# BIO-INSPIRED SEGMENTED SELF-CENTERING ROCKING FRAME

Kara D. Kea

Thesis submitted to the faculty of the Virginia Polytechnic Institute and State University in partial fulfillment of the requirements for the degree of

Master of Science
In
Civil Engineering

Matthew Eatherton, Chair
Roberto Leon
Ioannis Koutromanos

May 6, 2015
Blacksburg, Va

Keywords: Lateral Force Resisting System, Self-Centering Rocking Frame

# BIO-INSPIRED SEGMENTED SELF-CENTERING ROCKING FRAME

Kara D. Kea

## ABSTRACT

This paper investigates the development, design and modeling of a human spine-inspired seismic lateral force resisting system. The overall goal is to create a design for a lateral force resisting system that reflects human spine behavior that is both practical and effective. The first phase of this project involved a literature review of the human spine and rocking structural systems. The goal of this phase was to identify concepts from the spine that could be transferred to a lateral force resisting system. The second phase involved creating a 3-dimensional model of the lumbar region of the spine in SAP2000 and using it to examine concepts that could be transferred to a lateral force resisting system. The third phase consisted of creating possible system designs using concepts and principles identified through phases one and two and identifying a final system design. The last phase involved modeling the final lateral force resisting system design in SAP2000, validating the model and testing the design's effectiveness. This paper shows that this system is a viable option to prevent permanent structural damage in buildings during a seismic event.

Acknowledgments

Thank you to my parents, Karen Spencer-Kea and Jerry Kea, whose love, support and guidance have gotten me to where I am today. I love you guys. Thank you to my research advisor and committee members, Dr. Eatherton, Dr. Leon, and Dr. Koutromanos, for investing their time, effort and belief in me. They have taken me farther down the rabbit hole than I ever thought I would go and I couldn't be happier. Thank You to my loyal fans, Kandace Kea, Jackie Thomas, Kayla Ragland, Mathu Davis, Fred Harris, Guillermo and my other friends, for keeping me motivated, driven and sane. Lastly, I'd like to thank everyone who has impacted my life up until this point. Whether you know it or not, you've helped mold me into the person I am today.

## Table of Contents

## Contents

## List of Tables

## List of Figures

## List of Equations

# Chapter 1 Introduction

The human spine is the primary source of strength and stiffness in the human body. Not only does it protect the spinal cord but it also provides support for the upper body, controls posture, and allows for rotation, flexibility and movement in the human body. Over time the spine has evolved to allow upright posture, increased mobility, and injury prevention. These qualities make the human spine an excellent source of inspiration for a resilient lateral load resisting structural system. The spine has the capability to experience large deformations while sustaining little or no damage. Most regions in the spine can rotate substantially and are extremely flexible. Thus the spine presents methods for resisting torsion, lateral bending, rotation, compression and overextension. In addition, it is relatively small in proportion to the mass it supports and thus represents an extremely efficient structure.

Over the course of a day, the spine experiences many different types of loading scenarios, after which the spine returns to its neutral position. The surrounding support system, mostly muscles and ligaments, contribute to the overall stability and strength of the spinal structure. However, one of the most interesting capabilities of the spine is its ability to undergo large deformation with very little contribution from the muscles to resist it. This shows that the passive elements (ligaments, vertebral bodies and intervertebral discs) or elements that don't require use of the brain to be utilized of the spine significantly contribute to its' capabilities, which is very attractive when trying to transfer these same capabilities to a structural system. Overall, the human spine is extremely efficient in how it addresses the physical demands of everyday life on the human body and these concepts can be applied to the lateral force resisting system of a building.

Drawing inspiration from the human spine is not a simple task. The spine has a number of intricate parts that work together to perform various objectives. These parts handle the loads applied to the body due to a multitude of internal and external forces. Therefore it was essential to define the scope of forces being

observed, their effect on the spine and the components of the spine whose capabilities could be transferred to structural systems. Completing this task was the first objective of the proposed research. In order to understand the complexity of the spine and its components, an extensive literature review was conducted. From this review, a model of the spine was developed, including realistic dimensions, applicable passive components, material properties and appropriate load cases. Next the model was transferred to SAP2000, a powerful computer program for structural analysis and design. The model was then subjected to various loading cases that were deemed applicable to the research. Lastly, conclusions were made about the spine and its components based on the results obtained from the different loading scenarios.

The second objective was to create a lateral load resisting system based on the observations obtained from the SAP2000 model and further observations made through literature review. This was done by drafting up multiple system ideas and working through the logistics of each system. Next the ideas were categorized based off of what the system accomplished and how. Then all of the categories were simplified into one generic design that could be modeled in SAP2000. The best category was determined and used as the lateral force resisting system design. Lastly, the simplified model was inputted into SAP2000 and subjected to various loading conditions to ensure that the system behaved as expected.

The following report documents the processes used and results obtained from creating a lateral force resisting system that is inspired by the spine. The report is divided into seven chapters. Chapter 1, entitled “Introduction”, provides a brief introduction to the human spine and the features of the spine that can be applied to a structural system. Chapter 2, “Biomechanics of the Human Spine”, covers basic concepts of the spine, the center of mass of the body, spinal terms, motions of the spine, regions of the spine, details of the components of the spine, reactions of the spine to different loading conditions and relates the biomechanics of the spine to structural systems. Chapter 3, “SAP2000 Spine Model”, includes the process of creating a simplified model of the spine, the SAP2000 model, justification for simplifying the model and observations made from the SAP2000 model. Chapter

4, “Literature Review”, includes a literature review on rocking frame systems. Chapter 5, “System Ideas”, includes the general parameters of the system, details on each of the system design approaches, and a simplified model of general approach 1. Chapter 6, “Lateral Force Resisting System”, provides details about the lateral force resisting system, the design-building layout, the SAP2000 model of the system and the model verification process. Chapter 7, "Ground Motions in SAP2000", includes a description of the ground motions used to assess the capabilities of the lateral force resisting system design. Chapter 8, "SAP2000 Model Results", includes the results of four models ran in SAP2000 with ten sets of ground motions. Chapter 9, "Summary and Conclusions", provides and brief summary of the research and final conclusions. Lastly, chapter 9.3, entitled “Future Work”, includes a detailed summary of future work.

# Chapter 2 Biomechanics of the Human Spine

## 2.1 The Basics

The human spine is a complex structure consisting of bone, ligaments, muscle and viscous fluids. The layout of the spine is shown in Figures 1 and 2. The spine provides the body with support, stability and protects the spinal cord (Eidelson 2002). The segmented bone structure of the spine allows for the human body to experience a wide range of motion without damaging the individual components (Schafer 1987). The spine consists of three major elements; the spinal column, the neural elements and the supporting structures (Eidelson 2002). The spinal column is comprised of vertebrae and intervertebral discs(Eidelson 2002). The vertebrae, which provide support, are analogous to building blocks. Each building block is connected in the front of the spine by intervertebral discs (Schafer 1987). The intervertebral discs are simply gel pads bound together by tissue. These discs support the spine and also allow it to move (Schafer 1987). The neural elements include the spinal cord and nerve roots (Eidelson 2002). The spinal cord runs from the base of the brain down to the lower back (Schafer 1987). At each vertebra a pair of nerve roots spread out to the rest of the body (Schafer 1987). The supporting structures are the ligaments and muscles, which support and stabilize the spinal column (Schafer 1987).

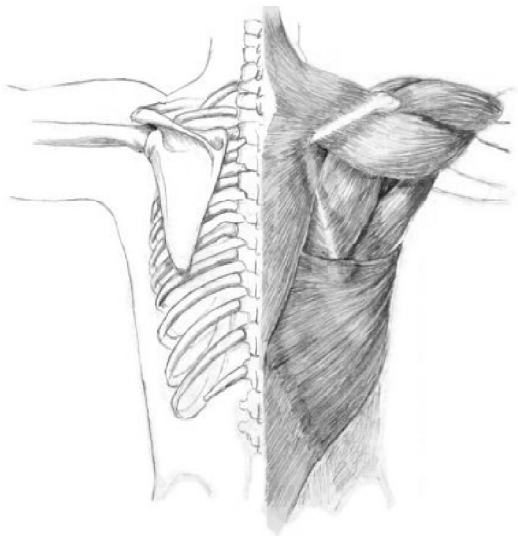

Figure 1: Spine and Muscles, Barcsay, Jenő. (1978). Anatomie voorde kunstenaa. Cantecleer, 1978. Print, Used under fair use, 2015.

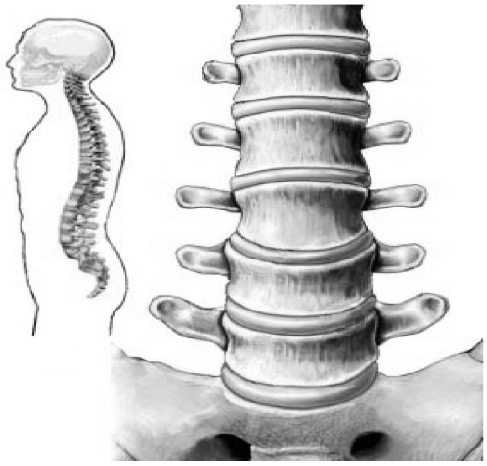

Figure 2: Vertebral and Intervertebral Discs, Beardmore, R. (2013, January 23). Reciprocating Mechanisms. Retrieved January 16, 2015, from http://roymechx.co.uk/Useful_Tables/Cams_Springs/Reciprocating.html. Used under fair use, 2015.

The human body is a bilaterally symmetric structure. This concept of bilateral symmetry significantly impacts the location of the center of mass of the body. The center of mass of a human being varies depending on weight distribution, gender and location of the limbs. Weight distribution plays an enormous role in how the spine reacts to outside stimuli and forces. A study conducted by Clauser et al. (Clauser and Young) showed that the center mass of the human body ranges from 39.4-43.1 percent of the person's stature or natural height (Clauser and Young). It is also important to understand the relevance of the location of the center of mass of each individual body segment and its contribution to the force exerted onto the spinal column. The numerous locations and masses of various body segments result in various stresses being applied to different portions of the spine. The location of the center of mass by segment is shown in the study conducted by Clauser (Clauser and Young) and some of the results can be seen in Table 1 below. The segment lengths and center of mass locations are measured from the top of each segment.

Table 1: Summarized Results from Clauser Study, Clauser, Charles, John T. McConville, and J.W. Young. "Weight, Volume, and Center of Mass of Segments of the Human Body." *National Technical Information Service*. (1969), Used under fair use, 2015.

| Segment | Mean Segment Weight/Body Weight | Mean Center of Mass Location of Segment/Segment Length |
|---|---|---|
| Head | 7.3% | 46.6% |
| Trunk | 50.7% | 38% |
| Total Arm | 4.9% | 41.3% |
| Total Leg | 10.1% | 38.2% |

The results in Table 1 show that the center of mass of each segment is highly affected by the weight distribution of each segment. For example the location of the center of mass of the total leg is located closer to the top of the leg. This can be attributed to the distribution of the weight between the thigh and the lower leg. This same concept can be transferred to looking at the center of mass of the entire body. While segments like the arms and head do contribute to its location, the center of mass is more so affected by larger segments like the trunk or legs. The location of the center of mass of the human body is key when examining how the spine distributes and dissipates the effects of applied forces. The spine must be able to accommodate the volume of these external forces as well as the location at which they are applied. The amount of force that the spine must provide support for is directly related to the magnitude of the force and its distance from the center of mass of the body. Therefore, the physical attributes of the five regions of the spine change to accommodate different types of loading scenarios.

### 2.3 Spine Location Terms and Descriptors

In order to simplify the description of both the spinal column's movement and component location relative to the body several generic terms are used. These terms are listed in the Table 2.

Table 2: Body Component Position Terms

| | |
|---|---|
| Anterior | refers to an object located in front of a structure |
| Posterior | refers to an object located behind a structure |
| Proximal | refers to an object located near the center of the body |
| Inferior | refers to an object located below or directly downward |
| Superior | refers to an object located above or directly upward toward the head |
| Lateral | refers to an object located away from the midline of the body |
| Anterolateral | refers to an object located on the front or side of |
| Medial | refers to an object located close to the midline of the body |

Sections of the body are often defined in terms of planes. The human body is broken into three planes as shown in Figure 3. The lateral plane is known as the sagittal plane. The frontal plane is known as the coronal plane. The transverse plane is known as the axial plane. When referring to the direction of movement, location of spinal elements and other relevant body components a coordinate system is defined. Figures 4 and 5 define the planes of the body and each vertebral body.

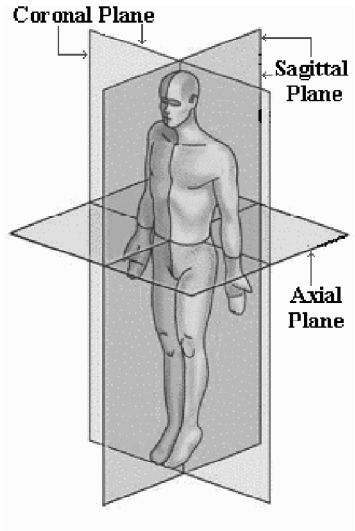


Figure 3: Planes of the Human Body, Eidelson, Stewart. *Saving Your Aching Back and Neck, A Patient's Guide* . 2nd ed. San Diego, California: SYA Press, Inc, 2002. Print, Used under fair use, 2015.

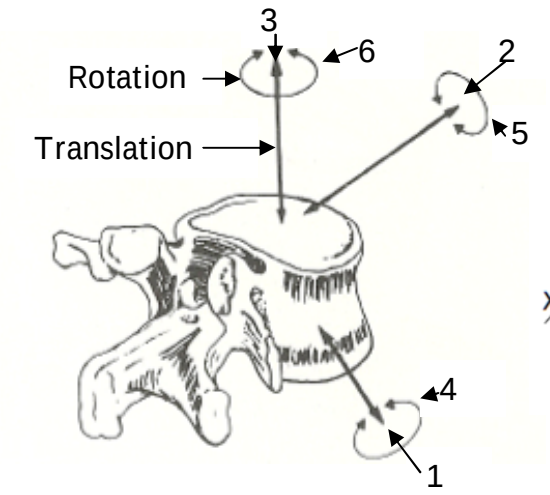


Figure 4: Spinal Vertebrae degrees of freedom, Boundless. “Center of Mass of the Human Body.” Boundless Physics. Boundless, 14 Nov. 2014. Retrieved 14 Jan. 2014 from https://www.boundless.com/physic /textbooks/boundless-physics-textbook/linear-momentum-and-collisions-7/center-of-mass-72/center-of-mass-of-the-human-body-305-1641/, Used under fair use,2015.

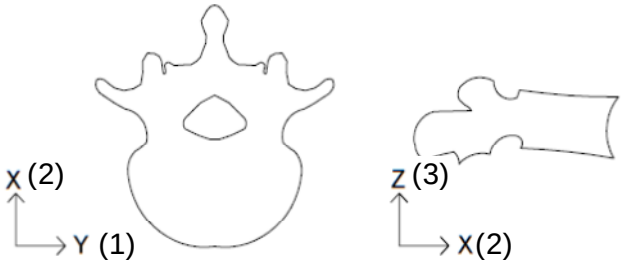


Figure 5: Vertebrae Coordinate System

## 2.4 Motions of the Spine

The spine allows for the transfer of moments and loads from the upper body to the pelvis, provides a point about which the head can pivot and acts as a shock absorber. When a force is applied to the human body several events occur. First, the force is distributed along the length of the body into the spine region. Next, the load moves through the vertebral bodies, which make up seventy-five percent of the spine. Lastly, the remaining forces passes through the intervertebral discs, ligaments and muscles. The spine has a high load and deformation capacity and sustains little to no damage during the vast majority of loading events. If it is over-exerted, either due repetitive movements or over-loading or over-extension,

permanent damage can occur over time. There are several types of motion that account for different loading scenarios to occur within the spine.

The types of motion primarily experienced by the spine include flexion, extension, side bending, rotation and translation. Flexion and extension describe the forward and backwards bending movements of the spine, respectively. Side bending occurs when the spine bends to the left or right. Rotation is the movement of one vertebrae to another on its' normal axis. Translation is described as vertebral body displacement.

## 2.5 Vertebrae and Intervertebral Disks

The vertebrae increase in size down the length of the spine. These bony structures carry a majority of the load experienced by the body including weight and any applied forces. The load is directed from the superior endplate to the inferior endplate. They are smallest in the cervical region and largest in the lumbar region. The vertebra, shown in Figure 6, consists of several components including the vertebral body, the pedicles, the foramen, the laminae, spinous process, the transverse facet and the superior facet. All of these components help distribute upper body weight through the spinal column, sacrum and coccyx.

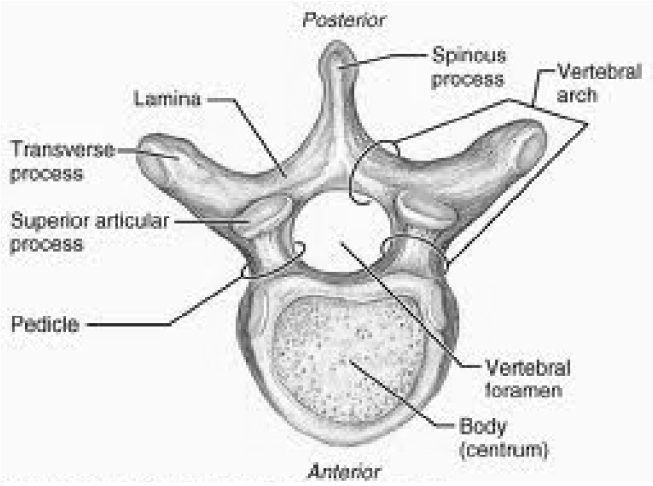


Figure 6: Vertebrae Layout, Marieb, Elaine. *Human Anatomy & Physiology.* 5th ed. San Francisco, California: Benjamin Cummings, 2001. Print, Used under fair use, 2015.

The intervertebral discs, shown in Figure 7, act as shock absorbers for the spinal column as well as allow for some flexion and extension. The discs work together to provide larger ranges of motion.

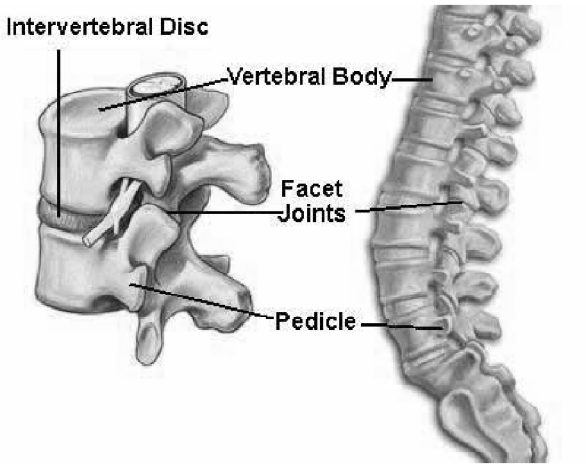


Figure 7: Intervertebral Disc Location, Eidelson, Stewart. *Saving Your Aching Back and Neck, A Patient's Guide* . 2nd ed. San Diego, California: SYA Press, Inc, 2002. Print, Used under fair use, 2015.

The discs consist of three components that allow for varying stress distribution under flexion, extension, bending, rotation and translation. These three components are the nucleus pulposus, annulus fibrosus and endplates. The layout of these components can be seen below in Figure 8.

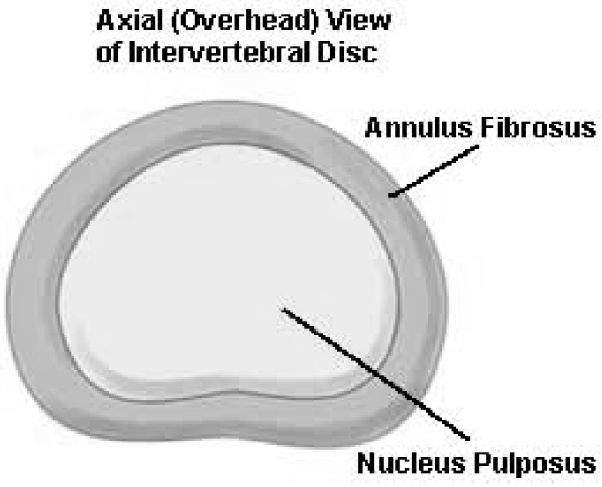


Figure 8: Intervertebral disc, Eidelson, Stewart. *Saving Your Aching Back and Neck, A Patient's Guide* . 2nd ed. San Diego, California: SYA Press, Inc, 2002. Print, Used under fair use, 2015.

The nucleus pulposus is comprised of water, collagen and proteoglyceans. Proteoglyceans are particles that attract and hold water. The nucleus pulposus is bound by the annulus fibrosus. The annulus fibrosus is a strong circular structure comprised of sheets of collagen fibers that are connected to the vertebral endplates. These components work together to allow the nucleus pulposus to move within the disc when subjected to various loading conditions. This accounts for the capability of the intervertebral disc to distribute and absorb loads of varying direction and magnitude.

The facet joints, seen in Figure 9, consist of two facet plates, one from each adjacent vertebra. Each vertebra has two sets of facet joints. A facet plate extends from the top and bottom of the vertebral body on both the right and left hand side.

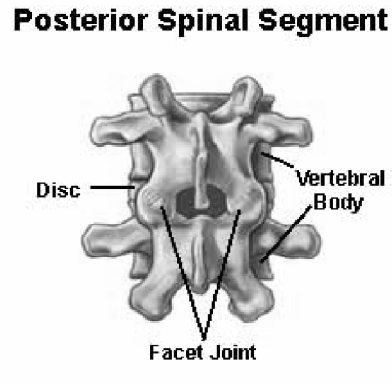


Figure 9: View of the posterior elements between two vertebral bodies, Eidelson, Stewart. *Saving Your Aching Back and Neck, A Patient's Guide* . 2nd ed. San Diego, California: SYA Press, Inc, 2002. Print, Used under fair use, 2015.

Facet plates are connected by ligaments in some places and muscles in others. They limit flexion, extension and rotation of the spinal column. The facet joints provide the spinal column with stability and support due to their interlocking nature between adjacent vertebrae. The facet joints angle changes depending on the vertebral body location within the spinal column. This change, which is most prominent in the lower region of the spine, is due to the need to limit different types of motion. The touching surfaces of facet joint are covered with cartilage. This allows one plate to glide smoothly upon another.

## 2.6 Regions of the Spine

The spine is separated into five regions that are shown in Figure 10. These regions are the cervical region, the thoracic region, the lumbar region, the sacrum and the coccyx. The cervical region consists of seven vertebrae, C1-C7. This region is identifiable with the neck on the human body. It accommodates large rotations and provides a pivot point for the head. The thoracic region consists of twelve vertebrae, T1-T12. This region has a limited range of motion due to the vertebrae connection to the ribcage and long spinous processes. The shape of these vertebrae is defined by their small pedicles, long spinous processes, and large neural passageway. The lumbar region consists of five vertebrae, L1-L5. This region supports most of the body's weight and applied stresses. In this region the spinous processes are round and square, the pedicles are wider and longer, and the neural passageway is larger. Movement in this region is restrained to flexion, extension and small amounts of rotation. The sacrum consists of five fused vertebrae, S1-S5, and forms the pelvis. The coccyx consists of three vertebrae collectively known as the tailbone.

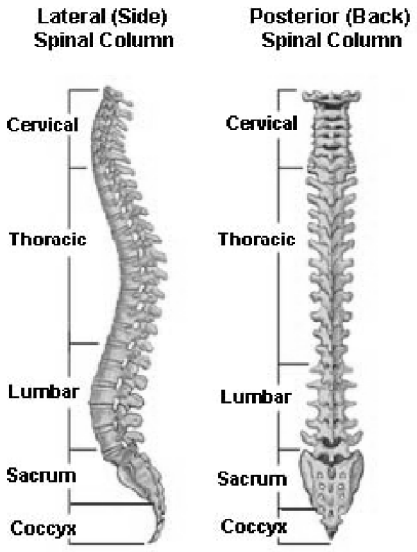


Figure 10: Spinal column layout, Eidelson, Stewart. *Saving Your Aching Back and Neck, A Patient's Guide* . 2nd ed. San Diego, California: SYA Press, Inc, 2002. Print, Used under fair use, 2015.

## 2.7 Ligaments

The ligaments of the spinal column, shown in Figure 11, act as passive elements in the control of the spine's deformation. They limit the motion experienced by the system and provide resistance when excessive force is applied to the body. The six main sets of ligaments in the spine are the anterior longitudinal ligament (ALL), posterior longitudinal ligament (PLL), intertransverse ligament, ligamentum flava, interspinal ligament, and supraspinous ligament. These ligaments provide the spine with stability and support. They are considered passive control elements, unlike the muscles that surround the spine.

The anterior longitudinal ligament is a thick ligament that runs down the anterior surface of the spine. It runs along all of the vertebral bodies and intervertebral disks. It consists of three layers: the superficial layer, the intermediate layer and the deep layer. The posterior longitudinal ligament runs down the posterior of the vertebral bodies, inside the spinal canal. This ligament consists of longitudinal fibers that are denser than those in the ALL. The intertransverse ligament runs between adjacent transverse processes of each vertebra. Some of these ligaments are replaced by muscle. The ligamentum flava connect the laminae of adjacent vertebrae. These ligaments assist the vertebrae in transitioning back to their original position after flexion and preserve posture.

The interspinal ligament is a thin and membranous ligament that connects adjoining spinous processes. It helps limit flexion of the spine. The supraspinous ligament is a strong fibrous cord that connects the spinous processes between vertebrae. It consists of several layers including the deep, intermediate and superficial fibers. The deep fibers connect adjacent spinous processes. The intermediate fibers connect two or three adjacent vertebrae. Lastly the superficial connects three or four vertebrae. All of these ligaments work in collaboration to limit the range of spine movement..

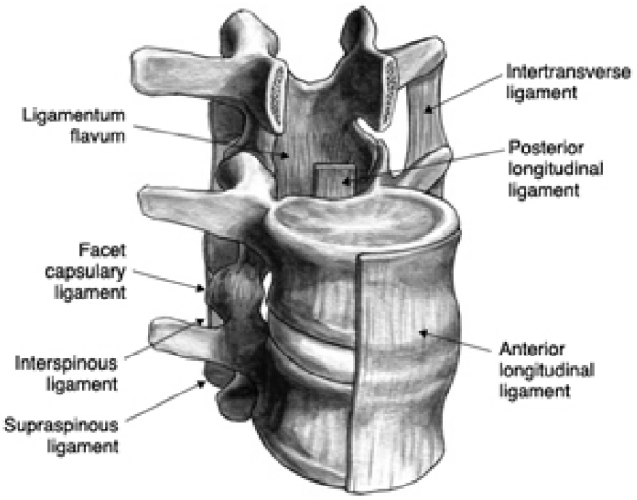


Figure 11: Spinal ligament layout, Spine Center. (n.d.). Retrieved January 6, 2014, from http://www.uvaspine.com/ligaments-tendons-and-muscles.php, Used under fair use, 2015.

## 2.8 Reaction of Spine to Various Loading Conditions

There are several reactions the spine can experience due to various loading conditions and the effects of gravity. These loading conditions and reactions include preloading, disc bulging, flexion, extension, tension, compression, and torsional stress. The preloading of an intervertebral disc can be compared to the tension in a pre-tensioned cable. Disc bulging occurs when the spinal column experiences flexion or extension. During these movements the intervertebral disc will bulge. When the spine moves the peripheral annulus of the intervertebral disc bulges in the posterior direction during extension and bulges anteriorly during flexion. The disc bulges towards the side during lateral bending. When the disc bulges, Poisson's effect takes over on the non-bulging edge, and it contracts on the contralateral side.

When the spinal column experiences tension or compression, the intervertebral discs elongate and flatten, respectively. The tension force causes the vertebral bodies to separate, disc thickening, nuclear pressure reduction and vertical annular fiber tension increase (Boundless Physics 2014). The compression forces causes the vertebral bodies to condense together, intervertebral disk

flattening, a nuclear pressure increase and annular fiber tension to increase(Boundless Physics 2014). If either of these forces is exerted in excess they can cause permanent damage to the intervertebral discs. Torsional stress is believed to cause the most damage to the discs. When an intervertebral disc is subjected to torsion, both a horizontal and vertical shear stress of equal magnitude develop. These forces become extremely dangerous when they are perpendicular to the fiber direction. The intervertebral discs and facets work to resist this force. The shape of the intervertebral discs also plays a role in the spines' ability to handle torsional rotation. Rounder discs are more torsion resistant than oblong or kidney shaped discs.

## 2.9 Lessons from Spine Biomechanics for Structural Systems

There are several spine biomechanics concepts that can be instructive for structural systems.

1. The spine is a segmented modular structure where each level consists of a near rigid unit (vertebra) connected together with elements (intervertebral discs) that allow deformations. The modular rigid units add significant stiffness to the spine system and could do similar for a structural system.
2. The spine system as a whole can undergo axial, lateral, and sagittal rotations and axial, lateral and anterior/posterior translations. Therefore it is capable of deformations in all six degrees of freedom without permanent damage. Allowing deformations in all six degrees of freedom without permanent damage would be very useful for a structural system when resisting seismic effects.
3. Each vertebra consists of a posterior neural arch and an anterior vertebral body, which absorb a portion of load applied to the body. Also each vertebra has facets that limit motion and transfer compressive forces. In a structural system, specialized connections between modular units could be designed to limit motion in some degrees of freedom while transferring compression forces to the base.

4. The intervertebral discs transmit body forces through hydrostatic pressure, acting as a shock absorber in between each vertebra body. The discs provide a viscous type of damping that could be emulated in a structural system.
5. The ligaments protect the spinal cord and other neural structures by limiting the motion of the spine and absorb energy during excessive motion. Similar passive control systems could be envisioned for structures. Post-tensioning elements with a two-phase behavior might transition from elastic behavior into a hardening regime that limits peak displacements while dissipating energy.
6. Many individual ligaments have varying length. As a consequence of these varying lengths, the spine creates an inherent system of overlapping ligaments adding redundancy to the system. The different lengths add a variety of displacement limitations. Assuming uniform strain capacity, shorter ligaments will have less displacement capacity. A range of displacement capacities in the ligaments can be used to control different types of motion.
7. Muscles act as an active control system that can bring the spine back to its neutral position after a large perturbation. Active structural systems that have the capability to plumb a building after a large event could be envisioned.
8. Many of the elements of the spine system have the ability to heal if damaged. Implementing healing characteristics into structural systems is an exciting prospect.

# Chapter 3 SAP2000 Spine Model

## 3.1 Simplified structural model of Lumbar Region

A simplified model of the lumbar section of the spine was created in Google Sketchup(Google, Inc. 2006) using geometric spine dimensions found in the paper written by Zhou, S.H. et. al. (Zhou et al. 2000). Figures 12 and 13 below illustrate the dimensions taken from literature.

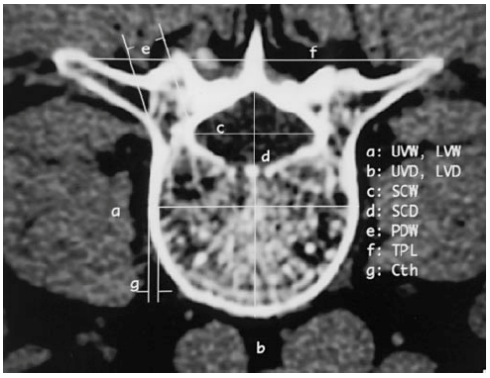


Figure 12: Cross Sectional Vertebral Body Dimension Labels, Zhou, S.H., I.D. McCarthy, A.H. McGregor, R.R.H Coombs, and S.P.F. Hughes. "Geometrical Dimension of the Lower Lumbar Vertebrae-Analysis of Data from Digitised CT Images ." *European Spine Journal*. 9. (2000): 242-248. Print, Used under fair use, 2015.

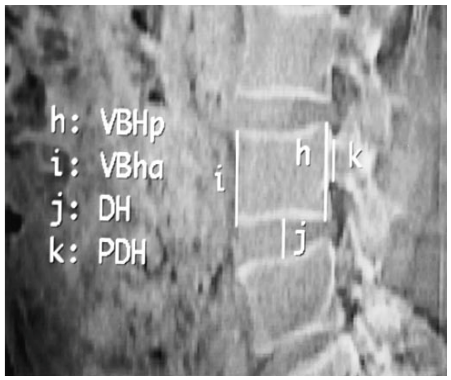


Figure 13: Lateral View of Lumbar Spine Dimension Labels, Zhou, S.H., I.D. McCarthy, A.H. McGregor, R.R.H Coombs, and S.P.F. Hughes. "Geometrical Dimension of the Lower Lumbar Vertebrae-Analysis of Data from Digitised CT Images ." *European Spine Journal*. 9. (2000): 242-248. Print, Used under fair use, 2015.

Each label in Figures 12 and 13 consists of an abbreviation that represents various dimensions on the vertebrae. UVW and LVW stand for the upper and lower vertebral width. UVD and LVD stand for the upper and lower vertebral depth. SCW stands for the spinal canal width. SCD stands for the spinal canal depth. PDW stands for the pedicle width. TPL stands for transverse process length. Cth stands for cortical bone thickness. VBHp stands for the posterior vertebral body height. VBha stands for the anterior vertebral body height. DH stands for intervertebral disk height and PDH stands for pedicle height.

In order to simplify the structural model, several assumptions were made. Figures of a simplified model of the lumbar region of the spine are shown below in Figures 14-17. The L1-L5 vertebrae were assumed to have the same dimensions and material properties. The transverse processes were assumed to be frame elements extending from vertebral body. The facets were represented by solid square elements whose contact angle could be easily modified. The spinous process was modeled as a pentagon shaped element that protruded from the back of the spinal canal wall. The bony posterior elements were assumed to consist of one material instead of soft cancellous bone surrounded by hard cortical bone. The vertebral body was assumed to be one constant width and height. The intervertebral disc was assumed to consist of one material. Lastly, the ligaments were divided into three layers: deep, intermediate and, superficial. Each of these layers was represented as cable elements that spanned one, two or three vertebrae. The following Table shows the geometric dimensions used in the Google Sketchup model.

Table 3: Geometric Properties of Simplified Spine Model

| | |
|---|---|
| Vertebral Body Width (VBW) | 2” |
| Vertebral Body Height (VBH) | 1 3/8” |
| Spinal Canal Width (SCW) | 1 3/16” |
| Spinal Canal Depth (SCD) | 1 3/8” |
| Transverse Process Length (TPL) | 1 9/16” |
| Spinous Process Depth (SPD) | 9/16 – 11/16” |
| Cortical Bone Thickness (CTh) | 0.05” |
| Intervertebral Disk Width (UDW) | 2” |
| Intervertebral Disk Height (DH) | 9/16” |

Creating a model of the lumbar region of the spine in Google SketchUp allowed for a closer examination of the geometry, configuration, and essential elements of the spine. The following observations were made when creating the model. The intervertebral bodies of the spine are held together by several different sets of ligaments and muscle groups. The ligaments act as passive elements, limiting motion, while the muscles act as active elements, controlling motion. The transverse

frame processes have the same effect on the spine as cantilever beams do on a structural floor system. The facet plates translate torsion from one intervertebral body to the next. The angle of contact of the facet plates play a significant role in the amount of torsion a region of the spine can accommodate. The intervertebral discs are meant to act as energy dissipaters whereas the intevertebral bodies provide the spine with structure and support.

These observations allowed for several simplification ideas to be used later on during the SAP 2000 spine modeling process. The transverse processes in the spine were equated to extended frame elements in a structural system. The intervertebral bodies had to be represented using two different materials, a harder outside shell and a softer interior. The discs could be represented using a single material property. The facet plates were simplified into extruded square shaped elements. The integrity of the shape of the spinal canal could be maintained when representing the transverse processes as frame elements. Lastly, it was important to model the spinal ligaments to properly represent the connectivity of the system.
The following Figures 14-17 illustrate the model created in Google Sketchup.

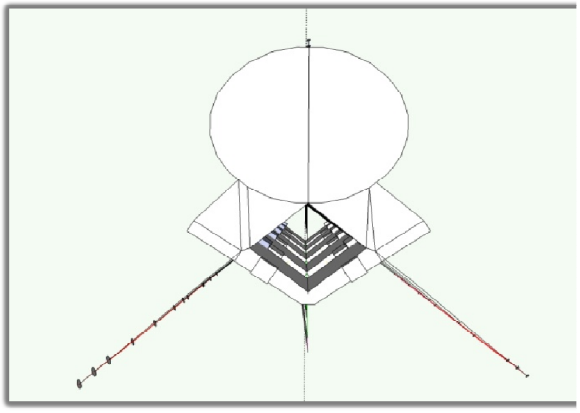

Figure 14: Plan view of Simplified Lumbar Region Model

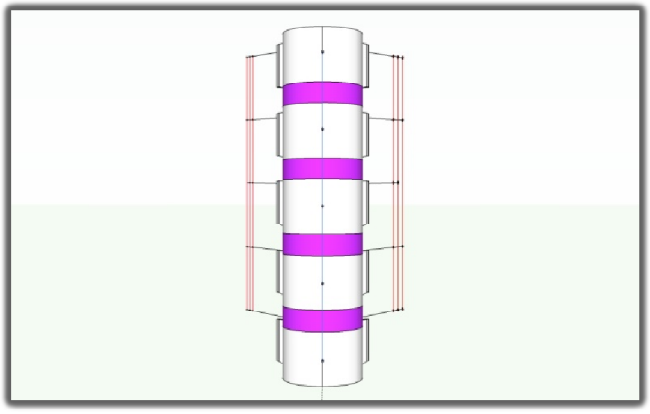

Figure 15: Front View of Simplified Lumbar Region Model

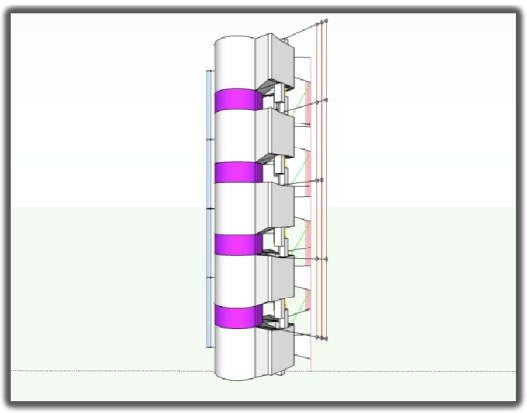

Figure 16: Side View of Simplified Lumbar Region Model

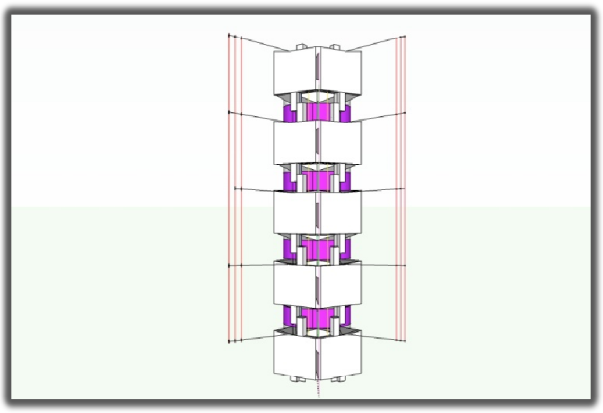

Figure 17:Rear View of Simplified Lumbar Region Model

Table 2 describes the material properties of the spinal ligaments. These material properties are not included in the Google Sketchup model. The ligaments are color-coded in the Google Sketchup model to show where the ligaments will be placed in SAP2000 model. The listed properties, taken from (Goel et al. 1994), include the Young's modulus, the shear modulus, Poisson's ratio, density, and cross-sectional area. Each ligament is color coded to match a model created in Google Sketchup.

Table 4: Spine Material Properties, Goel, Vijay K., Hosang Park, and Weizeng Kong. "Investigation of Vibration Charateristics of the Ligamentous Lumbar Spine Using the Finite Element Approach." *Journal of Biomedical Engineering*. 116. (1994): 378-379. Print, Used under fair use, 2015.

| Material | Color in Model | Young's Modulus(Mpa) | Shear Modulus (Mpa) | Poisson's Ratio | Density (kg/mm 3) | Cross-Sectional Area (mm2) |
|---|---|---|---|---|---|---|
| Cortical Bone | White | 12000 | 4615 | 0.3 | $1.7X10^{-6}$ | |
| Cancellous Bone | White | 100 | 41.7 | 0.2 | $l.lxl0^{-6}$ | |
| Bony Posterior Elements | | 3500 | 1400 | 0.25 | $1.40X1^{-6}$ | |
| Annulus (Fiber) | Purple | 175 | - | - | $1.0xl0^{-6}$ | |
| Nuclus Pulposus | Purple | 1,660 | - | - | $1.02X1^{-6}$ | |
| Ligaments | | | - | - | | |
| Anterior Ligament (AL) | Blue | 7.8-20.0 | - | - | 1.0X10^ -6 | 63.7 |
| Prosterior Ligament (PL) | Light Green | 10.0-20.0 | - | - | $1.0X10^{-6}$ | 20 |
| Ligamentum Flavum (LF) | Yellow | 15.0-19.5 | - | - | $1.0X10^{-6}$ | 40 |
| Intertransverse Ligament (TL) | Red | 10.0-58.7 | - | - | $1.0X10^{-6}$ | 3.6 |
| Capsular Ligament (CL) | | 7.5-32.9 | - | - | $1.0X10^{-6}$ | 60 |
| Interspinous Ligament (IS) | Pink | 7.5-32.9 | - | - | $1.0X10^{-6}$ | 40 |
| Supraspinous Ligament (SS) | Neon Green | 8.0-15.0 | - | - | $1.0X10^{-6}$ | 30 |

## 3.2 SAP2000 Model of the Simplified Lumbar Region Spine Model

Once the simplified model of the lumbar region of the spine was created in Google Sketchup, a second model was created in SAP2000 (Berkeley 2007). The model is shown below in Figure 18. This model was used to observe reactions of the

spine when subjected to various loading scenarios and the contributions of various processes to the reaction of the spine. In order to successfully transfer the model from Google Sketchup to SAP2000, several changes had to be made. The vertebral bodies were modeled using sixteen node solids surrounded by another thirty-two-node solid, creating an inner portion and outer portion. This was done to represent the two different materials that the vertebral bodies consist of, the cortical and cancellous bone. The oval shape used for the vertebral body could not be exactly replicated in SAP2000. Therefore an octagon shape was used for the vertebral body. The inner solid was then subdivided into twenty-seven smaller eight-node solids and the outer solid into twenty-four eight-node solids. The inner solids were assigned cancellous bone material properties and the outer solids cortical bone material properties.

The intervetebral discs were modeled using eight-node octagon shaped solids as well. The discs solids were then subdivided into eighteen smaller eight-node solids. The disc solids were assigned the appropriate disc material properties. The vertebral arches were modeled using eight node solid elements that were then subdivided into three layers in the Z direction. The layout of the arches included a hollow channel to represent the vertebral foramen. The solids were assigned the bony posterior element material property. The transverse processes were modeled using frame elements. The frame elements were represented as small, circular tubes with a very small inner hole diameter. The elements were assigned the bony posterior element material property.

The spinal ligaments were modeled as single cable elements. Instead of modeling all three layers of each individual ligament, the three layers of the spinal ligaments were combined into a single layer with the same material properties. The cables were not pretension due to the inability to find numerical data on pre-tensioning on ligament in situ. The facets were eliminated from the model entirely since SAP2000 unable to model the contact surface between two facets. Since all of the solid elements shared at least one face SAP2000 treated them as a single solid discretized element.

The properties used for the SAP2000 model can be seen in Table 3 and Table 4. When assigning modulus of elasticity for the ligaments, the lower value from Table 4 was assumed to produce a worst-case scenario. The model of the lumbar region of the spine was simplified to make modeling in SAP2000 easier. This process included removing some of the solid elements, such as the transverse processes, and replacing them with frame elements. This made it easier to run analyses in SAP2000 since there were less elements in the model. It also included making a standard vertebral body size and shape to simplify the modeling process.

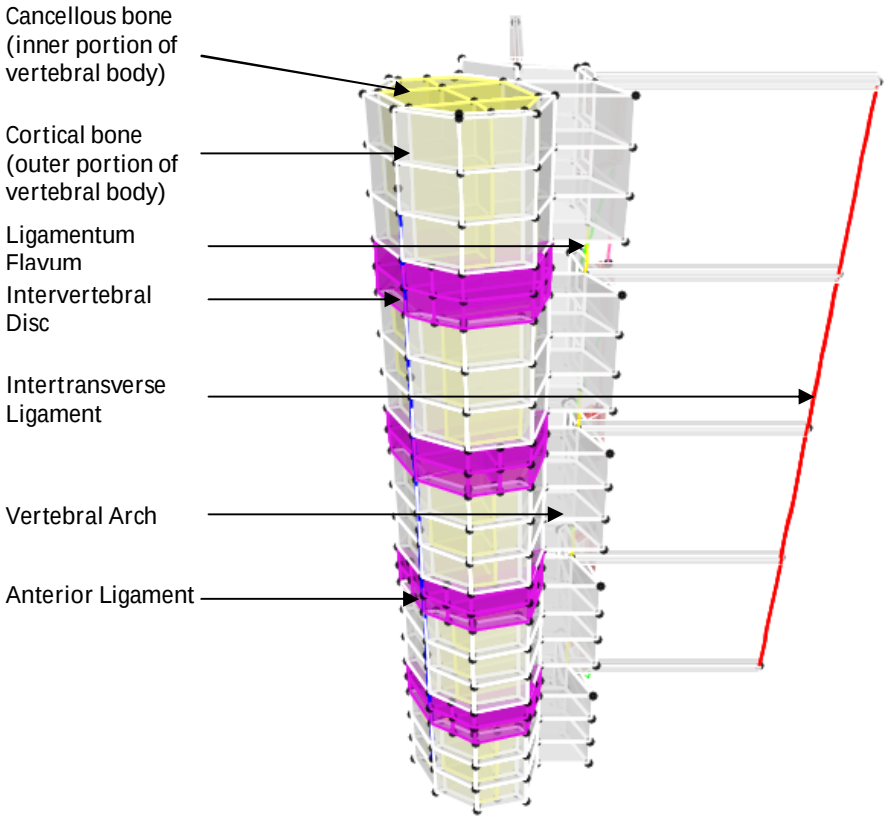


Figure 18: 3-D View of Lumbar Region of Spine in SAP200

## 3.3 Model Verification

The SAP2000 model went through several iterations to be deemed valid. Two techniques were used to validate the model. The first technique involved comparing the deflection of the model under compressive forces to an already completed nonlinear 3-D finite element model, with 6 degrees of freedom. This technique

helped to define the boundary conditions of the structure and confirm the material properties. A three vertebrae structure was created in SAP2000 (representing L4, L5 and S1). A 3-D view of the model is shown in Figure 19 below. Each vertebral body and intervertebral disc was meshed into a 3 by 3 and 2 by 2meshing pattern respectively. It was fixed in all directions at a single point on the inferior surface of the S1 vertebrae and a single point along the spinous process.

A compressive force of 0.1 kips was applied to the model by distributing it on each nodal point on the superior surface of the vertebral body. Ninety percent of this load was applied to the L4 upper vertebra surface and ten percent was applied to the L4 superior facet elements. This loading method is shown in Figure 20. The vertical deflection of a single point on the model was then compared to the resulting deflections at the same point of the model used in the study. A deflection of 0.0318 inches at a point along the cortical bone on L5 was compared to a deflection of 0.0386 inches obtained from the SAP2000 model at the same point. While this process helped confirm the material properties under a compressive axial force, when a lateral force was applied to the same structure the lateral deflections of the model seemed relatively small. Thus a second technique was needed to validate the model.

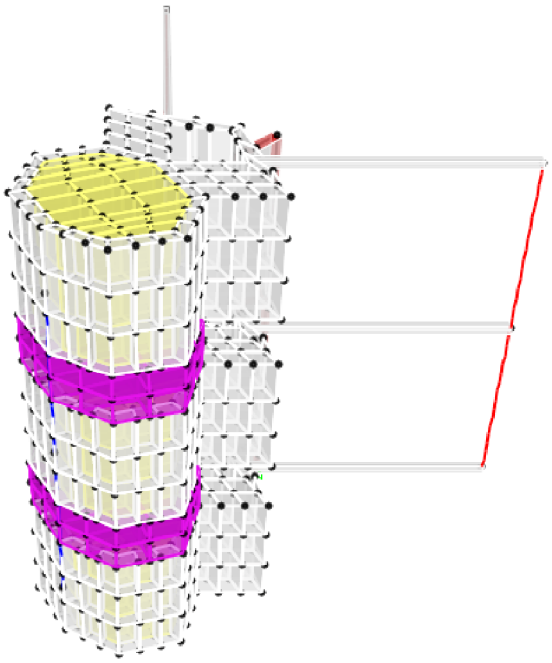

Figure 19: SAP2000 Spine Model A

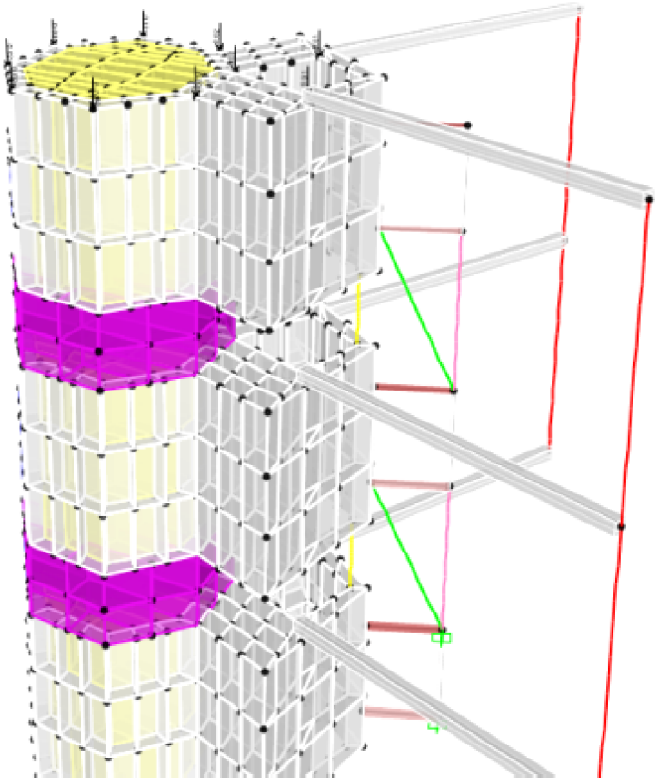

Figure 20: Load Configuration of Spine Model A

The second method involved comparing the deflections of a model comprised only of the vertebral bodies and intervertebral discs of the lumbar region in SAP2000 to hand calculated deflections. This process was used to confirm the correct process was being used to construct the model. The equation for the deflection of a cantilever beam was used to find the hand-calculated deflections. An $(EI)_{effective}$ was used when calculating the deflections by hand. This $(EI)_{effective}$ of 107 ksi, was derived by looking at the system a series of springs acting in series. A 100 lb load was used to calculate the deflections. The resulting deflection derived by hand was 0.240 inches. The model used during this process was constructed from single octagon shaped tower in SAP2000. The model was subdivided into nine sections in the Z direction to account for the vertebral bodies and intervertebral discs. It is important to note that the meshing sequence of the model played a vital role in the lateral deflections. If meshed incorrectly the SAP2000 model would greatly underestimate the lateral deflections. The properties for the vertebral bodies and intervertebral bodies are shown in Table 4. This model can be seen below in Figure 21. A 100 lb load was applied to the model in the positive x direction. The resulting deflection from the model was 0.268 inches. Comparing the hand calculated deflection of the model and the deflection obtained from SAP2000 showed the model was being developed correctly.

### 3.5 Observations From SAP2000 Simplified Lumbar Region Model

Understanding how the spine deforms when subjected to various loads was one of the main goals behind creating a 3D model of the spine in SAP2000. The first question posed was: when subjected to lateral loads, is spine deformation shear or flexure dominated? In order to determine this, the difference between shear dominated and flexure dominated was looked at in terms of the angle of rotation. When an object experiences predominately flexural deformations and perpendicular to the member longitudinal axis. In an object that experiences shear dominated deformations the deformed sections do not remain plane and are no

longer perpendicular to the longitudinal axis. Therefore the angle of rotation is closer to zero. The angle of rotation, $\theta$, and deflection, $\delta$, were calculated using the following equation derived from a cantilever beam:

$$\theta = PL^2 / 2(EI)_{eff} \quad \text{(Equation 1)}$$

$$\delta = PL^3 / 3(EI)_{eff} \quad \text{(Equations 2)}$$

where,

P = Applied Load

L = Length

$(EI)_{eff}$ = derived in section 3.3

From these two equations a ratio can be developed to determine if a system is flexure or shear dominated. This equation is shown below.

$$\text{Ratio} = \theta / \delta \quad \text{(Equation 3)}$$

where,

$\theta$ = angle of rotation

$\delta$ = deflection

Due to the angle of rotation being closer to zero during shear deformation, if this ratio is close to zero the system can be assumed to be shear dominated. In order to calculate the theoretical value for flexure, the behavior of a fixed-free rod consisting of nine layers of alternating materials when subjected to 100 lbs of force was calculated using equations 1 and 2. The theoretical value for flexural deflection and the angle of rotation were calculated to be 0.240 in and 0.039 rads respectively making the theoretical ratio value for flexure 0.163. Spine Model B shown in Figure 21, was used to find the ratio in SAP2000. This model was subjected to 100 lbs of force. The model ratio was calculated to be 0.163265 with deflection and angle of rotation values of 0.268 in and 0.043755 respectively. Therefore it was concluded that lumbar region of the spine undergoes flexure-dominated deformations.

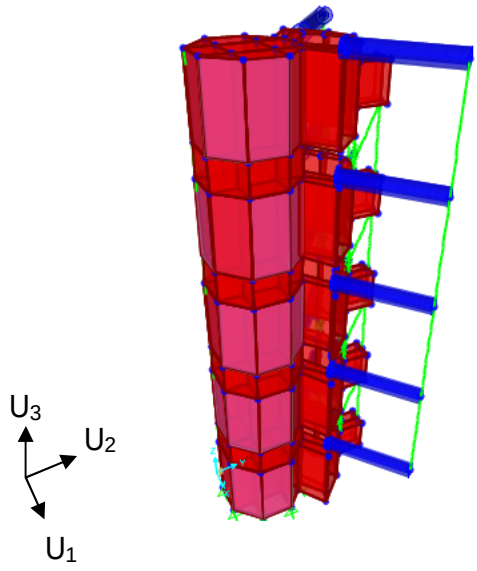


Figure 21: 3-D View of Model in SAP2000

The second question was: how much and in what way do the ligaments affect the deformations of the spinal model? In order to answer this, a 100 lb load was applied to the model with and without ligaments. The deformations from each model were recorded. The deformations for the model with ligaments were U1=0.0098 in, U2 = 0.246 in and U3 = 0.0326 in. The deformations for the model without ligaments were U1 = 0.0093 in, U2 = 0.2478 in and U3 = 0.0328 in. Comparing U2 from both models showed that the ligaments had very little impact on the overall deformation of the spine. The same ratio utilized in the previous section was also used to determine the shear versus flexure dominated deformation balance of the models. The model with ligaments had a ratio of 0.163 and the model without had a ratio of 0.163 showing the spinal model was still flexure-dominated and that the ligaments once again had little impact on this behavior. This finding directly contradicted the fact that ligaments have been shown to hold the vertebrae together and stabilize the spinal column (Hines 2013). Therefore it was concluded that the model does not correctly model the behavior of the ligaments. It is speculated that this is due either to SAP2000 treating all of the eight node solids with touching faces as a single solid element or ligament pretensioning being neglected in the model. This eliminates the notion of the vertebral bodies and

intervertebral discs as being separate entities that must be connected by ligaments.

The third question was: how does the vertical stiffness of the spine compare to the lateral stiffness. In order to answer this question, the compressive behavior of the lumbar region spine model was investigated. This was done by treating the lumbar region of the spine like a short column whose critical buckling load was significantly greater than the load applied. The critical buckling load was calculated using the following equation:

$$P_{cr} = \pi^2 EI / L^2 \qquad \text{(Equation 4)}$$

where,

E= Modulus of Elasticity

I = Moment of Inertia

L = Length of Column

The calculated Pcr of 12,510 lbs was signifigantly greater than the applied P of 100 lbs. Therefore the following equation was used to calculate the deflection of the model due to a compressive force:

$$\delta = PL / EA \qquad \text{(Equation 5)}$$

where,

P = Applied Load

L Length of Column

E = Modulus of Elasticity

A = Area

The deflection was then calculated to be -0.004382 inches. This calculation did not include the effects due to the posterior neural arch or ligaments. A deflection of -0.0029 inches was obtained from Spine Model A shown in Figure 21. Even though the calculated amount was greater the difference can be attributed to the addition of the components that make the posterior neural arch and the ligaments. A deflection of -0.003 in was obtained when a uniformly distributed compressive force totaling 100 lbs was applied in the negative Z direction. When subjected to a lateral load of 100 lbs in the positive X direction the model deflected 0.24 in. From this data, the vertical and lateral stiffness of the model was calculated to be 33 k/in and 0.42 k/in

respectively. The ratio of vertical to lateral stiffness was calculated to be 80 k/in.

The fourth question was: what is the maximum lateral displacement the spine can endure before a ligament would break. This question was answered by calculating the drift ratio for each ligament using the maximum in vivo strain to find the maximum deflection the ligament will experience. The following chart shows the maximum in vivo strain each ligament experiences and the type of motion that causes it.

Table 5: Maximum In Vivo Strain of Spinal Ligaments, White, A., & Panjabi, M. (1990). *Clinical biomechanics of the spine* (2nd ed.). Philadelphia: Lippincott, Used under fair use, 2015.

| Ligament | Maximum In Vivo Strain (%) | Type of Motion |
|---|---|---|
| ALL | 13 | Flexion |
| PLL | 13 | Extension |
| LF | 15 | Flexion |
| CL | 17 | Torsion (Not Examined) |
| ISL | 28 | Flexion |

The drift ratio is measured as the lateral drift divided by the height of the structure. To find the drift ratio for the model was subjected to both of the load types listed above in Table 5 (flexion and extension) and the displacement of each ligament was recorded. In both scenarios the load was increased in 0.1K increments until 1.0K was reached to achieve a large range of ligament strains. The results from an applied extension force are shown in Table 6.

Table 6: Deflection of Ligaments Exposed to Extension

| Force (k) | ALL Deflection (in) | PLL Deflection (in) | LF Deflection (in) | ISL Deflection (in) | SSL Deflection (in) |
|---|---|---|---|---|---|
| 0.1 | 0.2503 | 0.1843 | 0.1912 | 0.2043 | 0.2043 |
| 0.2 | 0.4963 | 0.3743 | 0.3781 | 0.4043 | 0.4043 |
| 0.3 | 0.7423 | 0.5543 | 0.5649 | 0.6033 | 0.6033 |
| 0.4 | 0.9883 | 0.7443 | 0.7518 | 0.8033 | 0.8033 |
| 0.5 | 1.2343 | 0.9343 | 0.9387 | 1.0042 | 1.0042 |
| 0.6 | 1.4817 | 1.1243 | 1.1256 | 1.2042 | 1.2042 |
| 0.7 | 1.7265 | 1.3043 | 1.3125 | 1.4041 | 1.4041 |
| 0.8 | 1.9723 | 1.4943 | 1.4994 | 1.6041 | 1.6041 |
| 0.9 | 2.2183 | 1.6843 | 1.6862 | 1.8041 | 1.8041 |
| 1 | 2.4644 | 1.8643 | 1.8731 | 2.0041 | 2.0041 |

The recorded displacements were then translated to ligament strains by dividing the displacements by the ligament lengths. These strains were then plotted against the initial displacement for each individual ligament. These results can be seen in Table 7.

Table 7: Ligament Strain

| Force (k) | ALL Strain (%) | PLL Strain (%) | LF Strain (%) | ISL Strain (%) | SSL Strain (%) |
|---|---|---|---|---|---|
| 0.1 | 3% | 3% | 3% | 3% | 3% |
| 0.2 | 7% | 6% | 6% | 6% | 6% |
| 0.3 | 10% | 9% | 9% | 9% | 8% |
| 0.4 | 14% | 12% | 12% | 11% | 11% |
| 0.5 | 17% | 15% | 15% | 14% | 14% |
| 0.6 | 21% | 18% | 18% | 17% | 17% |
| 0.7 | 24% | 20% | 21% | 20% | 20% |
| 0.8 | 27% | 23% | 24% | 23% | 22% |
| 0.9 | 31% | 26% | 26% | 25% | 25% |
| 1 | 34% | 29% | 29% | 28% | 28% |

The maximum in vivo strain from Table 5 was then used to find the maximum displacement on the graph and the lateral drift ratios were calculated. The following Table 8 displays the calculations of the results.

Table 8: Lateral Drift Ratios of Spinal Ligaments

| | Length (in) | Maximum in vivo Strain | Deflection at Maximum In Vivo Strain (in/in) | Lateral Drift Ratio |
|---|---|---|---|---|
| ALL | 7.19 | 13% | 0.95 | 0.10 |
| PLL | 6.38 | 13% | 0.88 | 0.09 |
| LF | 6.38 | 15% | 0.97 | 0.11 |
| ISL | 7.09 | 28% | 2.00 | 0.22 |
| SSL | 7.19 | 31% | 2.24 | 0.24 |

# Chapter 4 Literature Review

## 4.1 Rocking Systems

Roke, et al. (2009) describe a method to design steel self-centering concentrically braced frames (SC-CBF) and validate their method. The authors describe how post tensioned (PT) strands of cable can be used and designed to bring a building back to center after a seismic event. The paper begins by describing the system behavior of SC-CBFs. The gravity loads and PT strands resist column uplift and provide a restoring force while the beams, columns and braces remain elastic (19). The authors then go on to describe how to design the system and their analysis procedure. Overall the authors show that the design procedure creates SC-CBF systems that behave as expected when exposed to seismic forces. This paper was used to gain an understanding of how self-centering systems worked and review possible test to perform on a lateral force resisting system to verify its success.

Sause, et al. (2006) investigated the responses of self-centering seismic-resistant steel concentrically-braced frames (SC-CBF) when subjected to earthquake loading. In order to do this the authors conducted pushover and dynamic analyses on a prototype frame design. In the article, the authors describe the typical behavior of a SC-CBF system, a prototype building, the SC-CBF design process, and the pushover and seismic response of the system. The authors' work concluded that the designed SC-CBF system behaved as expected when subjected to both the pushover and dynamic analyses. The work also produced identified several limit states of the system including PT yielding and decompression. Overall this paper offered insight into applicable design procedures of a SC-CBF, potential limit states, expected results and possible tests to further verify the effectiveness of the system.

Wiebe et al. (2011) explored steel rocking frame designs that mitigate the amplification effects experienced by a frame in the higher modes. The authors utilized two techniques to mitigate higher mode effects on the system. The first

technique involved using an energy dissipation device at the first-story level of the building to control base shear. The second technique consisted of adding a rocking joint between the fourth and fifth stories of the building to control the moment near the mid-height of the building. The paper also described the laboratory setup, utilized ground motions, and test results. Overall, the authors work showed that while the techniques used were effective in limiting peak forces experienced by the building, the interstory drift did increase. It also showed that the energy dissipation device was more effective than the rocking joint at reducing shear forces. This paper provided some examples of effective spine-like concepts that have been utilized in previous self-centering rocking frame systems.

Eatherton, et al. (2014) describe the characteristics, design concepts, limit states, and design methods for controlling limit states for controlled rocking systems. The article begins by describing the importance of developing systems that can control the location of inelastic deformations and contain elements that can keep the building plumb. The system described in the article consists of three elements including a braced steel frame, vertical post-tensioning, and an energy dissipation device. These components work together to prevent major structural damage and residual drift a building experiences during a seismic event. Each of these elements are described in detail including potential failures. Through this process, the authors identify equations that can be used to predict the limiting strain for the PT strands, required minimum energy dissipation, global uplift and self-centering force required. The authors also identify equations to describe the behavior of the frame including the system yield moment, uplift moment, yield strength and uplift stiffness. Overall, this article provided valuable equations to be used for the design and validation processes of the spine-inspired self-centering frame. It also provided some inspiration when creating system designs in Chapter 5 of this paper.

Priestley, et al. (2000) tested a five-story precast building under seismic loading conditions. From these tests, they were able to obtain results from five different precast structural systems. This was done by constructing two different types of precast frames. The first precast frame used pre-stressed precast concrete

beams to provide lateral resistance on opposing sides of the building in one response direction and a structural wall to do the same in the other direction. The second precast frame used mild steel across the beam to column connections and a structural wall to accomplish the same feet, respectively. Four different types of connections were used throughout the building. A hybrid connection was used on the lower three floors of the pre-stressed frame. These connections consisted of single bay beams connected between continuous columns by unbonded post-tensioning.

A pre-tensioned frame connection was used on the upper two floors of pre-stressed frame. In this connection continuous precast beams with pre-tensioned strands were bonded in external stub beams and debonded on the interior beam portion that spanned between the column faces that provided seismic resistance. A tension/compression gap yielding connection was used in the lower three floors of the non-prestressed frame. In these connections, beams were clamped to columns by unbonded post-tensioning thread bars engrained in fiber grout pads at the bottom of the connections. In the top two floors of the non-pre-stressed frame, a tension/compression yielding frame connection was used. In this connection, mild steel rebar was placed in grout ducts at the bottom and top of the connection. Lastly, a U-shaped flexure plates welded to embed plates in the wall panels were used in the orthogonal direction to connect four precast panels. The plates were used to provide energy dissipation and lateral resistance through shear coupling between two walls. Through testing of the building the authors used the obtained results to validate the displacement-based design approach of the precast walls. Overall this paper provided insight into concepts that could be used to create concrete rocking systems.

Overall the literature review showed that there are several structural systems that have already developed spine-like qualities. The SC-CBF system design procedure, created in the paper by Roke, et al. (2009), used post tensioned steel cables to apply a self-centering effect to structural systems. These PT cables act like the ligaments that span of the spin. In the paper by Sause, et al. (2006) the authors investigated the effects of using SC-CBF systems in a building subjected to

earthquake loading using pushover and dynamic analysis. Wiebe et al. (2011) explored the idea of using rocking joints to control the moment at the mid-height of a rocking system. This idea is similar to that of creating a segmented rocking system. Eatherton, et al. (2014) looked at design methods and concepts for controlled rocking systems, including self-centering mechanisms. Different configurations of rebar in pre-cast beam to column connections were examined in a paper by Priestley, et al. (2000), providing examples of the design process for concrete rocking systems.

# Chapter 5 System Ideas

## 5.1 System Idea General Parameters

The creation of new lateral force-resisting system concepts began by creating a list of objectives. Each design attempted to address multiple issues on the list. The objectives for the systems were as follows:

1. The components of the system must be capable of transferring shear from one floor to the next.
2. The system should be axially fixed. This means that the system will need to contain a continuous and relatively stiff load path that can transfer vertical loads throughout the system.
3. The system must contain components that limit the amount of deformation in the system. This is especially important between floors where the system would be free to deform.
4. The system must contain spaces on each floor that can be designated as definitive building spaces.
5. The system must have vertebrae like elements that are self-contained and shop fabricated. Making assembly of the system simpler, faster, and providing definitive building space.
6. The system must provide a method of lateral load resistance.
7. The system must provide a way to resist overturning moment.

Through the design creation process, these requirements evolved. Each system consisted of six stacked frames or six levels in total. These frames acted as the vertebrae and provided building space. Several different concepts were explored during the creation process including a mock nucleus design, using pre-tensioned strands for self-centering, dampers, viscoelastic material, spherical surfaces, springs, rubber isolaters, and woven mesh fabric limiters. In order to simplify the creation of models in SAP2000, each of the stacked frame lateral force resisting system designs was placed into one of three categories labeled general approach one, two and three.

## 5.2 General Approach 1

The first category, referred to here as general approach one, allowed for rotation at the vertical intersection of two frames (between floors), vertical loads to be carried through a central column, energy dissipation through axial deformation at the frame edges during frame rotation and the pre-tensioned cables at the edges acted as ligaments (limiting displacement) and self-centering. The following Figures show some of the system design sketches. The system shown in Figure 22 consists of 3-Dimensional steel frames or “steel cages” supported on 3-Dimensional concave surfaces with viscoelastic material filling in the empty space between frames. The concave surface in this system allows the frame to freely revolve around the concave surface. The viscoelastic material provides the frame with a buffer or energy-dissipating element that prevents the frame from gaining too much momentum as it revolves around the concave surface. On the bottom of each frame is a solid steel plate. These plates are pinned to the concave surface, creating a central pivot point for each frame.

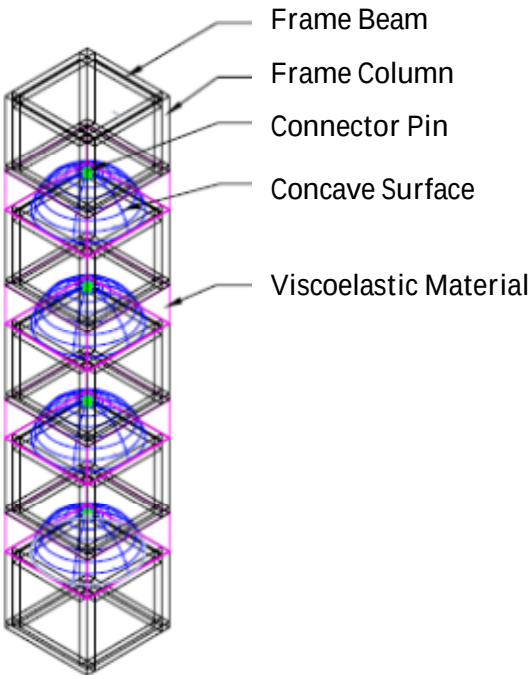


Figure 22: 3-D Design 1- Intevertebral Disks as Concave Surface with Viscoelastic Material as Energy Dissipation

The system in Figure 23 consists of 3-D steel frames supported by solid spheres in between each frame. The remaining space between each frame is filled with an energy dissipating material shown in purple. The cylindrical elements in green represent post-tensioned cables that connect each frame in the system. The light blue rectangular elements are plates that connect the post-tensioned cables to each frame. The idea behind this system is that the frames can rotate about the spherical surfaces and the post-tensioned cables will limit their displacement. The energy dissipating materials helps decrease the displacement as well as dissipates some energy.

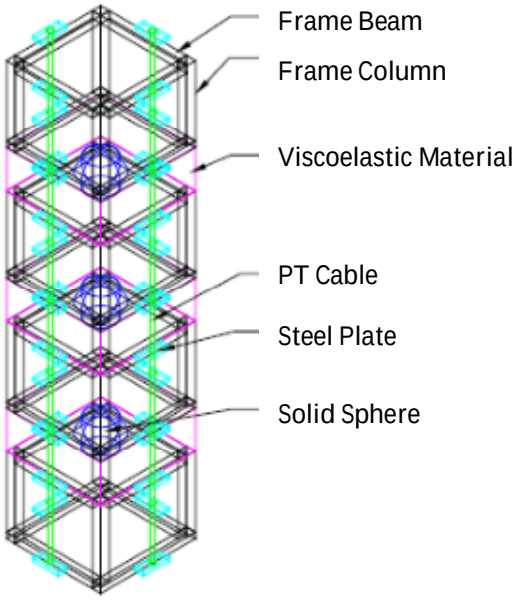


Figure 23: 3-D Design 2- Self Centering Frame System with Viscoelastic Energy Dissipation and Spherical Pivot Surface

The system shown in Figure 24 consists of a 3-dimensional steel frames that rests upon an intervertebral disc inspired support system. The support system consists of a round bar in the center used to provide the frame with additional support. The round bar is connected to the frame above and below it using a ball and socket type or pin connection. This allows the frame to rotate around the bar at that the point. A block of energy dissipating or bumper like material surrounds the bar. This material is meant to prevent excess movement and dissipate energy. Two

separate metal boxes that are connected to either the frame above or the frame below the material then surround the block of energy dissipating material. The purpose of these boxes is to limit the amount of displacement that occurs between floors.

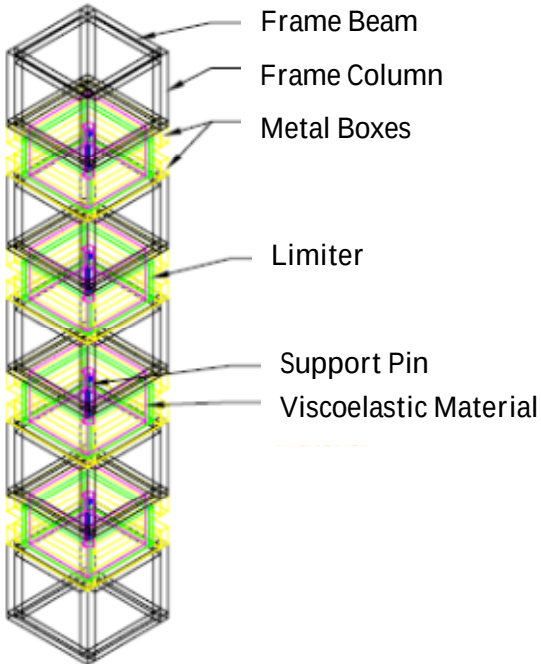


Figure 24: 3-D Design 3- Ball and Socket Intervertebral Disk with Viscoelastic Energy Dissipation and Deflection Limitors

The 2-dimensional system shown in Figure 25 is designed to be located within the walls of a building. It consists of steel plate shear walls secured inside steel frames. Each frame is designed to interlock with the frame above and below it using a ball and socket like concave surface, leaving a gap between each floor. This is done to allow the frame to rotate around the central point of the concave surface. Each frame is connected with post-tensioned strands that continuously run from the top to the bottom of the system. These post-tensioned strands are meant to limit displacement and provide a restorative force after initial displacement of the system.

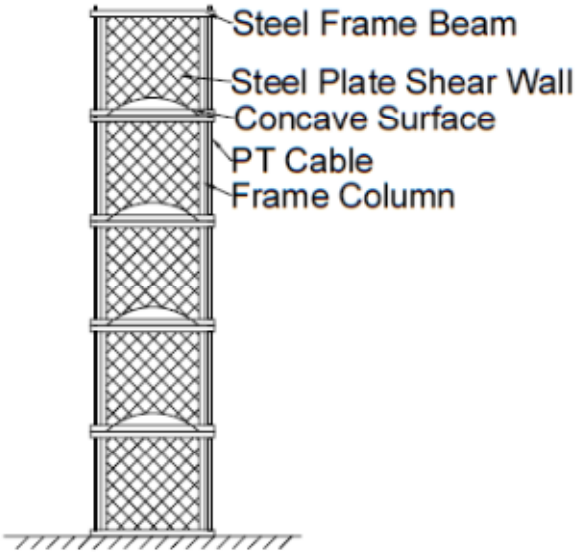


Figure 25: 2-D Design 1 - Concave Rocking Surface with PT Self-Centering

The 2-dimensional system shown in Figure 26 is designed to be located within the walls of a building. The system consists of a two-beam two-column steel frame that is braced by damping apparatuses. The frames sit upon intervertebral disc inspired elements. Each disc inspired section consists of a vertical support column surrounded by an energy dissipating material. The material is shaped has an oval-like shape to encourage the frame to move along the outer perimeter of the material around the support column. Steel plates to further encourage the displacement pattern described above surround the energy dissipating material.

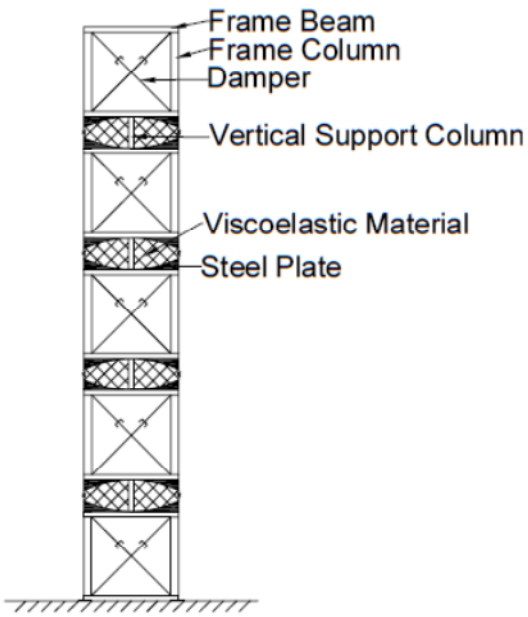


Figure 26: 2-D Design 2- Intervertebral Disk Shaped Viscoelastic Material with Dampers and Vertical Support Columns

### 5.3 General Approach 2

The second category, referred to as general approach two, consisted of lateral force resisting systems comprised of pulleys and cables. These elements were intended to limit the systems deflection, bring the system back to center and dissipate energy. Though there were many designs that fell into this category it was ultimately decided that this approach would not be used. This was due to its' difficulty to model, variation in system designs and the complication of the systems.

## 5.4 General Approach 3

The third category, referred to here as general approach three, was comprised of lateral force resisting systems that controlled the deformation mode of system. These modes ranged from forcing the system into shear deformation or elastic deformation to using concept taken from the gimble, Philon's inkpot and other mechanisms. The gimbal and stroke mechanism are shown below in Figures 27 and 28. As with general approach 2, this approach was also not used due to its' difficulty to model, variation in system designs and the complication of the systems.

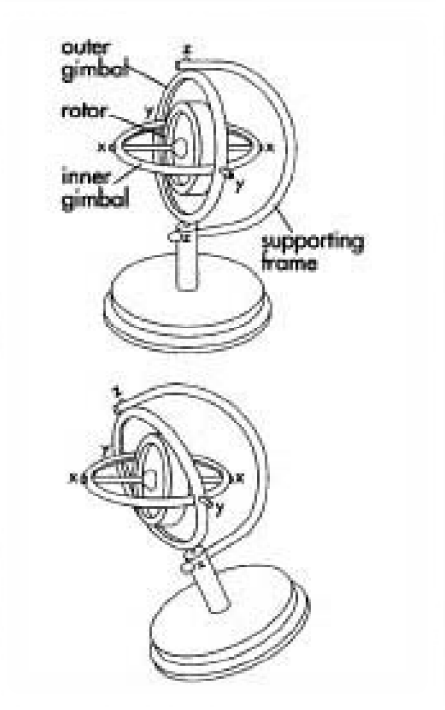


Figure 27: Gimbal, Holmes, G. (n.d.). How Products Are Made. Retrieved January 16, 2015, from http://www.madehow.com/Volume-6/Gyroscope.html, Used under fair use, 2015.

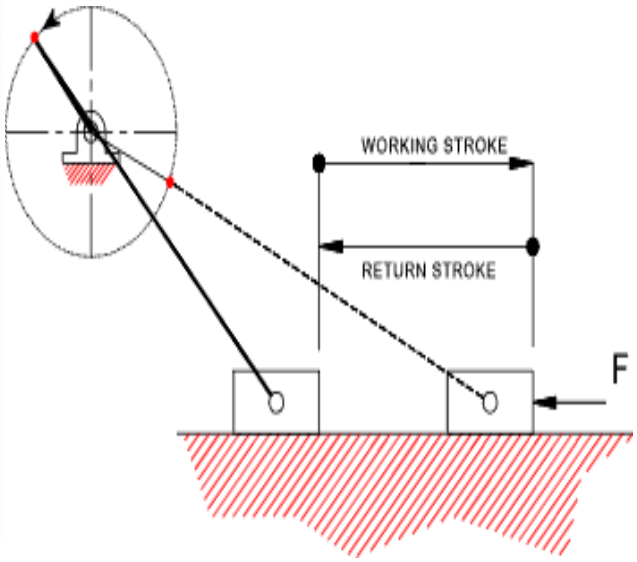


Figure 28: Stroke Mechanism, Beardmore, R. (2013, January 23). Reciprocating Mechanisms. Retrieved January 16, 2015, from http://roymechx.co.uk/Useful_Tables/Cams_Springs/Reciprocating.html, Used under fair use, 2015.

## 5.5 Simplified Model of General Approach 1

As stated in sections 5.4 and 5.4 upon further inspection it was decided that only general approach one would be modeled in SAP2000 (Berkeley 2007). This was in part due to the simplicity of modeling the approach as well as the fact that most of the system designs fell within this category. Each of the designs under General Approach 1 could be simplified into one generic 2-D model in SAP2000 since each system implemented the same principles. These concepts included a centralized pivot point for each frame, damping material, pre-tensioned cables for self-centering and coupling devices. This model can be seen in Figure 29 below.

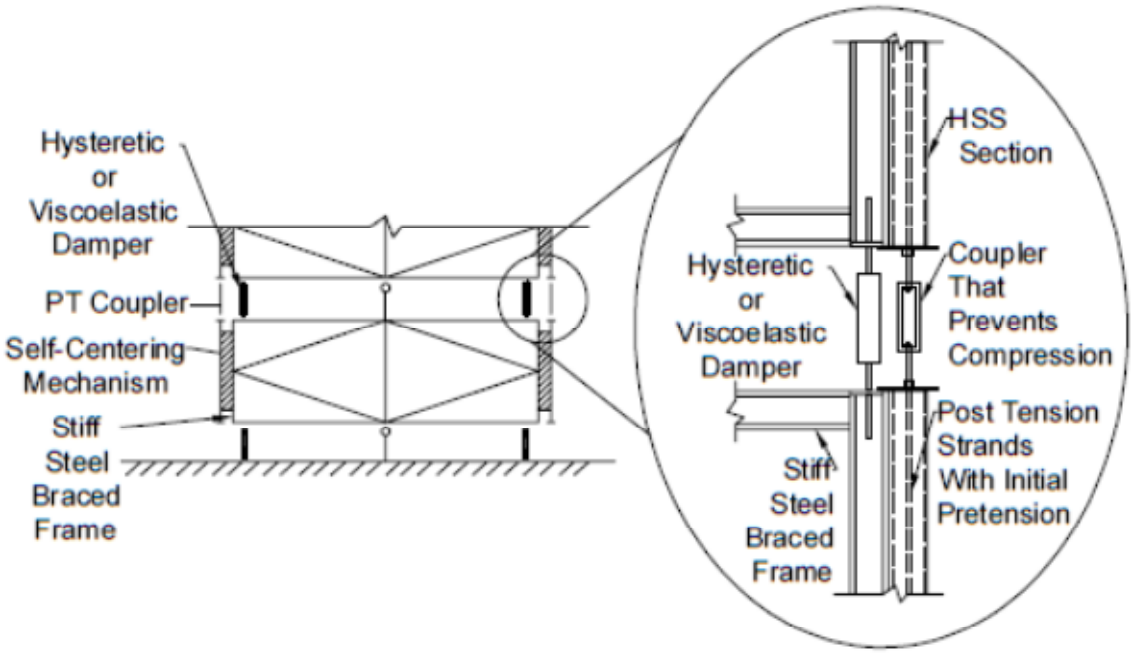


Figure 29: Simplified Model of General Approach 1

# Chapter 6 Lateral Force Resisting System Model

## 6.1 Prototype Building Layout

To evaluate the proposed lateral force resisting system, a prototype building layout, design loads and frame locations were developed. The test building layout and design loads were taken from the 2012 International Building Code Volume 4 Examples for Steel Framed Buildings (SEAOC 2012) and are shown in Figures 30, Figure 31 and Table 9 respectively. The prototype building consists of a three by four bay core with a two bay protrusion on each side. The 150' by 120' office building has a total of six 12' stories.

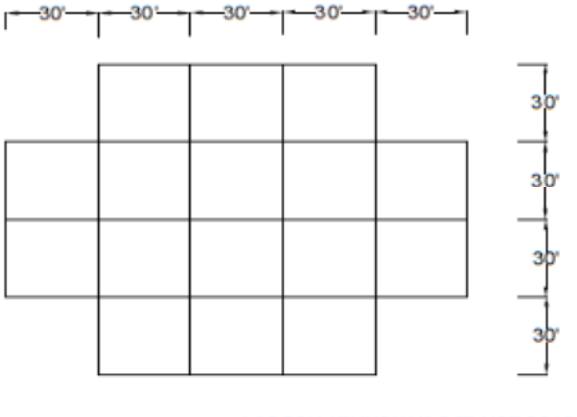


Figure 30: Plan View of Prototype Building

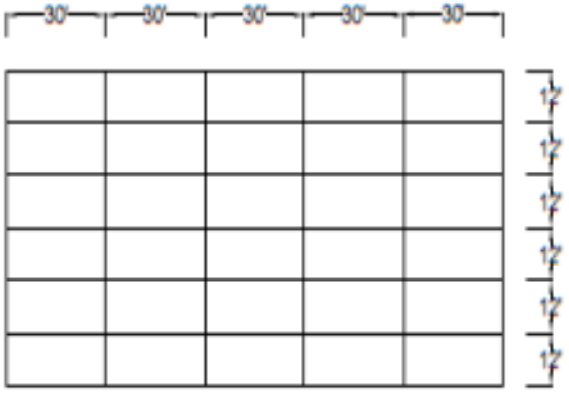


Figure 31: Elevation View of Prototype Building

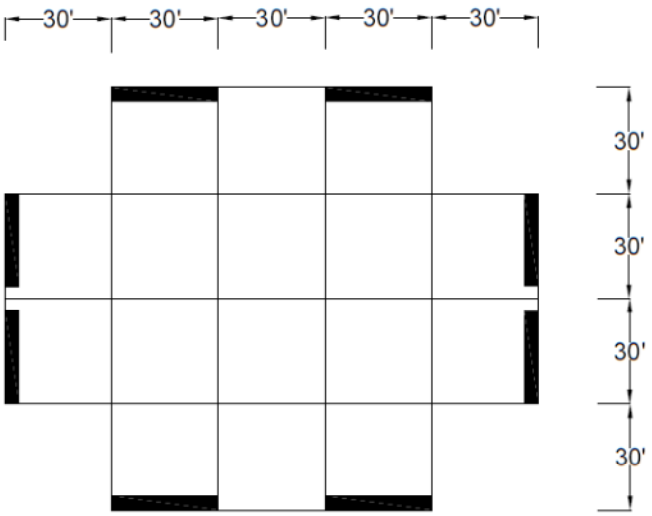


Figure 32: Plan View Frame Locations

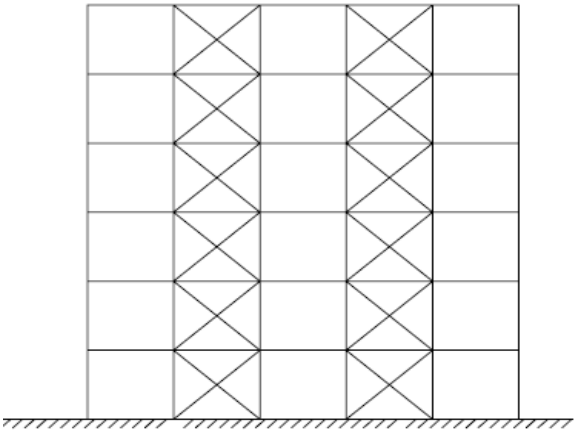

Figure 33: Elevation View of Frame Location

The following loads were applied to the building as per the design example in the IBC.

Table 9: Typical Floor and Roof Loads For Prototype Building

| Typical Floor Loads | | |
|---|---|---|
| Dead Loads | Gravity Load (psf) | Effective Seismic Weight (psf) |
| Floor Finish | 5 | 5 |
| 2 in, 18-ga deck | 2.7 | 2.7 |
| 3 1/4" lightweight concrete fill | 39 | 39 |
| steel framing | 10 | 10 |
| mechanical/plumbing/electrical | 4 | 4 |
| ceiling | 4 | 4 |
| partitions | LL | 10 |
| micellaneous | 3 | 3 |
| Total Dead Load | 67.7 | 77.7 |
| Live Loads | | Live Load (psf) |
| Lobbies and stairs | | 100 |
| Office | | 65 |
| Corridors above 1st Floor | | 80 |
| Total Live Load | | 245 |
| Roof | | |
| Dead Loads | Gravity Load (psf) | Effective Seismic Weight (psf) |
| Built Up Roof | 6 | 6 |
| Insulation | 2 | 2 |
| Metal Roof Deck | 4 | 4 |
| Steel Framing | 8 | 8 |
| Mechanical/Plumbing/Electrical | 4 | 4 |
| Ceiling | 4 | 4 |
| Partitions | 0 | 5 |
| Miscellaneous | 3 | 3 |
| Total Dead Load | 31 | 36 |
| | | |
| Live Loads | | Live Load (psf) |
| Ordinary Flat Roof | | 20 |
| Total Live Load | | 20 |
| Exterior Wall | | |
| Dead Loads | Gravity Loads (psf) | Effective Seismic Weight (psf) |
| Cladding | 7 | 7 |
| Metal Studs | 2 | 2 |
| Insulation | 2 | 2 |
| 5/8 in gypsum board | 3 | 3 |
| miscellaneous | 5 | 5 |
| Total Dead Load | 19 | 19 |

Table 10 shows the weight, seismic weight and mass for the roof and floors.

Table 10: Floor and Roof Weights and Mass

| Floor | Weight (k) | Mass (k-s²/in) | Seismic Weight (k) |
|---|---|---|---|
| Roof | 580 | 3.4 | 656 |
| Typical Floor | 1163 | 1.7 | 1315 |

Table 11 and Table 12 display the assumptions made about the site location, building type, soil type and other parameters necessary for calculating the story shear resisted by each individual frame in the lateral load resisting system.

Table 11: General Information

| | |
|---|---|
| Location | California |
| Site Class | D |
| Occupancy | Office Occupancy on all Floors |
| # of Lateral-Force Resisting Systems in Each Direction | 4 |

Table 12: Seismic Design Category

| | |
|---|---|
| Risk Category | II |
| Importance Factor | 1.0 |
| Short Period Seismic Design Category ($S_{DS}$ = 1.0g) | D |
| 1-Sec Seismic Design Category ($S_{D1}$ =0.6g) | D |

The equivalent lateral force (ELF) method was used to calculate the lateral forces applied at each floor that were used in the design of the lateral force resisting system. Table 13 shows the assumptions made while conducting the ELF method.

Table 13:Design Base Shear Assumptions and Variables

| | |
|---|---|
| R | 8 |
| $W_o$ | 2.5 |
| $C_d$ | 5 |
| $C_s$ | 0.101 |
| Total Base Shear (V) | 730 k |

These lateral forces can be seen in Table 14.

Table 14: Vertical Distribution of Shear by Floor

| Floor | Floor Height (ft) | $F_x$ (kip) |
|---|---|---|
| Roof | 72 | 128 |
| 6th | 60 | 210 |
| 5th | 48 | 164 |
| 4th | 36 | 118 |
| 3rd | 24 | 75 |
| 2nd | 12 | 35 |

## 6.2 Lateral Force Resisting System

### 6.2.1 System Layout

The lateral force resisting system consists of spine inspired segmented frames in four bays in both the N-W and E-S directions of the building. The frames are designed to be two-dimensional systems located in the walls of the building. The intent of the stacked frames is to work together to create a highly flexible region in the structure that allows large displacements and has the capability to bring the structural system back to its' original position after the system experiences drifts dye to seismic forces. The systems are placed in a total of eight locations in the building layout. The location of the systems can be seen in Figures 32 and 33 in Section 6.1. An elevation view of the stacked frames can be seen below in Figure 34.

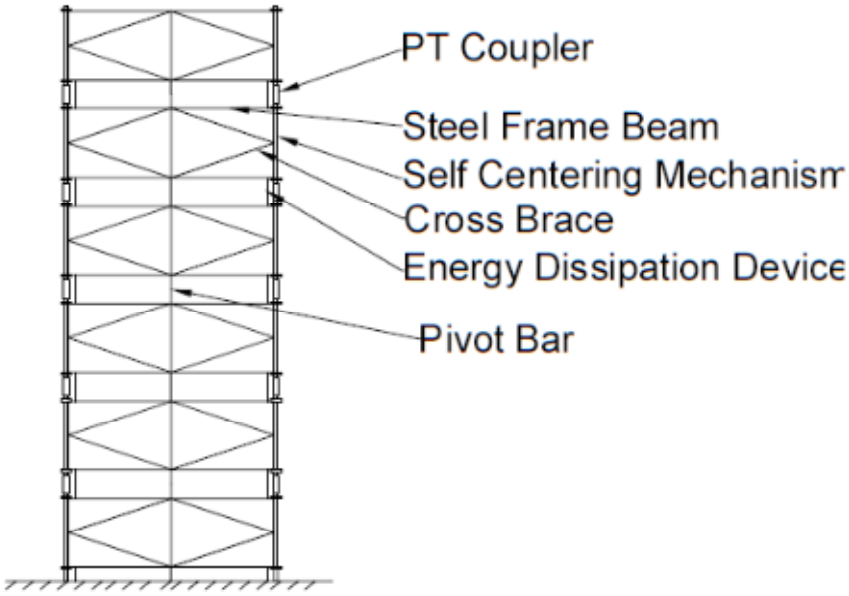


Figure 34: Stacked Frame Elements

Each individual stacked component consists of a steel frame, energy dissipaters, self-centering mechanisms, a pivot point, a support column, and cross braces. The location of these components is shown in Figure 29. The steel frame provides the system with the capability to transfer loads from one frame to the next and to support some inherent gravity loads. The energy dissipators are located at the bottom corners. The energy dissipators, as the name suggest, dissipates some of the energy created when the applied seismic forces cause the system to displace. These energy dissipaters can be represented by many things including viscoelastic material, dampers, etc. The self-centering mechanism was designed to work in pairs to bring each individual frame back to center after being displaced by lateral seismic forces. These mechanisms consist of a hollow steel tube with plates on each end. A post-tensioned (PT) strand is used to connect each plate through the tube. This

creates an element that can expand on either side, limits the displacement of the system, provides some resistance when the tensioning in the PT isn't exceeded by the applied force, and brings itself back to its' original position when the force is removed. Each of these devices will be connected to each other using a coupler device which carries no tension under normal loading conditions and does not support compression loads. A detailed drawing of the self-centering mechanism is shown in Figure 35 and 36.

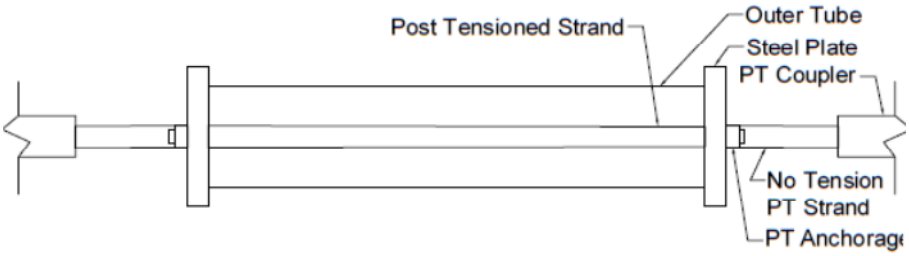


Figure 35: Self-Centering Mechanism without Gap Opening

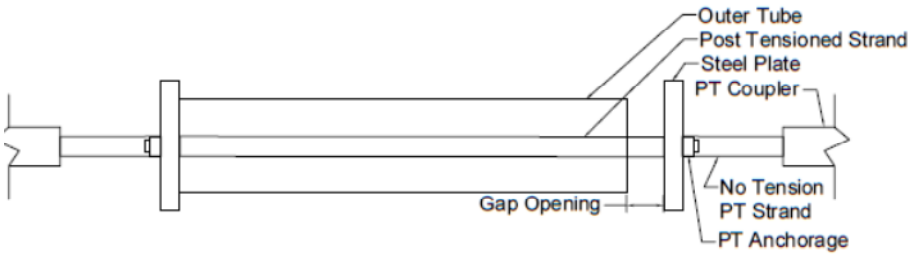


Figure 36: Self-Centering Mechanism with Gap Opening

The pivot point and support column is used to represent a member that provides the individual frame with a point around which it can pivot, allowing for displacement in multiple directions. This pivot point could take the form of a ball and socket type connection, a spherical surface, or pin connection. The support column, which has a pivot point at the top, supports the gravity loads of the system

and helps transfer shear between frames. Lastly the cross braces transfer shear forces in frame.

### 6.2.2 Preliminary Member Design

All of the frames were designed for the worst-case level, which took place in the bottom frame. The columns and beams of the steel frame were sized to withstand an axial force, P, due to Fx and story shear, V calculated using equations 6 and 7. Then cross braces were designed to carry a portion of the story shear. The support column was designed for a total axial load, P, resulting in a very stout member. The variable P, was divided by four to account for four lateral force resisting systems in both the x and y direction.

$$P = \frac{\sum F_i * H_i}{L} \qquad \text{(Equation 6)}$$

where,

$F_i$ = force applied at floor due to seismic load

$H_i$ = height to floor from base of system

L = length of moment arm

$$V = \frac{R_o}{R_N} * V_o \qquad \text{(Equation 7)}$$

where,

$V_o$ = Original Story Shear at Base of Structure (Taken from IBC design example 2)

$R_o$ = Original Redundancy Factor (Taken from IBC design example 2)

$R_N$ = New Redundancy Factor (adjusted per researchers discretion)

The redundancy factor used in the IBC design example was selected due to the system type (Special concentrically braced frame and special moment frame) and number of lateral force resisting frames in the building. This was altered due to the decrease in the amount of systems used and the variation of system type. The resulting story shear, V, was calculated to be 160 kips, when $R_0$ was 6, $R_N$ was 8 and $V_0$ was 213 kips. The resulting axial load of 602 kips was used to find the area and

amount of pre-tensioning in the PT strands. The area of the pt strands was calculated using the following equation:

$$A_{pt} = \frac{1}{2}\left[\frac{P}{0.5*Fu}\right] \quad \text{(Equation 8)}$$

where,

$A_{pt}$= area of PT Strand

P = Total Force for Lateral Force Resisting System Applied to System

Fu= Ultimate Strength of PT Strand

In equation 8 the factor of 1/2 comes from assuming that half of the overturning moment is resisted by post-tensioning and the rest is resisted by a hysteretic damper. The 0.5 factor, applied to the $F_u$ term, assumes that the PT strands were stressed to 50% of ultimate stress. The area of the PT strands was determined to be 2.23 $in^2$, when $F_u$ was assumed to be 270 ksi. Using this calculated area, the force in the PT strands was calculated using the following equation:

$$F_{PT} = 0.5 * Fu * A_{PT} \quad \text{(Equation 9)}$$

The resulting $F_{pt}$ was 301 kips. This force is the amount of tensioning needed in each PT cable to resist overturning moment.

### 6.2.3 Energy Dissipation Devices

There are two types of internal damping used in the lateral force resisting system; hysteretic and viscoelastic. Hysteretic damping is described by the characteristic that the stress-strain curve of the material forms a hysteretic loop, shown in Figure 37 below. Hysteretic damping is achieved through the yielding of material (i.e. low strength or high strength steel). This form of damping is independent of frequency.

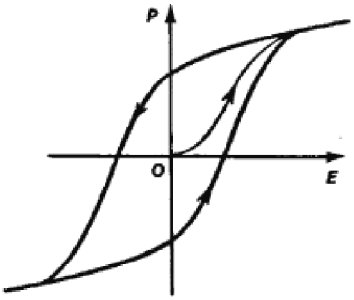


Figure 37: Hysteretic Loop of Hysteretic Damper

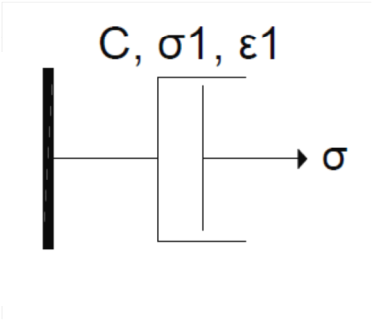


Figure 38: Schematic of Hysteretic Damper

The yield strength of the hysteretic dampers was derived from the yield strength needed to resist the applied design lateral loads shown in Table 14. This was done by assuming an amount of lateral load force that would be accommodated by the PT and the hysteretic dampers. It was assumed that the PT would accommodate one half of the lateral load force and the hysteretic dampers would accommodate the remaining half. Then the area of the hysteretic damper was calculated by dividing the yield strength by an assumed typical yield stress of 36 ksi. Lastly, the stiffness was calculated using the following equation:

$$k = \frac{A*E}{L} \qquad \text{(Equation 10)}$$

where,

k = stiffness (k/in)

L = length of hysteretic damper (in)

A = Area of hysteretic damper ($in^2$)

E = Modulus of Elasticity (210 Gpa or 30457 ksi)

The yielding exponent controls the sharpness of the transition from the inital stiffness of the hysteretic damper to the yielded stiffness. The post yield stiffness ratio is the post-yielded stiffness divided by the initial stiffness.

Table 15: Hysteretic Damper Properties

| | |
|---|---|
| Stiffness (k/in) | 10571 |
| Yield Strength (kip) | 300 |
| Post Yield Stiffness Ratio | 0 |
| Yielding Exponent | 2 |

Viscoelastic describes a set of materials whose force-displacement (or stress-strain) has either viscous or viscoelastic properties, meaning the materials have both a damping component and a stiffness component. The modulus of elasticity of these materials contains both a stored and dissipative energy component. Therefore the stiffness and damping properties are a function of both temperature and frequency. There are many different mathematical models that are used to represent viscoelastic damping. For the purpose of this paper viscoelastic material will be modeled using the Kelvin model. This model is shown below in Figure 39.

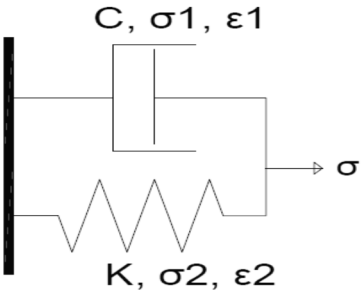


Figure 39: Kelvin Model of Viscoelastic Damper

The properties of both the damper and spring elements of the viscoelastic material are shown in the Table 14 below. The properties of the viscoelastic material were based on numerical values from a paper by Lyan-Ywan Lu, et al. (2011) and were compared to values obtained is a paper by Costi, et al. (2002).

Table16: Viscoelastic Damper Properties

| Damper | | Spring | |
|---|---|---|---|
| Stiffness (k/in) | 1000 | Stiffness (k/in) | 5.71 |
| Damping Coefficient | 0.57 | Damping Value | 0 |
| Damping Exponent | 1 | | |

### 6.2.4 System Configurations

Two different system configuration models of the lateral force resisting system were created in Sap2000. Both models attempted to capture the behavior of the self-centering mechanisms in two different ways. The first configuration, shown below in Figures 40 and 41, used a system of alternating tensioned and non-tensioned steel cables in conjunction with compression and tension only springs to mimic the behavior of the self-centering mechanisms. The goal of this configuration was to create a build-up of tension in the non-tensioned cable elements until gap openings occurred along the height of the stacked frame system.

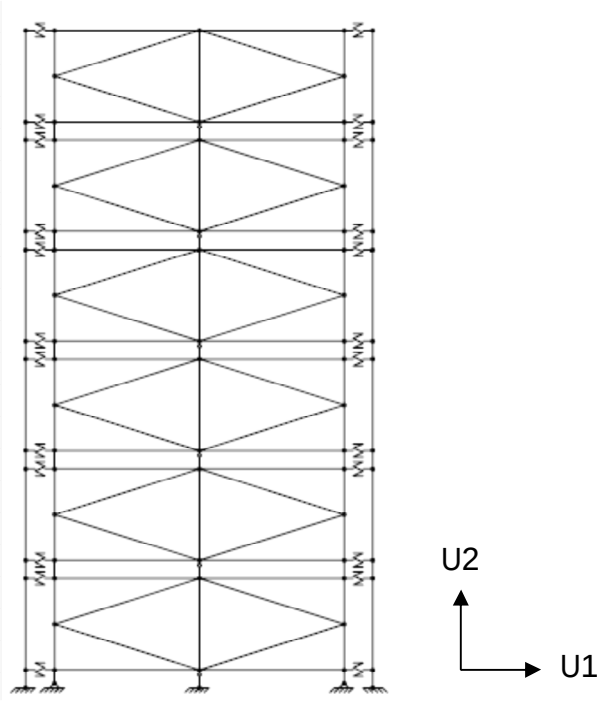


Figure 40: Stacked Frame System Configuration 1 in SAP2000

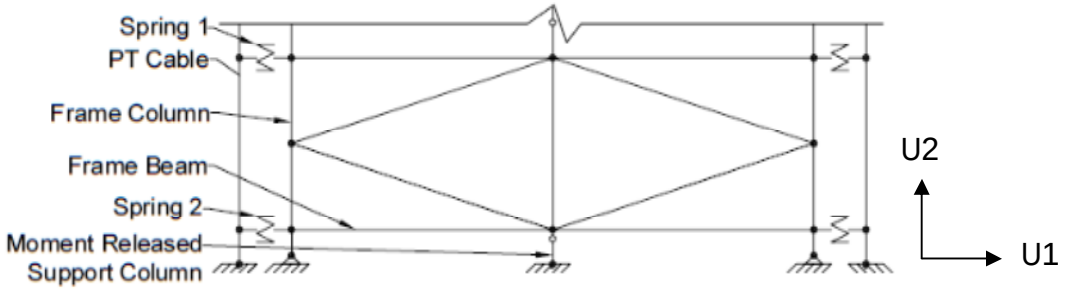


Figure 41: Isolated Floor of Stacked Frame System Configuration 1 in SAP2000

The second configuration, shown in Figures 42 and 43, utilized continuous pre-tensioned steel cables, which ran from the top to the bottom of the system, and compression only gap opening elements.

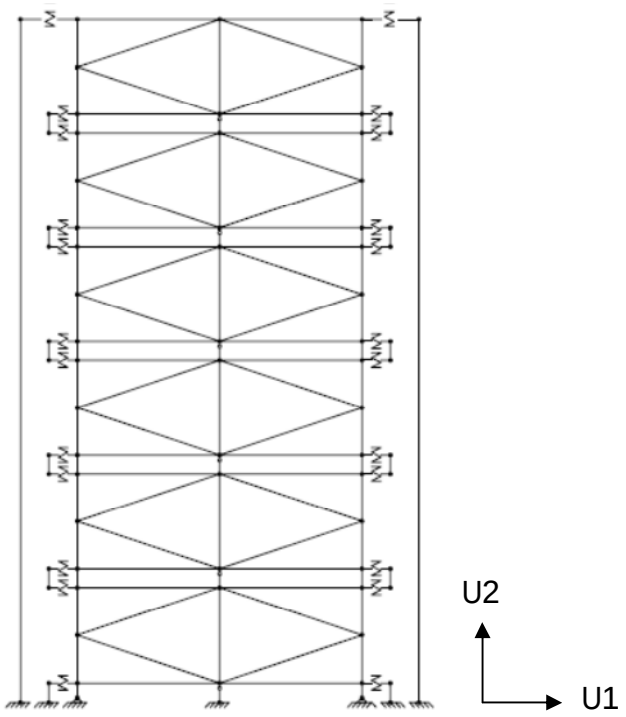


Figure 42: Stacked Frame System Configuration 2 in SAP2000

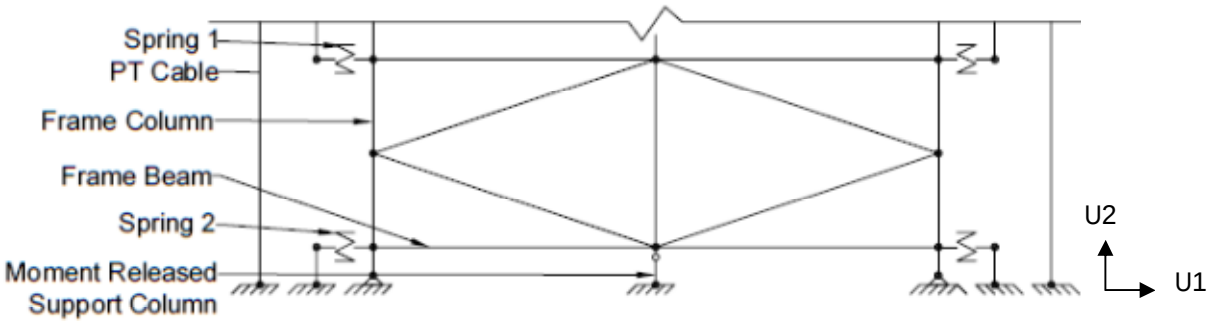


Figure 43:Isolated Floor of Stacked Frame System Configuration 2 in SAP2000

The gap opening components of this configuration consisted of non-tensioned steel cables, which were connected to the frame by a spring that allowed compression only in the Vertical or U2 direction on one end and fixed to the adjacent frame at the other end. The goal of this configuration was to reduce the amount of axial force experienced by the PT strands when gaps began to open in the stacked frame system. Both system configurations had identical frame and energy dissipater layouts. The configuration of the steel cables and springs were the only components that varied between configurations.

### 6.2.5 Member Design in SAP2000

The final member sizes for both models were determined by using the design option in SAP2000. In order to begin this process, each floor of the system was assigned a separate diaphragm restraint along the Z axis. This created a total of six levels (the roof and 2nd-6th floors) that the vertical distribution of shear could be applied to. The vertical distribution of shear, which was taken from example 3 of the IBC, was calculated using the following equation:

$$F_x = C_{vx} * V, \quad \text{where } C_{vx} = w_x h_x^k / \sum w_i h_i^k \qquad \text{(Equation 11)}$$

where,

$F_x$ =portion of the seismic base shear, V, induced at Level x

$C_{VX}$ = vertical distribution factor

$w_x$, $w_i$ = portion of *W* that is located at or assigned to *Level x* or i

$h_x^k$, $h_i^k$ = the height above the base to Level i or x, respectively

The vertical distribution of shear loads were applied to the system using a load pattern whose loads were user defined. The loads were then multiplied by the over strength factor, $\Omega_0$. The calculated design quake load pattern was then ran through a non-linear load case. The same procedure was used to run a non-linear load case, where the utilized load pattern was generated from the 2012 version of the international building codes with an automated process in SAP2000. Four load combinations were defined for the design procedure. The section properties of all members in the system except the steel cables, PT strands and links were assigned an auto-select list. The two load cases were then run using the run analysis function. Once the analysis were complete the design of the frame members could begin.

First the utilized load combinations for the design process were set. Then the design process was initiated. During this process SAP2000 assigns each member a section property from the assigned auto-select list. The design phase repeated until both the analysis and design sections match. Lastly, it was verified that all members passed the stress/capacity checks performed by SAP2000 using the "Verify All Members Passed" function.

## 6.3 Models in SAP2000

### 6.3.1 Model Creation

In both models the steel fame was created using the same process. First the steel frame was created using frame elements. Then cross braces were modeled as frame elements and designed to carry a portion of the story shear. Then the pivot bar was created with a frame member, which had a moment release about the major and minor axis at the start of the member only. This allowed the frame to pivot or rock about a specified location in the model. Next the energy dissipaters were modeled using two joint link elements, which had assigned material properties of various viscoelastic materials. It is important to note that for initial analysis purposes these components were not assigned properties. The self-centering mechanisms had to be broken down into several components including the PT strands and springs.

In model 1, the tube elements were eliminated from the mechanism completely. Instead a tensioned pt strand was connected to the frame cage by two springs. The properties of these springs can be seen in Figure 44. This allowed a connection, which was extremely stiff in tension and flexible in compression, to be placed on the top of the frame and a connection with the opposite capabilities to be placed on the bottom. The springs were also programmed to be very stiff in the horizontal or U1 direction. This prevented excessive lateral displacement from occurring at the connection points. The result was connections that mimicked the behavior of the steel tubes, which allow a limited amount of displacement in both directions.

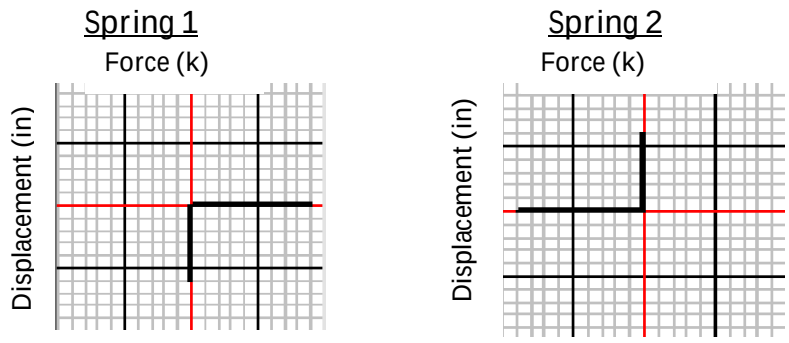


Figure 44: Force-Displacement Properties of Spring

In model 2, the tube elements were eliminated from the mechanism completely. Instead a single pre-tensioned steel cable ran from the top of the system to the ground on each side of the frame. The top of the PT strand was connected to the frame using a tension only spring (Spring 1 from Figure 44). The bottom of the PT strand was fixed to the ground. Non-tensioned steel cables and compression only springs (Spring 2 from Figure 44), represented as frame and link elements, were used to connect adjacent frames. The springs allowed compression only in the U2 direction on one end of the steel cable and an equal constraint was used to fix the other end to the adjacent steel frame. Lastly, in both models, the floor weight and mass supported by each frame were distributed over two and three floor joints, respectively, of each frame in the stacked frame system. Once the two system configurations were modeled in Sap2000 the energy dissipation devices were added.

In order to input a post-tensioning effect into the cables a temperature gradient was utilized. The temperature gradient required to cause the correct tension force in the PT strands was calculated using the following equation:

$$\Delta T = \frac{P}{\alpha * E * A} \qquad \text{(Equation 12)}$$

where,

DT = temperature change

P = Total Force Applied to System

$\alpha$ = temperature coefficient of resistance

E= modulus of Elasticity (ksi)

A = area of pt strand

DT was calculated to be -707 ◦ F. When modeling elements with temperature gradients in SAP2000, DT is likely to change depending on the PT strand's position in the system. This is due to the programs tendency to distribute the forces caused by the temperature gradient into the system. Therefore it is important to adjust the gradient value along the height of the structure to accommodate this to ensure that each PT element has the same amount of tensioning, 300k.

Both hysteretic and viscoelastic dampers were utilized as energy dissipation devices in the systems. Therefore a total of four models were created. These four systems and their characteristics can be seen below in Table 17.

Table 17: System Models

| System Name | System Configuration | Energy Dissipation Device | PT-Force |
|---|---|---|---|
| Segmented PT Strand and Hysteretic Damper | 1 | Hysteretic Damper | 300 kips |
| Segmented PT Strand and Viscoelastic Damper | 1 | Viscoelastic Damper | 300 kips |
| Continuous PT Strand and Hysteretic Damper | 2 | Hysteretic Damper | 300 kips |
| Continuous PT Strand and Viscoelastic Damper | 2 | Viscoelastic Damper | 300 kips |

The hysteretic dampers were modeled using a 2 joint plastic (wen) nonlinear link element. The properties of these dampers can be seen below in Table 16. The viscoelastic dampers were modeled using a nonlinear exponential damper link element and a linear link element in parallel. These two elements represented the damping and stiffness component of the viscoelastic material.

### 6.3.2 Mass and Weight Distribution for System

For the purpose of designing a lateral force resisting system, the forces experienced by a building equate to the mass of the building multiplied by the buildings' acceleration. In this case the acceleration is supplied by inputting the ground motion accelerations for various earthquakes. Therefore, in order to get the correct building response, the building masses and weights must be correct. The individual floor and roof masses in the Y direction where calculated by examining the overall contribution of each frame, laterally, to resisting the applied forces.

According to the tributary area distribution each frame in the lateral force resisting system must accommodate 3,805 $ft^2$ of floor or roof mass and 1,747.5 $ft^2$ of exterior wall cladding when resisting lateral loads. The mass of each floor and the roof was calculated using the following equations:

$$M = \frac{W_F}{a} \quad \text{(Equation 13)}$$

where,

$W_F$ = Weight of Tributary Area of Floor Supported by Frame

a = acceleration due to gravity ($386 \frac{in}{s^2}$)

The mass applied on each level of the stacked frame system in the y direction or direction of ground motion (GM) acceleration was calculated to be 0.852 $\frac{K-sec^2}{in}$ for the 2nd -6th floor and 0.422$\frac{K-sec^2}{in}$ for the roof. This mass was then distributed between three points on each floor frame. Finding the amount of weight accommodated by each stacked frame system was a slightly different procedure.

In order to calculate the weight supported by each floor of the stacked frame system, the tributary area of the frame was utilized with respect to the gravity loads. In these calculations, the weight supported by the stacked frame system on each floor and the roof was 67 kips and 39 kips, respectively. These loads were then distributed, with respect to the tributary area contribution, as point loads acting on the two corners of each frame on each floor.

## 6.4 Model Verification

### 6.4.1 Pushover Analysis

A pushover analysis was used to examine where the self-centering mechanisms would begin to open in both models. First, a descending load pattern, starting at 6 kips, was applied to the system at each floor. The applied load pattern, called "pushover", can be seen below in Figure 45.

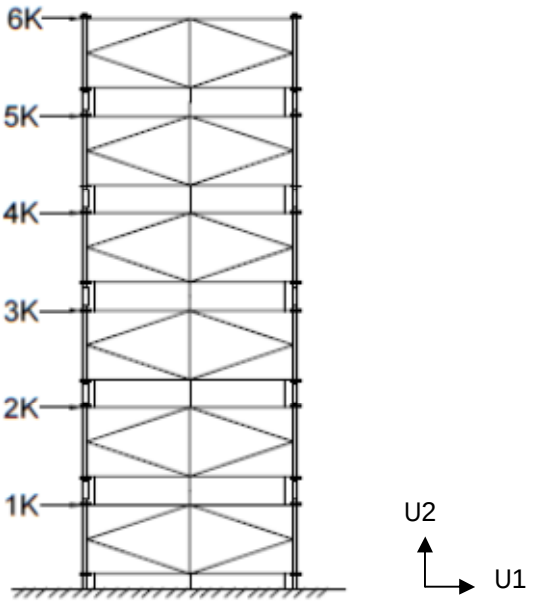


Figure 45: Pushover Analysis Load Pattern

Then a nonlinear static load case was defined where the pushover load pattern was applied. The load case was set to be full load controlled, to save at least 25 steps, and the applied load was scaled up till gap opening was achieved. It is important to note, the point at which the gap opening began to develop changes depending on the applied scale factor. In order to see if gaps were opening in the system the base shear versus the roof displacement in the U1 direction were plotted. When the slope of the resulting line changed is where the gap opening occurred. This value was then compared to a calculated gap opening value. The calculated base shear that would cause gap opening in the pushover analysis was calculated using the following equation:

$$V = \frac{F*L}{\frac{2}{3}h} \qquad \text{(Equation 14)}$$

where,
V = base shear

F = force in the PT strands

L = length of the moment arm (horizontal distance from PT strands to center of frame)

Equation 8 calculates the base shear for a system that has no dampers and assumes an inverted triangular load pattern. The equation is modified when hysteretic dampers are included. The following Table 18 displays where the gap opening should occur for each systems configuration with either hysteretic dampers, viscoelastic dampers or no dampers.

Table18: Gap Opening Occurrence

| System | Calculated PT Force (k) | SAP2000 PT Force (k) | Calculated Base Shear (k) | SAP2000 Model Base Shear (k) |
|---|---|---|---|---|
| Segmented Pt Strands and Hysteretic Damper | 300 | 308 | 283 | 105 |
| Segmented PT Strands and Viscoelastic Dammper | 300 | 307 | 94 | 92 |
| Continuous PT Stand and Hysteretic Damper | 300 | 299 | 283 | 126 |
| Continuous PT Strand and Viscoelastic Damper | 300 | 305 | 94 | 92 |
| Segmented PT w/o dampers | 300 | 301 | 94 | 92 |
| Continous PT w/o dampers | 300 | 302 | 94 | 92 |

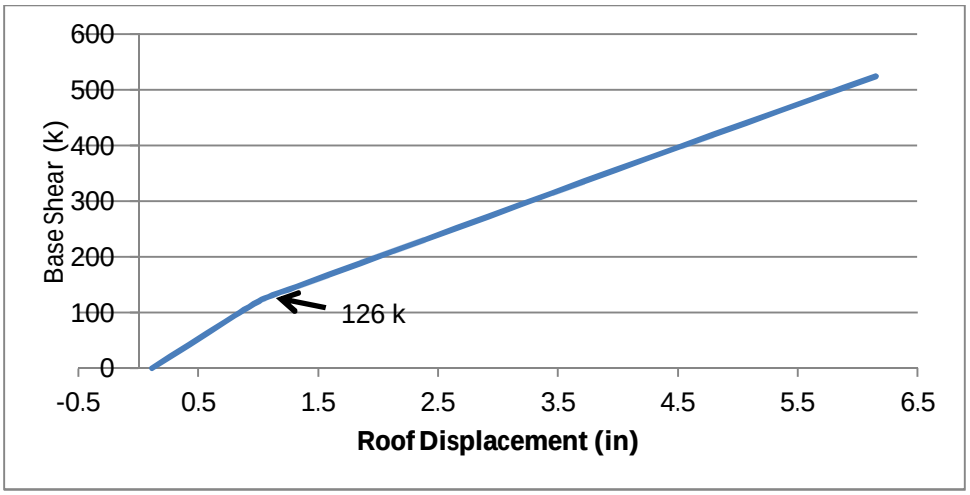


Figure 46: Continuous PT Strands and Hysteretic Damper Pushover Curve

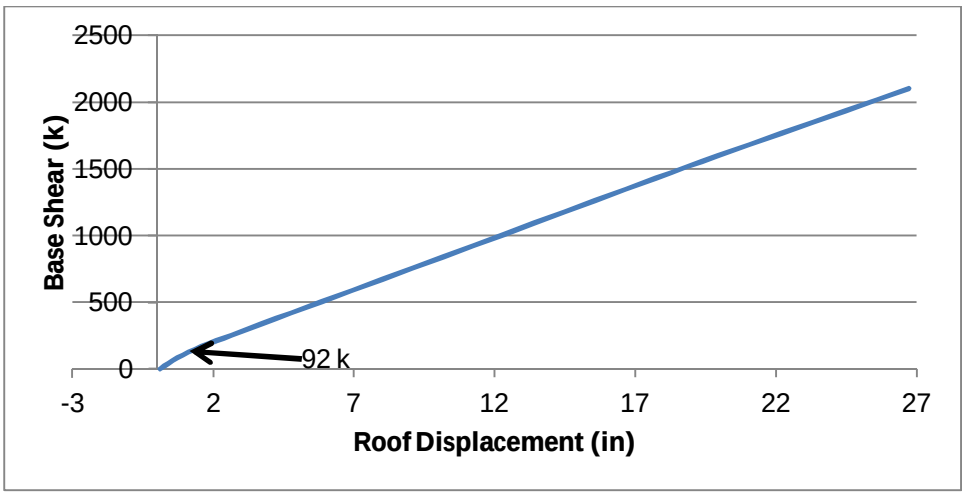


Figure 47: Continuous PT Strand and Viscoelastic Damper Pushover Curve

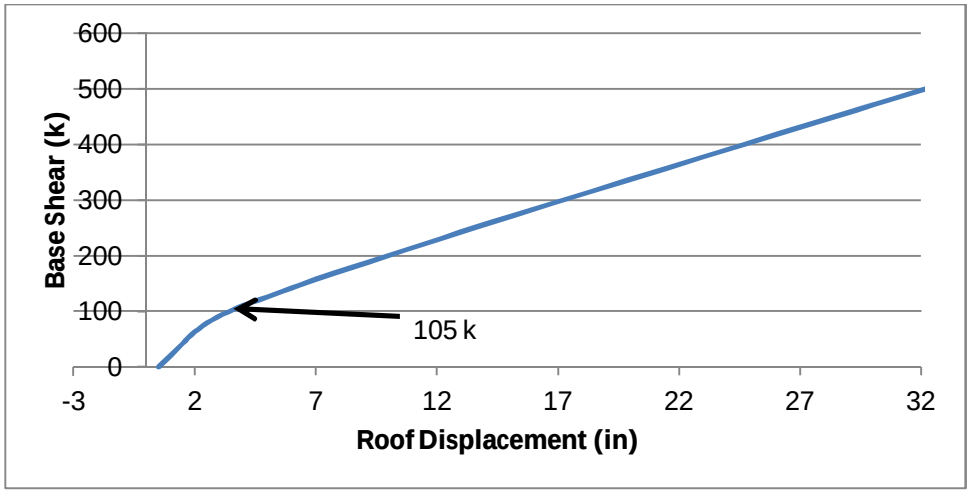


Figure 48: Segmented PT Strand and Hysteretic Damper Pushover Curve

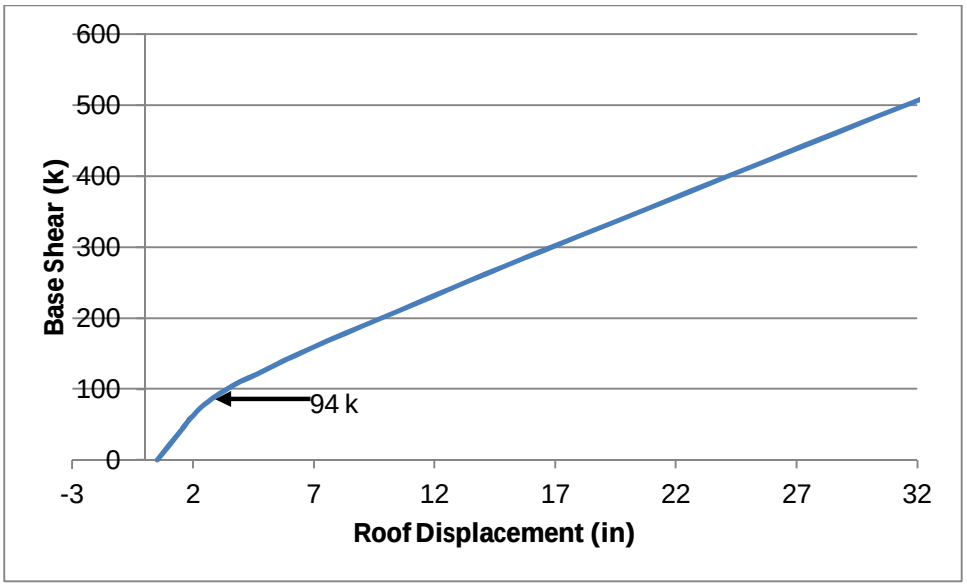


Figure 49: Segmented PT Strand and Viscoelastic Damper Pushover Curve

Figures 46-49 show the pushover curve plots for each of the four models. Gap opening occurs when the system experiences a change in stiffness due to one of the gap mechanisms being activated. On the Figures 46-49 the location of this occurrence is marked with a data label. As seen is Table 15, the gap opening occurs at the calculated value of around 94 k of base shear in the system 1 and system 2 configuration when dampers were not present . This is an accurate value due to the calculations being base off of a system without damping components. The same can be said about the calculated base shear versus SAP2000 base shear for both system configurations with hysteretic and viscoelastic dampers. It is important to note that when the load pattern was scaled up the location of the gap opening changed. However there was no clear indication in the base shear-roof displacement plots that the subsequent gaps were opening on other floors in either system configuration.

When the column size was increased dramatically, multiple slope changes occurred in the plots. This confirmed that the sections assigned to the system during the design phase could not properly accommodate the tensioning force in the PT strands in the SAP2000 models. This differs from a real life scenario where the tension in the PT strands would be limited to just the PT elements and not passing through the rest of the system. At this point the frame sections were adjusted. The

same member sections were chosen for the 1st-3rd frames (bottom to top) and 4th-6th frames. The final member sections for all the models can be seen below in Figure 50.

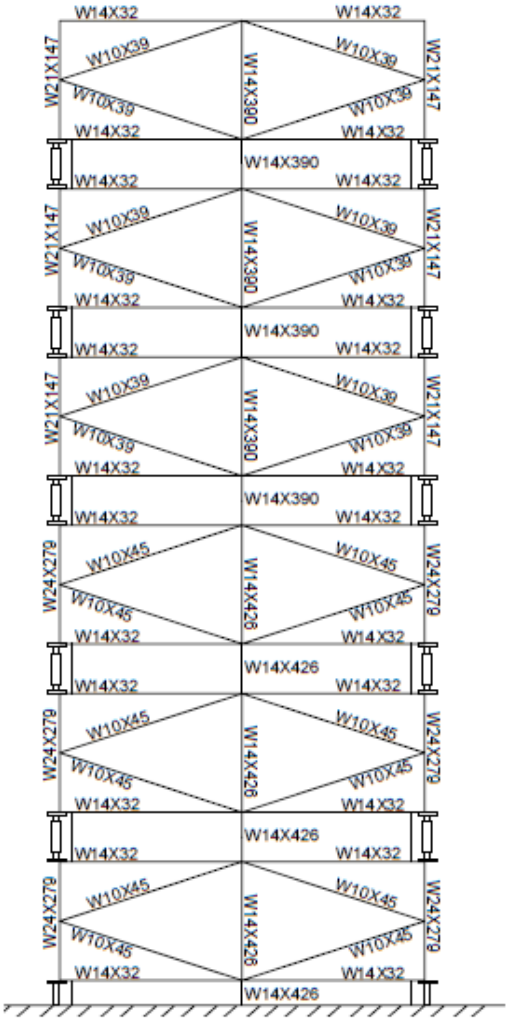


Figure 50: Frame Member Section Sizes

### 6.4.2 Natural Period

The natural period of both system configurations with viscoelastic and hysteretic dampers were found by applying an impulse load to the system and calculating the period from a plot of the roof displacement versus time. This was done because the natural periods calculated in SAP2000 for the models were incorrect. The 1st, 2nd and third mode natural periods and frequencies calculated in

SAP2000 were found using a modal load case analysis which did not included the tension force of the PT strands. Therefore these values were incorrect for the models and the alternate method described above was utilized instead.

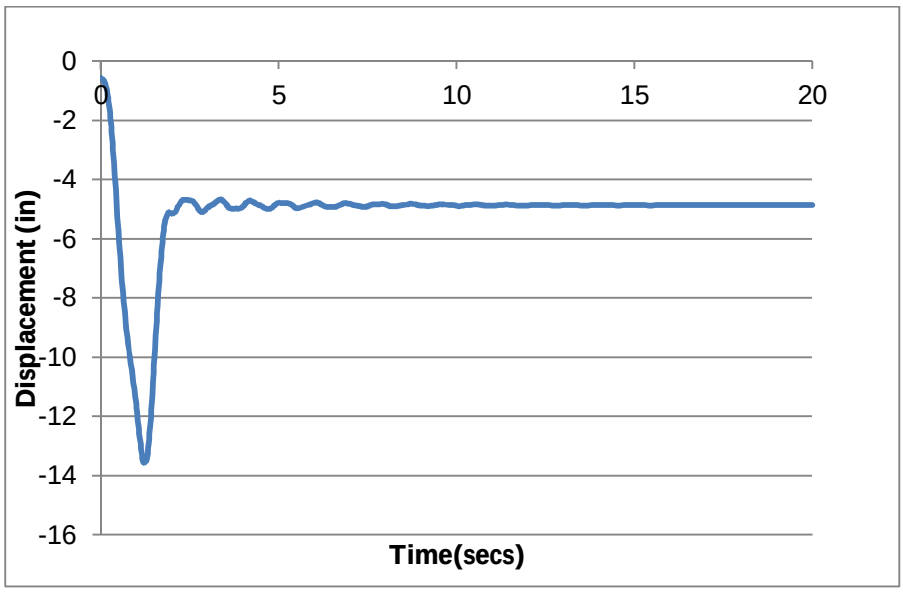


Figure 51: Segmented PT Strands Hysteretic Damper Impulse Load

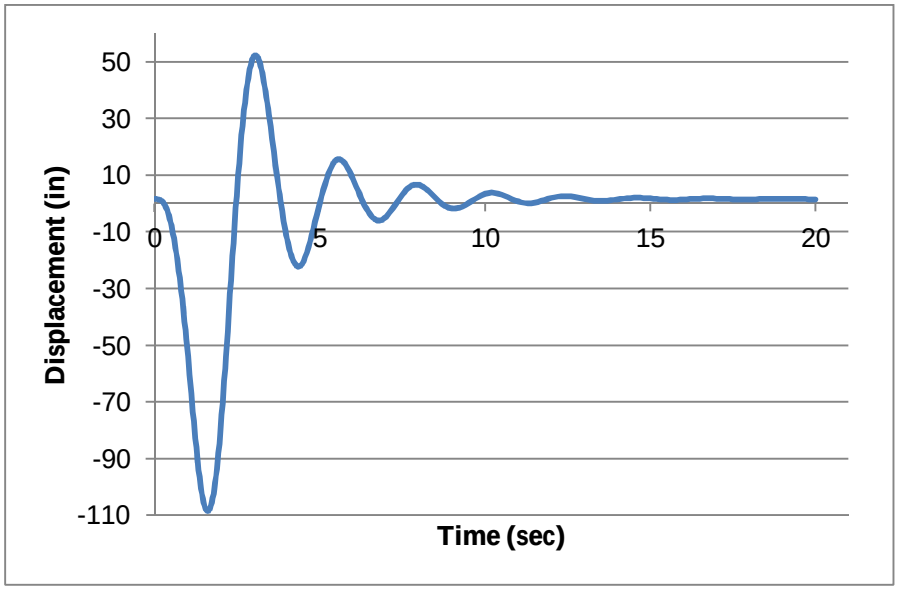


Figure 52: Segmented PT Strands and Viscoelastic Damper Impulse Load

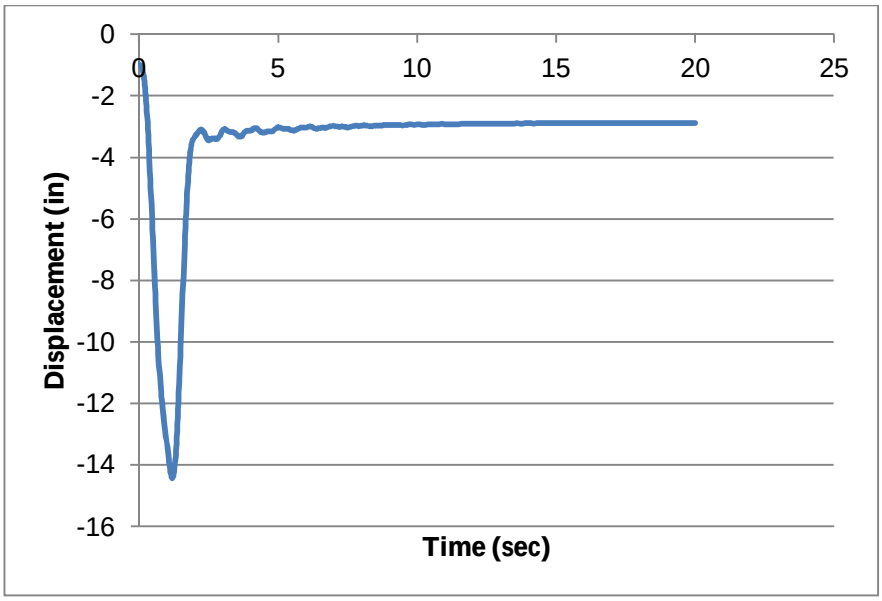


Figure 53: Continuous PT Strand and Hysteretic Damper Impulse Load

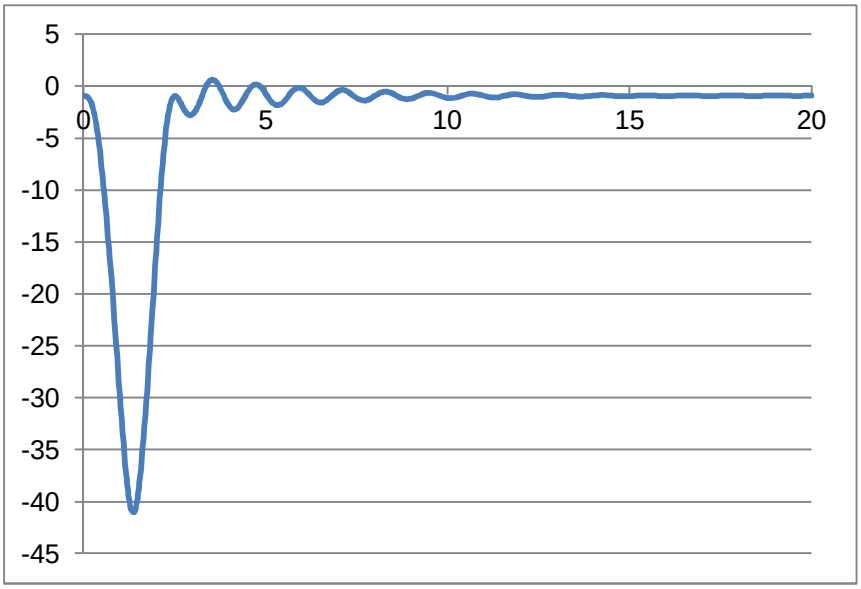


Figure 54: Coniunuous PT Strand and Viscoelastic Damper Impulse Load

As seen in the Figure 51 above the peak roof displacement after the impulse load was applied occurred at 2.22 seconds. Another peak roof displacement occurred at 5.57 seconds. During this time interval a total of 5 cycles occurred. Therefore the natural period of the system was determined using the following equation:

$$T_n = \frac{T_2 - T_1}{\#\ of\ Cycles} \quad \text{(Equation 15)}$$

where,

$T_2$ = time at which displacement occurred at 2

$T_1$ = time at which displacement occurred at 1

The calculated natural period in a first mode response of the system configurations can be seen below in Table 19. These natural periods were not comparable to the natural periods obtained from modal analysis due to the fact that SAP2000 doesn't consider the initial PT pre-tensioning of the system.

Table 19: Natural Period of System Configurations

| System Configuration | T2 | T1 | # of Cycles | Tn |
|---|---|---|---|---|
| 1 | 3.86 | 2.41 | 5 | 0.29 sec |
| 2 | 7.28 | 2.97 | 5 | 0.862 sec |
| 3 | 3.92 | 2.28 | 5 | 0.328 |
| 4 | 5.62 | 3.61 | 5 | 0.404 |

### 6.4.3 Seismic Drift

The seismic drift of the building, with the stacked frame system as its' lateral force resisting system, was checked against the seismic drift limit provided in ASCE 7-12. The seismic drift limit or allowable story drift is defined in Table 12.12-1 of ASCE 7-12 as the following equation:

$$D = 0.025h_{sx} \quad \text{(Equation 16)}$$

where,

$h_{sx}$ = the story height below Level, $x = (h_x - h_{x-1})$

The allowable story drift for the roof was calculated to be 3.6 inches.

The drift of the lateral force resisting system was calculated using the following procedure. First a typical $C_d$ factor was assumed. It was assumed that the system behaves similar to a steel special concentrically braced frame, therefore a $C_d$

factor of 5.0 was used. Next the seismic base shear, V, was calculated using the following equation:

$$V = C_s * W \quad \text{(Equation 17)}$$

where,

$C_s$ = seismic response coefficient

W = the effective seismic weight

$$C_s = \frac{S_{DS}}{\frac{R}{I}} \quad \text{(Equation 18)}$$

where,

$S_{DS}$ = the design spectral response acceleration parameter in the short period range as determined (Table 11)

R = response modification coefficient (8)

I = the importance factor (Table 11)

The seismic base shear was then distributed vertically to each floor using the equivalent lateral force (ELF) method. These deflections were then used to calculate the 6th floor story drift using the following equation:

$$D = C_d * d_{el} \quad \text{(Equation 19)}$$

where,

$C_d$ = 5.0

$d_{el}$ = Roof Drift, inches

The drifts for each system configuration, calculated using equation 12, can be seen below in Table 20. The continuous PT strand systems had drifts below 3.6 in.

Table 20: Roof and 6th floor Deflections and Story Drift

| System Configuration | Roof Deflection (in) | 6th Floor Deflection (in) | Story Drift (in) |
|---|---|---|---|
| Segmented PT Strand and Hysteretic Damper | 35.7 | 30.1 | 5.62 |
| Segmented PT Strand and Viscoelastic Damper | 38.9 | 31.9 | 7.01 |
| Continuous PT Strand and Hysteretic Damper | 5.05 | 4.5 | 0.55 |
| Continuous PT Strand and Viscoelastic Damper | 8.23 | 7.18 | 1.05 |

# Chapter 7 Ground Motions and Analysis Methods in SAP2000

## 7.1 Ground Motions

After verifying that the models were working correctly, the four systems were further analyzed in SAP2000. A nonlinear direct integration history analysis was used to subject each system to ten different ground motions. The ground motions varied in intensity, location (near fault), pulse occurrence, magnitude and duration. Table 18 shows the ground motions used for analysis and their properties. The goal of this analysis was to see how the system will react under varying non-linear load conditions. The desired outcome was to be able to state what the best and worst-case conditions are for the systems, identify locations where the system would be best implemented, and identify any potential problems the system may have in different environments. These parameters were quantified by examining the system's peak displacements, residual displacements, inter-story drift, maximum base shear, and force deformation plots.

## 7.2 Scaling of Ground Motions

The four system configurations were subjected to the ten different ground motions shown below in Table 18. These un-scaled and un-rotated ground motions were retrieved from the Pacific Earthquake Engineering Research Center (PEER) ground motion data base.

Table 21: Ground Motion Data

| Event Name/Year | Magnitude | Recording Station/ Component | PGA (g) | Site Class/$V_{s30}$ (m/s) | Source Distance (km) | Ground Motion Type | $D_{rms}$ | SSE |
|---|---|---|---|---|---|---|---|---|
| Hector-Mine/1999 | 7.1 | Hector/ Component 000 | 0.23 | C/685 | 11.7 | Far Field | 0.029 | 230 |
| Landers/1992 | 7.3 | Yermo Fire Station/ Component 270 | 0.25 | C/523 | 23.6 | Far Field | 0.028 | 88 |
| Manjil, Iran/ 1990 | 7.4 | Abhar/ Component 057 | 0.13 | C/724 | 13 | Far Field | 0.021 | 359 |
| San Fernando/ 1971 | 6.6 | LA-Hollywood Stor/ Component 090 | 0.21 | D/219 | 22.8 | Far Field | 0.028 | 317 |
| Imperial Valley-06/ 1879 | 6.5 | El Centro Array#6/ Component 140 | 0.41 | D/203 | 1.4 | Near Field-Pulse | 0.028 | 36 |
| Erzican, Turkey/ 1992 | 6.7 | Erzican/ Component EW | 0.5 | D/275 | 4.4 | Near Field-Pulse | 0.02 | 8 |
| Cape Mendocino | 7 | Petrolia/ Component 000 | 0.48 | C/713 | 8.2 | Near Field-Pulse | 0.033 | 79 |
| Loma Prieta/1989 | 6.9 | BRAN/ Component 000 | 0.48 | C/376 | 10.7 | Near Field-No Pulse | 0.027 | 113 |
| Nahanni, Canada/1985 | 6.8 | Site 1/ Component 019 | 0.98 | C/660 | 9.6 | Near Field-No Pulse | 0.053 | 189 |
| Northridge-01/1994 | 6.7 | Northridge-Saticoy/ Component 090 | 0.37 | C/380 | 8.4 | Near Field-No Pulse | 0.023 | 60 |

These ground motions were chosen for their various characteristics including ground motion type, peak ground acceleration (PGA), site class and magnitude. Ten ground motions were selected to satisfy the ASCE-7 requirement

that a system be subjected to 7 or more ground motions when nonlinear analysis is utilized. The horizontal component with the highest PGA for each ground motion was applied to each system. Each ground motion was scaled to the design spectrum shown below in figure 54. The scale factor was calculated using equation 20 shown below:

$$\text{Scale Factor} = \frac{A_{DS}}{A_{RS}} \qquad \text{(Equation 20)}$$

where,

$A_{DS}$ = Acceleration of design response spectrum at 0.5 seconds

$A_{RS}$ = Acceleration of 5% damping response spectrum at 0.5 seconds

The selected period of 0.5 sec corresponded to the average value of the natural frequency for all four system configurations. Table 19 shows the calculated scale factors for each ground motion.

Table 22: Ground Motion Scale Factors

| Event Name/Year | Ground Motion Scale Factor |
|---|---|
| Hector-Mine/1999 | 2.44 |
| Landers/1992 | 1.83 |
| Manjil, Iran/ 1990 | 2.00 |
| San Fernando/ 1971 | 3.26 |
| Imperial Valley-06/ 1879 | 3.40 |
| Erzican, Turkey/ 1992 | 1.08 |
| Cape Mendocino | 1.07 |
| Loma Prieta/1989 | 0.66 |
| Nahanni, Canada/1985 | 1.69 |
| Northridge- 01/1994 | 1.45 |

Figures 56 and 57 display the pre-scaled pseudo-acceleration response spectrum for 5% damping versus the design spectrum and the scaled pseudo-acceleration response spectrum for 5% damping versus the design spectrum.

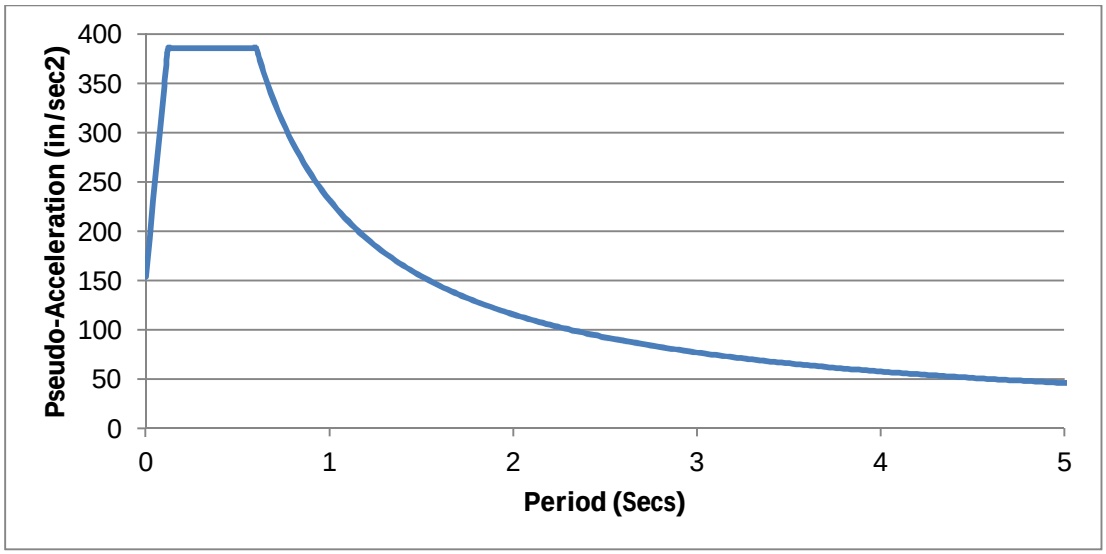


Figure 55: Design Response Spectrum

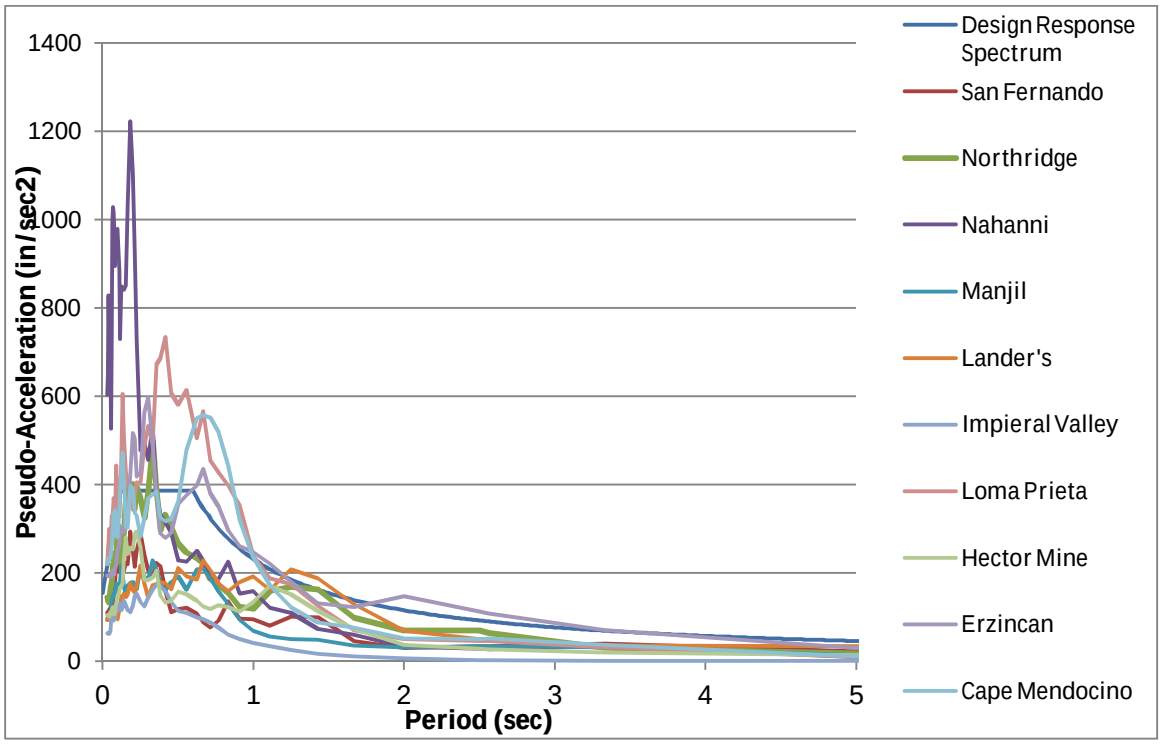


Figure 56: Pre-Scaled Ground Motion Response Spectrum

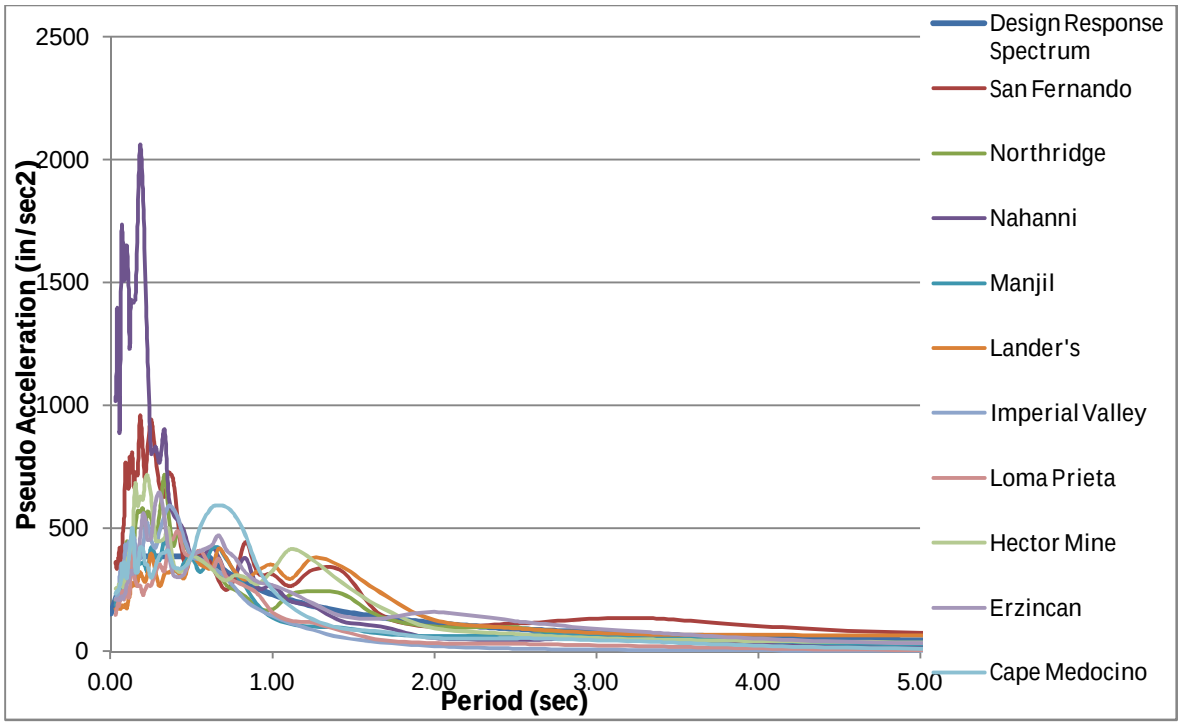


Figure 57: Scaled Ground Motion Response Spectrum

## 7.3 Importing Ground Motions into Sap2000

The ground motion data was put into SAP2000 using a user defined time history function that was imported into the program using text files. These text files were taken from the PEER database. These files provided the recorded accelerations of the ground motion over time in units of g and seconds, respectively. The time history function for each ground motion was then assigned to a non-linear direct integration load case that continued from the nonlinear dead load case. The dead load case contained the tensioning in the PT strands as a temperature gradient as well as the assigned joint loads that represented tributary system gravity weight. The ground motion time history functions were applied as an acceleration load type in the U2 direction. The scale factor used for each ground motion consisted of the acceleration of gravity (386.4 in/sec2) multiplied by the calculated scale factors shown in Table 19. The damping coefficients for each load case were defined by period as five percent. Once a load case was defined for each ground motion the

nonlinear direct integration analysis for all ten ground motions were run for each system.

# Chapter 8 SAP2000 Model Results

The Tables and figures on the following pages display the results obtained from running the ten different ground motions for the four system models in SAP2000. Figures 58- 61 are plots of the base shear versus system (roof) displacement for the Northridge ground motion. Tables 21- 24 display the interstory drift calculated for each floor of the four models. These figures and Tables were used to determine if the systems experiencing a reasonable amount of drift , base shear and to check if the system was over or under designed. The base shear values were taken directly from SAP2000. The interstory drifts, shown in Tables 21-24, were calculated based off of the displacements of the center joint of the floor above and below each story.

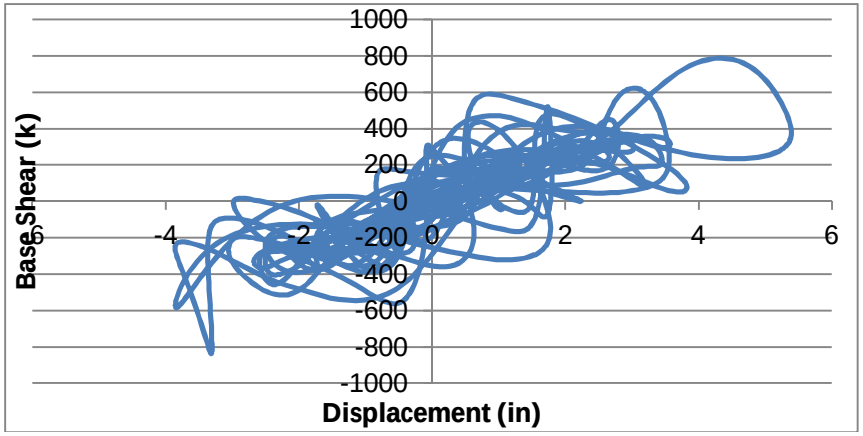


**Figure 58: Segmented PT Strands and Hysteretic Damper Northridge**

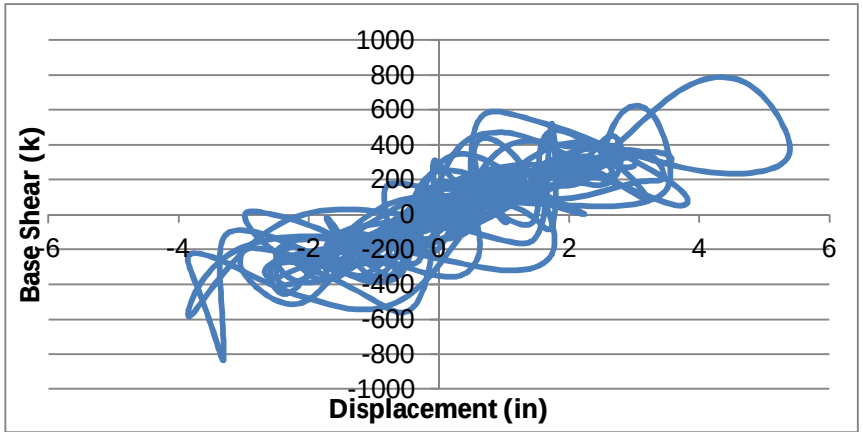


**Figure 59: Segmented PT Strands and Viscoelastic Damper Northridge**

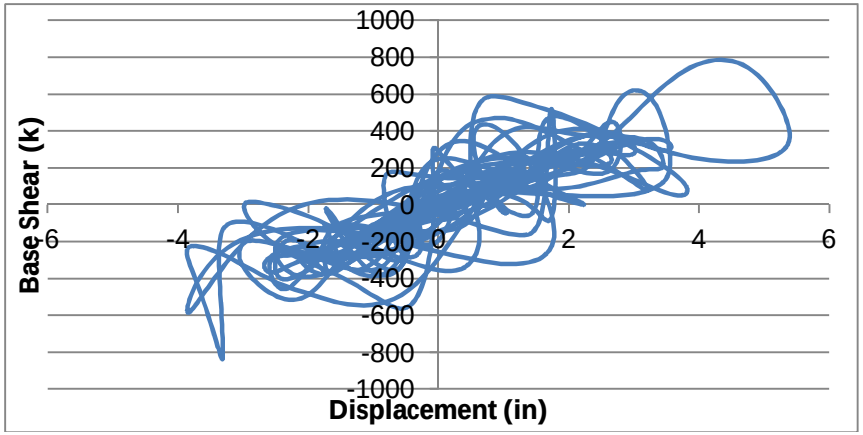


**Figure 60:Continuous PT Strands and Viscoelastic Damper Northridge**

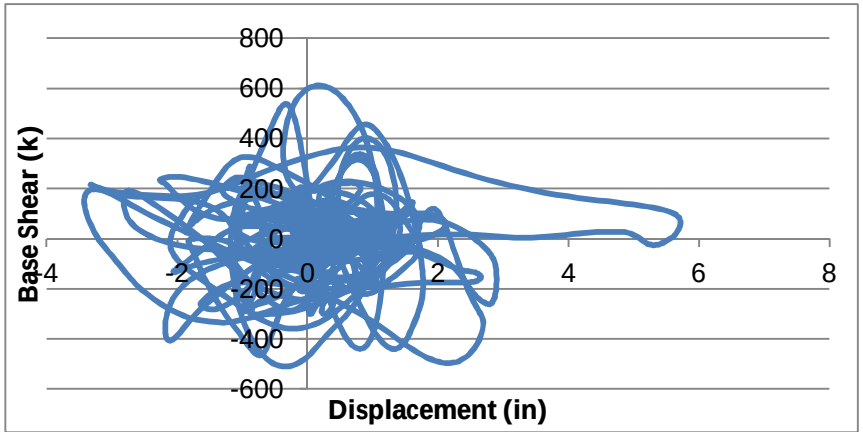


**Figure 61: Continuous PT Strands and Hysteretic Damper Northridge**

Table 23:Segmented PT Strands and Viscoelastic Damper System Interstory Drifts (in)

| | | Ground Motions | | | | | | | | | |
|---|---|---|---|---|---|---|---|---|---|---|---|
| Story | | Cape Menocino | Erzincan | Hector Mine | Imperial Valley | Landers | Loma Prieta | Manjil | Nahanni | Northridge | San Fernando |
| | 6th | 1.40 | 2.60 | 2.46 | 0.889 | 4.07 | 1.16 | 0.987 | 1.61 | 2.20 | 2.05 |
| | 5th | 1.44 | 2.66 | 2.51 | 0.566 | 4.18 | 1.11 | 0.992 | 1.37 | 2.16 | 2.11 |
| | 4th | 1.07 | 2.63 | 2.31 | 0.386 | 4.08 | 0.834 | 1.00 | 1.29 | 2.09 | 2.11 |
| | 3rd | 0.788 | 2.38 | 1.97 | 0.502 | 3.70 | 0.840 | 1.00 | 1.44 | 1.98 | 1.56 |
| | 2nd | 0.783 | 1.96 | 1.72 | 0.622 | 2.94 | 0.887 | 0.968 | 1.490 | 1.72 | 1.34 |
| | 1st | 0.574 | 1.15 | 1.07 | 0.569 | 1.64 | 0.718 | 0.689 | 1.08 | 0.998 | 1.18 |

Table 24: Segmented PT Strands and Hysteretic Damper System Inter-story Drifts (in)

| | | Ground Motions | | | | | | | | | |
|---|---|---|---|---|---|---|---|---|---|---|---|
| Story | | Cape Medencino | Erzincan | Hector Mine | Imperial Valley | Landers | Loma Prieta | Manjil | Nahanni | Northridge | San Fernando |
| | 6th | 1.09 | 133.39 | 1.62 | 0.27 | 1.56 | 0.80 | 0.86 | 1.63 | 1.25 | 1.22 |
| | 5th | 1.24 | 136.25 | 1.63 | 0.24 | 1.66 | 0.92 | 0.98 | 1.80 | 1.40 | 1.24 |
| | 4th | 1.27 | 133.66 | 1.65 | 0.30 | 1.68 | 0.97 | 1.09 | 1.51 | 1.41 | 1.08 |
| | 3rd | 1.17 | 117.79 | 1.63 | 0.35 | 1.70 | 0.92 | 1.06 | 0.97 | 1.29 | 1.08 |
| | 2nd | 1.10 | 90.01 | 1.64 | 0.42 | 1.71 | 0.85 | 0.96 | 1.11 | 1.17 | 1.10 |
| | 1st | 0.66 | 47.01 | 1.19 | 0.33 | 1.24 | 0.58 | 0.67 | 0.92 | 0.90 | 0.84 |

Table 25: Continuous PT Strands and Viscoelastic Damper System Inter-story Drifts (in)

| | | Ground Motions | | | | | | | | | |
|---|---|---|---|---|---|---|---|---|---|---|---|
| Story | | Cape Mendocino | Erzican, Turkey | Hector Mine | Imperial Valley | Landers | Loma Prieta | Manjil, Iran | Nahanni | Northridge | San Fernando |
| | 6th | 1.04 | 0.340 | 0.991 | 0.314 | 0.991 | 0.732 | 1.09 | 1.25 | 0.698 | 1.25 |
| | 5th | 1.46 | 0.351 | 1.10 | 0.462 | 1.37 | 1.02 | 1.48 | 1.55 | 0.914 | 1.61 |
| | 4th | 1.74 | 0.336 | 1.32 | 0.666 | 1.64 | 1.17 | 1.78 | 1.59 | 1.00 | 1.27 |
| | 3rd | 1.69 | 0.493 | 1.53 | 0.756 | 1.68 | 1.12 | 1.83 | 1.37 | 0.991 | 1.32 |
| | 2nd | 1.49 | 0.616 | 1.58 | 0.794 | 1.61 | 0.925 | 1.74 | 1.47 | 1.02 | 1.61 |
| | 1st | 0.927 | 0.473 | 1.13 | 0.525 | 1.07 | 0.551 | 1.16 | 1.17 | 0.746 | 1.23 |

Table 26:Continuous PT Strands and Hysteretic Damper System Inter-story Drifts (in)

| | | Ground Motions | | | | | | | | | |
|---|---|---|---|---|---|---|---|---|---|---|---|
| Story | | Design Cal Eq | Cape Mendocino | Erzincan | Hector Mine | Landers | Loma Prieta | Manjil, Iran | Nahanni | Northridge | San Fernando |
| | 6th | 1.11 | 0.66 | 0.58 | 0.54 | 0.73 | 0.50 | 0.78 | 0.93 | 0.69 | 0.54 |
| | 5th | 1.48 | 0.83 | 0.72 | 0.71 | 0.96 | 0.68 | 1.03 | 1.24 | 0.92 | 0.66 |
| | 4th | 1.69 | 0.76 | 0.86 | 0.84 | 1.16 | 0.76 | 1.22 | 1.33 | 1.07 | 0.67 |
| | 3rd | 1.62 | 0.75 | 0.96 | 0.92 | 1.24 | 0.73 | 1.25 | 1.01 | 1.08 | 0.80 |
| | 2nd | 1.54 | 0.78 | 1.17 | 0.92 | 1.29 | 0.72 | 1.22 | 1.14 | 1.06 | 1.08 |
| | 1st | 1.12 | 0.63 | 1.10 | 0.72 | 1.05 | 0.61 | 0.90 | 1.24 | 0.88 | 1.09 |

In order to determine how effective each system was three parameters were examined, the base shear, system roof displacement and residual drift. These values were taken from the results of the analysis conducted in SAP2000. For each ground motion the maximum base shear, peak displacement and maximum residual drift were identified for each system. These values are shown below in Tables 21-24.

Table 27: Segmented PT Strands and Viscoelastic Damper System Max Values

| Load Case | Maximum Base Shear (K) | Peak Displacement at Roof (in) | Max Residual Drift at Roof (in) |
|---|---|---|---|
| Hector Mine | 482 | 9.99 | 0.663 |
| Erzincan | 584 | 13.4 | 0.988 |
| Manjil, Iran | 340 | 5.64 | 0.191 |
| San Fernando | 547 | 13.1 | 0.675 |
| Loma Prieta | 381 | 5.56 | 1.00 |
| Nahanni | 805 | 8.30 | 1.19 |
| Northridge | 835 | 5.38 | 0.398 |
| Cape Mendocino | 318 | 6.18 | 0.683 |
| Imperial Valley | 532 | 4.27 | 0.794 |
| Lander's | 393 | 20.6 | 1.01 |

Table 28: Segmented PT Strands and Hysteretic Damper Material Max Values

| Load Case | Maximum Base Shear (K) | Peak Displacement (in) | Max Residual Drift (in) |
|---|---|---|---|
| Hector Mine | 759 | 9.36 | 0.177 |
| Erzincan | 12875 | 658 | 0.12 |
| Manjil, Iran | 411 | 5.62 | 0.9 |
| San Fernando | 662 | 7.37 | 0.48 |
| Loma Prieta | 447 | 5.04 | 0.32 |
| Nahanni | 660 | 7.95 | 1.3 |
| Northridge | 836 | 5.39 | 0.323 |
| Cape Mendocino | 549 | 6.53 | 0.13 |
| Imperial Valley | 561 | 4.83 | 0.145 |
| Lander's | 516 | 9.56 | 0.287 |

Table 29: Continuous PT Strands and Viscoelastic Damper Material Max Values

| Load Case | Maximum Base Shear (K) | Peak Displacement (in) | Max Residual Drift (in) |
|---|---|---|---|
| Hector Mine | 930 | 8.03 | 0.315 |
| Erzincan | 412 | 2.61 | 0.13 |
| Manjil, Iran | 916 | 9.11 | 0.12 |
| San Fernando | 963 | 8.32 | 0.165 |
| Loma Prieta | 474 | 5.52 | 0.43 |
| Nahanni | 983 | 8.42 | 0.29 |
| Northridge | 835 | 5.38 | 0.32 |
| Cape Mendocino | 832 | 8.35 | 0.196 |
| Imperial Valley | 619 | 5.16 | 0.5 |
| Lander's | 843 | 8.37 | 0.34 |

Table 30: Continuous PT Strands and Hysteretic Damper Material Max Values

| Load Case | Maximum Base Shear (K) | Peak Displacement | Max Residual Drift |
|---|---|---|---|
| Hector Mine | 1286 | 4.68 | 0.26 |
| Erzincan | 1112 | 5.87 | 1.00 |
| Manjil, Iran | 696 | 6.40 | 0.10 |
| San Fernando | 1099 | 6.87 | 0.20 |
| Loma Prieta | 677 | 4.21 | 0.40 |
| Nahanni | 969 | 6.88 | 0.40 |
| Northridge | 506 | 5.71 | 1.59 |
| Cape Mendocino | 970 | 8.57 | 0.09 |
| Imperial Valley | 892 | 4.64 | 0.30 |
| Lander's | 912 | 6.44 | 0.24 |

From the data collected from the models shown in Tables 21-28 the mean, variance and standard deviation of the maximum base shear, maximum peal displacement and maximum residual drift were calculated for each systems. The resulting values can be seen below in Tables 29 and 30.

Table 31: Continuous PT Strand Configuration Mean, Variance and Standard Deviation of Ground Motion Results

| Hysteretic Damper | | | |
|---|---|---|---|
| | Maximum Base Shear | Maximum Peak Displacement | Maximum Residual Drift |
| Mean | 912 | 6.03 | 0.57 |
| Variance | 48833 | 1.53 | 0.24 |
| Standard Deviation | 221 | 1.24 | 0.49 |
| Viscoelastic Damper | | | |
| | Maximum Base Shear | Maximum Peak Displacement | Maximum Residual Drift |
| Mean | 781 | 6.93 | 0.239 |
| Variance | 38000 | 4.03 | 0.018 |
| Standard Deviation | 194 | 2.00 | 0.134 |

Table 32: Segmented PT Strand Configuration Mean, Variance and Standard Deviation of Ground Motion Reults

| Hysteretic Damper | | | |
|---|---|---|---|
| | Maximum Base Shear | Maximum Peak Displacement | Maximum Residual Drift |
| Mean | 1828 | 6.8 | 0.523 |
| Variance | 13575860 | 38176 | 0.090 |
| Standard Deviation | 3685 | 195 | 0.299 |
| Viscoelatic Damper | | | |
| | | | |
| Mean | 522 | 9.25 | 0.710 |
| Variance | 29500 | 23.8 | 0.069 |
| Standard Deviation | 171 | 4.88 | 0.263 |

Once the data analysis techniques were complete for all four models, the behavior of one system and applied ground motion was further investigated. The segmented PT strand system with viscoelastic dampers when subjected to the Northridge ground motion was chosen for further analysis. The behavior of the individual frames or floor response of the system was examined by plotting the story shear versus story drift. These plots are shown below in Figures 62-67.

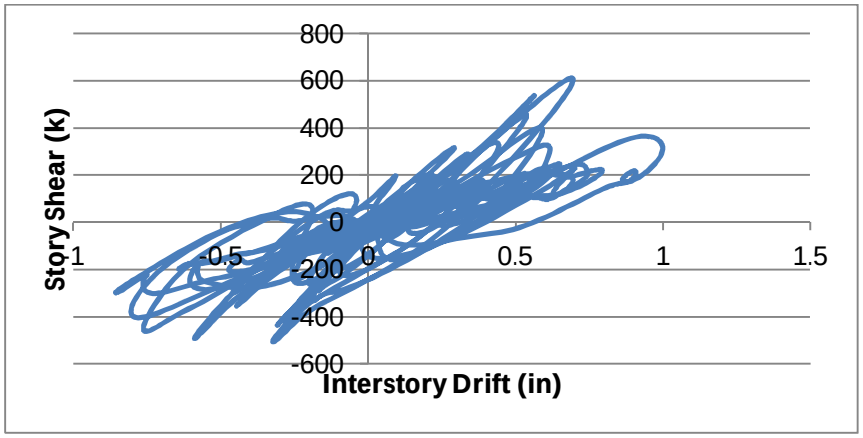


Figure 62:1st Floor Response Northridge Ground Motion

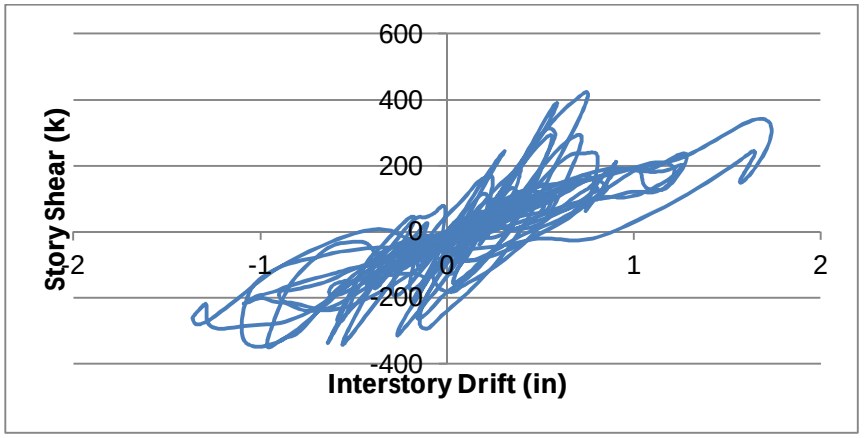


Figure 63: 2nd Floor Response Northridge Ground Motion

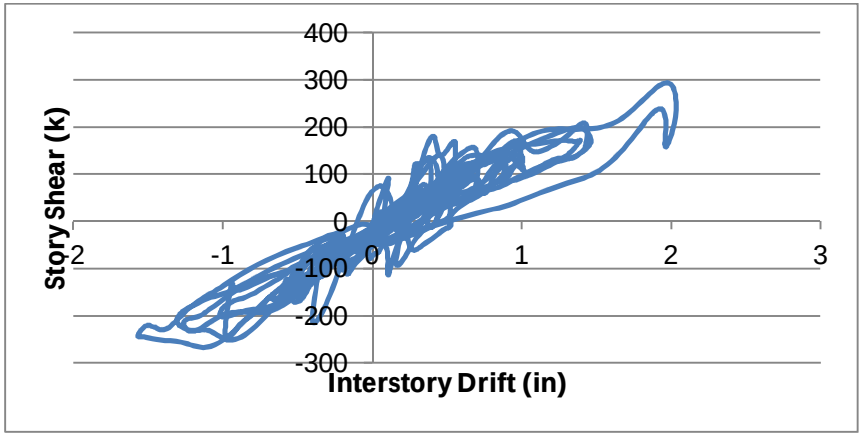


Figure 64: 3rd Floor Response Northridge Ground Motion

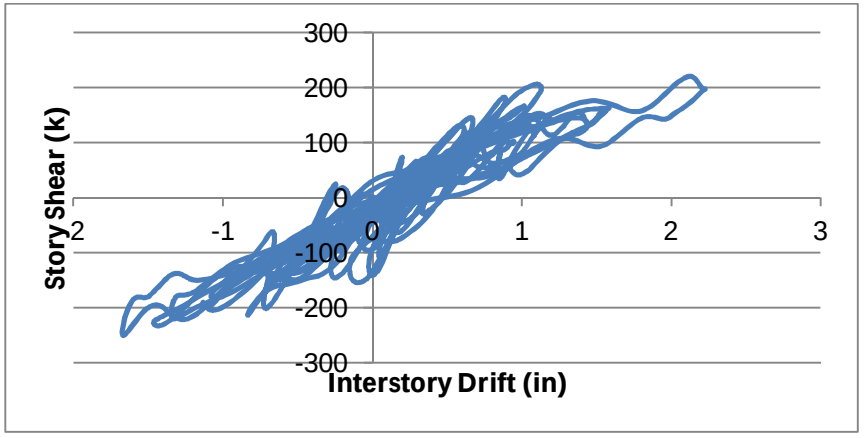


Figure 65: 4th Floor Response Northridge Ground Motion

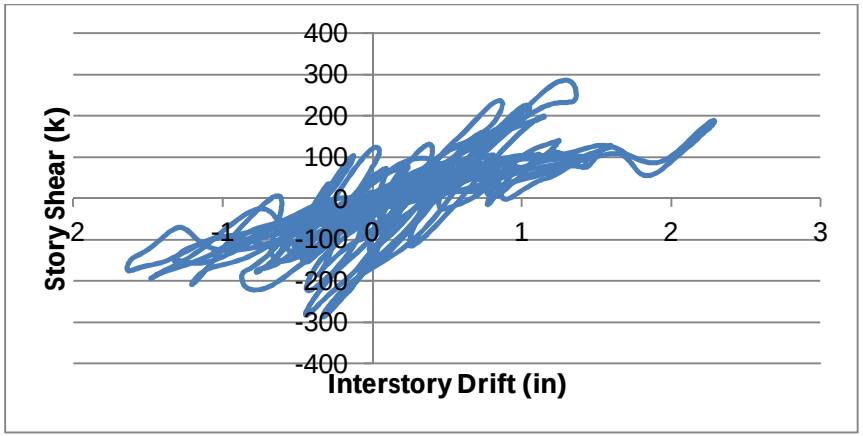


Figure 66: 5th Floor Response Northridge Ground Motion

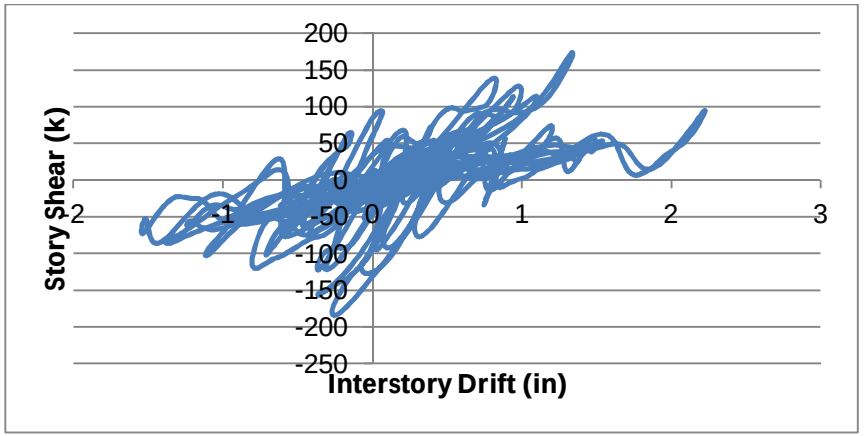


Figure 67:6th Floor Response Northridge Ground Motion

Next the member force distribution at the peak roof displacement was examined for the same system and ground motion. Figure 68 below shows the axial force distribution for the system taken from the SAP2000 model.

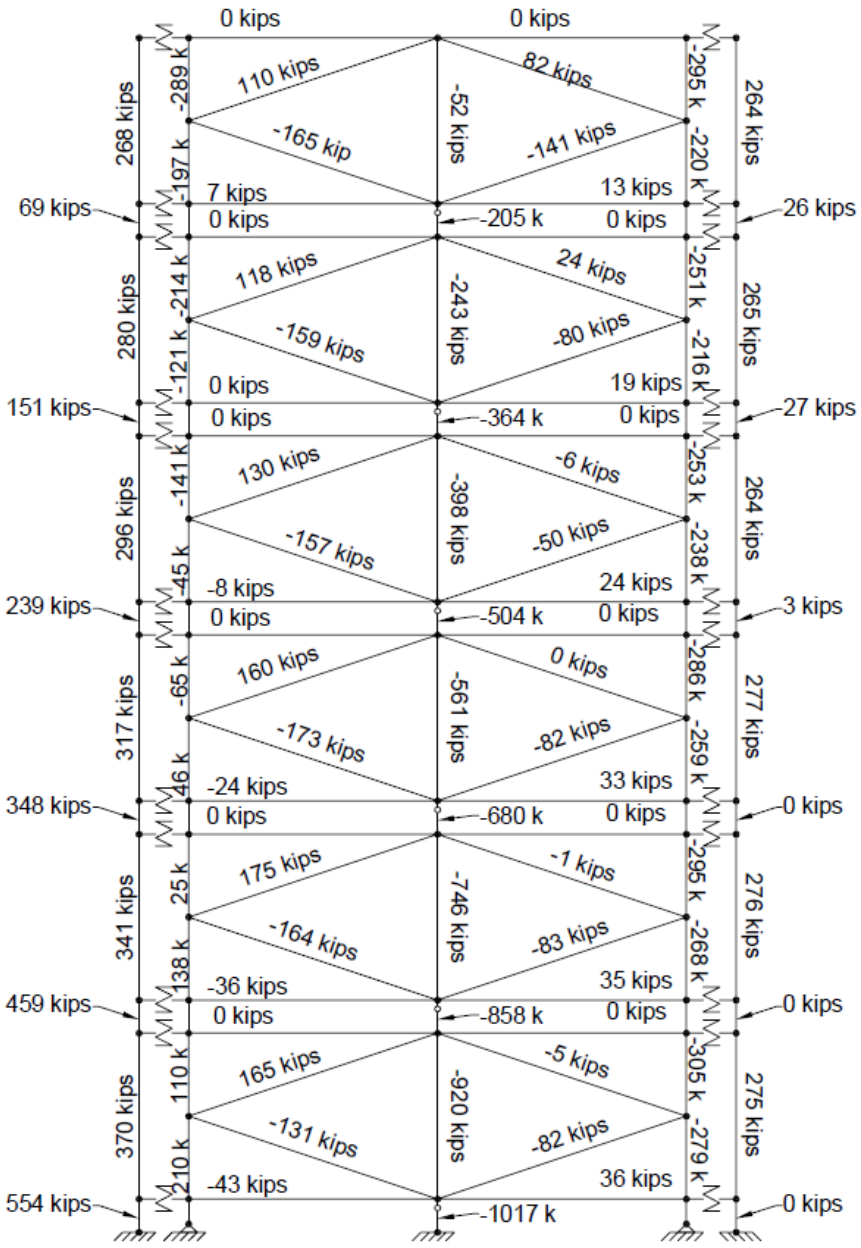


Figure 68:Northridge Ground Motion Member Force Distribution Segmented PT Strand System

From the results obtained, the following conclusions were made about the designed lateral force resisting system:

1. Two systems produced drifts that were well below the seismic drift limit of 3.6 inches when subjected to the design load case. The mean peak displacement for the continuous PT strand system with hysteretic dampers was 6.8 inches. The mean peak displacement for the continuous pt strand system with viscoelastic dampers was 6.93 inches. The mean peak displacement for the segmented PT strand system with hysteretic dampers was 6.8 inches. The mean peak displacement for the segmented PT strand system with viscoelastic dampers was 9.25 inches.
2. The "Segmented PT Strand" layout in Figure 39 provided more believable results in terms of system deflection than the "Continuous PT Strand" layout in Figure 42. The deflections at the roof of the "Continuous PT Strand" models were much smaller than those of the "Segmented PT Strand" models. For example when looking at the hector mine load case the continuous PT strand system with hysteretic dampers had a peak displacement of 4.68 inches and the segmented PT strand system with hysteretic dampers had a peak displacement of 8.03 inches.
3. The systems with viscoelastic dampers experienced larger displacements that the systems with hysteretic dampers. This trend can be observed in the base shear versus roof displacement plots shown in the appendix.
4. The systems with viscoelastic dampers experienced significantly smaller base shear than the systems with hysteretic dampers. This trend can be observed in the base shear versus roof displacement plots shown in the appendix.
5. The lateral force system was able to be effectively designed with consistent modular units that allow for easy construction assembly. All members were able to pass the stress/capacity check conducted in SAP2000.
6. The continuous PT strand system is extremely stiff. This can be seen in the all of the base shear versus roof displacement plots for the system.

7. The segmeted PT strand system with viscoelastic dampers experienced large and sudden changes in acceleration on multiple floors. This behavior can be observed in Figures 62-67,rapidly changes over very little displacement. This behavior results in steep slope changes when plotting story shear versus interstory drift.

# Chapter 9 Summary and Conclusions

## 9.1 Summary

The idea of using the human spine as the inspiration for a lateral force resisting system is introduced. The system will be able to take advantage of naturally occurring capabilities of the spine. These abilities included the spine's ability to undergo large deformations while sustaining little damage, restorative capabilities due to muscles and ligaments and the spine's ability to adequately support a large amount of weight using a relatively small structure.

First the concepts and principles of the spine were explored through an extensive literature review of the spine. A list of concepts from the spine that could be used in a lateral force resisting system was developed based off of this initial literature review. Then a model of the lumbar region of the spine was developed in SAP2000. The lumbar region was chosen to model due to the region's capability to support a large amount of weight and undergo large rotations. Several different methods were used to validate this model including checking the results against other scholarly articles that attempted to model the region using finite element programs and a series of hand calculations.

Next a literature review of rocking systems was conducted. This review explored the basic concepts of self-centering systems, the design process of self-centering systems, spine influenced concepts that have already been implemented into self-centering systems, and concrete rocking systems. Many of the articles reviewed during this review provided insight into several concepts used in the final lateral force resisting system design. The main concept being application and design of the self-centering mechanisms.

Once the literature review was complete enough information was collected to begin the design process. Ideas for the design of the system were created and drawn up. This included both two and three dimensional structures. A design for the system was created and inputted into SAP2000. This design process included creating a prototype building and system layout, selecting design criteria,

preliminary sizing of members, calculating the amount of tensioning required for the PT strands, sizing the PT strands and investigating viscoelastic material and hysteretic damper properties.

Then two approaches to modeling the system in SAP2000 were developed. The first system consisted of segmented PT strands and energy dissipation devices. The second system consisted of continuous PT strands and energy dissipation devices. Several verification methods were used to ensure the systems were working correctly in SAP2000. A set of ten ground motions were selected to use to analyze the models. These ground motions were scaled to a design spectrum and inputted into SAP2000 as time history function. The properties of each ground motion varied in terms of magnitude, location, source distance, site class, ground motion type and peak ground acceleration. The purpose of selecting these ground motions was to see how the models behaved under varying loading conditions.

Lastly each of the four models developed in SAP2000 were subjected to the set of ten ground motions. For each model the maximum base shear, peak displacement, maximum residual drift and inter-story drifts were calculated and recorded. These results were then used to determine the effectiveness of each system under the varying loading conditions.

## 9.2 Conclusions

### 9.2.1 Spine Literature Review

A list of concepts that could be transferred from the spine to a lateral force resisting system was developed during the spine literature review. The list comprised of the following points:

- Modular rigid units
- Capable of deformations without permanent damage
- Specialized connections limit motion and transfer compression forces
- Discs provide a viscous type of damping
- Ligaments protect the spinal cord and other neural structures

- Inherent system of overlapping ligaments add redundancy. Ligaments can be used to control different types of motion.
- Muscles act as an active control system
- Elements heal if damaged

These concepts were used during the lateral force resisting system design process to inspire different configurations of potential systems.

### 9.2.2 Lumbar Region SAP2000 Model

The lumbar region spine model that was created in SAP2000 was used to verify several different behaviors of the spine. From this analysis it was concluded that the lumbar region of the spine was flexure-dominated, the maximum lateral displacement before a ligament breaks were calculated and the lateral drift ratios for each spinal ligament were determined. The results from this analysis can be seen in chapter 3.5. These results proved very useful when developing ideas for a spine inspired lateral force resisting system. Especially the concept of the spine being flexure-dominated. This gave insight into how the final system design should behave when subjected to ground motion accelerations.

### 9.2.3 Lateral Force Resisting System Ideas and Design

Using the information collected in chapters 1-4 a list of objectives for system design was developed. This list consisted of the following objectives:

1. The components of the system must be capable of transferring shear from one floor to the next.
2. The system should be axially fixed. This means that the system will need to contain a continuous and relatively stiff load path that can transfer vertical loads throughout the system.
3. The system must contain components that limit the amount of deformation in the system. This is especially important between floors where the system would be free to deform.

4. The system must contain spaces on each floor that can be designated as definitive building spaces.
5. The system must have vertebrae like elements that are self-contained and shop fabricated. Making assembly of the system simpler, faster, and providing definitive building space.
6. The system must provide a method of lateral load resistance.
7. The system must provide a way to resist overturning moment.

The final design of the lateral force resisting system is shown in Figure 28. This system was comprised of cross braces, stout centrally located column members that provided a central pivot point and continuous vertical load path, pre-tensioned steel cables, PT couplers, energy dissipation devices and self-centering mechanisms.

### 9.2.4 Lateral Force Resisting System in SAP2000

Two different system configurations were developed in SAP2000 in order to accurately capture the theoretical behavior of the system. The first configuration consisted of a segmented PT strand schematic. The second configuration consisted of a continuous PT strand schematic. This was done in order to obtain a better understanding as to how the models were working in SAP2000. Two different types of energy dissipation devices, hysteretic and viscoelastic dampers, were also used in the models. This created a total of four models that were subjected to ground motions and assessed for effectiveness in SAP2000. Each model was subjected to the ten different ground motions. It was observed that the two system configurations behaved very differently, leading to the conclusion that while the models were behaving correctly, they were not behaving as anticipated.

### 9.2.5 System Verification in SAP2000

Through several verification procedures the following conclusions were made about the models:

1. The natural periods of each model were deemed reasonable, ranging from 0.29 seconds to 0.86 seconds.
2. The location of initial gap opening, shown in Table 15, could be accurately calculated in terms of the amount of base shear needed to cause gap opening. For example for the segmented PT strand system with hysteretic dampers it was calculated that the gap opening should occur at a base shear of 283.6 kips. In the SAP2000 model this opening occurred at 308 k. This difference can be accounted to the varying PT strand tensioning of 301 k in the model instead of the calculated value of 300 k.
3. The PT stands provided a successful approach to resisting overturning moment in the system. Caution must be used to ensure that the force in the PT strands will not reach a point that causes the strands to yield. This was proven while experimenting with different system configurations in SAP2000. A model with continuous PT strands and no gap opening elements(compression only cable members) experienced extremely high amounts of force in the PT strands. These forces were high enough to cause the strand to yield.
4. The self-centering or gap opening elements successfully reduced the amount of tension experienced by the PT strands. This was also proven while experimenting with different system configurations in SAP2000. Initially an idea to try different patterns of combinations of gap opening elements was explored. In other words the length of the PT strands were varied by changing the location of the gap opening elements. The amount of tension in the PT strands decreased as more gap opening elements that were included the model.
5. The gap elements, consisting of the non-tensioned cable strands and spring elements, exhibited an accurate behavior of experiencing an increase in

tension until the same amount of tension as the surrounding PT strands was reached.

6. The modal shapes of all four systems obtained through the use of modal ritz vectors were not accurate in SAP2000. This was attributed to SAP2000's inability to include the temperature gradient in the dead load(which was used to apply tension to the PT strands) to the modal load case.
7. While a four models in SAP2000 were verified to be working correctly, they did not work as anticipated by the researcher.

### 9.2.6 SAP2000 Model Results

1. The two models produced drifts that were below the seismic drift limit.
2. The deflections at the roof of the "Continuous PT Strand" models were much smaller than those of the "Segmented PT Strand" models.
3. The systems with viscoelastic dampers experienced larger displacements that the systems with hysteretic dampers.
4. The systems with viscoelastic dampers experienced significantly smaller base shear than the systems with hysteretic dampers.
5. The lateral force system was able to be effectively designed with consistent modular units that allow for easy construction assembly.
6. SAP2000 was able to model the lateral force resisting system. This modeling process involved manipulating SAP2000 into performing some of the researchers desired results. Therefore it may be beneficial to explore other modeling software options for future analysis.

## 9.3 Future Work

The research described in this proposal has investigated the possibility and practicality of using the spine as an inspiration in creating a spine inspired lateral force resisting system. Although the research conducted in this proposal has resulted in a working model of a spine inspired segmented frame design further testing of the model is needed to assess the effectiveness of the system.

1. Explore using other software programs such as Opensees to model the system. This would give the research better control of the system's material properties and nonlinear behavior.
2. Design the lateral force resisting system in detail. This process would include drafting precise details for all components of the system including the self-centering mechanisms.
3. Varying the properties of both the viscoelastic and hysteretic damper to determine which loading scenario each damper is most effective in.
4. Expose the models to a larger set of ground motion to increase the variability of the results.
5. Analyze the accelerations at each floor for each ground motion. Obtain the mean, variance and standard deviation for the maximum accelerations at each floor during each load case. Determine why there is a drastic change in acceleration on various floors (this would included magnitude and direction)
6. Develop a model whose behavior is more predictable by the researcher.

## References


Barcsay, Jenő. (1978). Anatomie voor de kunstenaa. Cantecleer, 1978. Print.

Beardmore, R. (2013, January 23). Reciprocating Mechanisms. Retrieved January 16, 2015, from http://roymechx.co.uk/Useful_Tables/Cams_Springs/Reciprocating.html

Boundless. “Center of Mass of the Human Body.” Boundless Physics. Boundless, 14 Nov. 2014. Retrieved 14 Jan. 2014 from https://www.boundless.com/physics/textbooks/boundless-physics-textbook/linear-momentum-and-collisions-7/center-of-mass-72/center-of-mass-of-the-human-body-305-1641/

Clauser, Charles, John T. McConville, and J.W. Young. "Weight, Volume, and Center of Mass of Segments of the Human Body." *National Technical Information Service*. (1969).

Costi, J., Hearn, T., & Fazzalari, N. (2002). The effect of hydration on the stiffness of intervertebral discs in an ovine model. Clinical Biomechanics, (17), 446-455.

*CSI Analysis Reference Manual* (11th ed.). (2007). Berkeley: Computers and Structures.

Eatherton, M., Ma, X., Krawinkler, H., Mar, D., Billington, S., Hajjar, J., and Deierlein, G. (2014). ”Design Concepts for Controlled Rocking of Self-Centering Steel-Braced Frames.” J. Struct. Eng., 140(11), 04014082.

Eidelson, Stewart. *Saving Your Aching Back and Neck, A Patient's Guide* . 2nd ed. San Diego, California: SYA Press, Inc, 2002. Print.

Goel, Vijay K., Hosang Park, and Weizeng Kong. "Investigation of Vibration Charateristics of the Ligamentous Lumbar Spine Using the Finite Element Approach." *Journal of Biomedical Engineering*. 116. (1994): 378-379. Print.

Hines, Tonya. *Spine Anatomy*. (2013, January 1). Retrieved January 15, 2015, from http://www.mayfieldclinic.com/PE-AnatSpine.htm#.VLbXs1pfkdo

Holmes, G. (n.d.). How Products Are Made. Retrieved January 16, 2015, from http://www.madehow.com/Volume-6/Gyroscope.html

Kurtz, Steven M., and Avram A. Edidin. *Spine Technology Handbook*. 1st edition. Burlington, Massachusetts: Academic Press, 2006. Print.

Lu, L., Lin, G., & Shih, M. (2011). An experimental study on a generalized Maxwell model for nonlinear viscoelastic dampers used in seismic isolation. *Engineering Structures, 34*, 111-123.

Marieb, Elaine. *Human Anatomy & Physiology.* 5th ed. San Francisco, California: Benjamin Cummings, 2001. Print.

Priestly, M., Sritharan, S., Conley, J., & Pampanin, S. (2000). Preliminary Results and Conclusions From the PRESSS Five-Story Precast Concrete Test Building. *PCMAC Technical Update,* 1-12.

Rodriguez, M. (2006). Analysis of Structural Damping. Lulea University of Technology.

Roke, D., Suase, R., Ricles, J., & Gonner, N. (2009). Design Concepts for Damage-Free Seismic-Resistant Self-Centering Steel Concentrically Braced Frames. *Structures Congress 2009,* 1-10.

Sause, R., Ricles, J.M., Roke, D., Seo, C.-Y., and Lee, K.-S.. "Self-Centering Seismic-Resistant Steel Concentrically-Braced Frames," STESSA 2006, Proceedings of the 5th International Conference on Behavior of Steel Structures in Seismic Areas, Yokohama, Japan, 2006, p. 85-90

Schafer, R.C. *Clinical Biomechanics: Musculoskeletal Actions and Reactions*. 2nd ed. Williams & Wilkins, 1987.

*SketchUp User's Guide*. (2006, June 16). Google, Inc. Retrieved January 3, 2015, from https://kpaccio.wikispaces.com/file/view/GSUUsersGuide-WIN.pdf

Slipped Discs, Disc Herniations, Disc injuries. Chiropractic Centres. (n.d.). Retrieved January 13, 2015, from http://www.isischiropractic.co.uk/chiropractic_disc_injuries.html

Specially Concentrically Braced Frame. (2012). In *2012 IBC SEAOC Structural/Seismic Design Manual* (Vol. 4, pp. 43-70). Sacramento: Structural Engineers Association of California (SEAOC).

Spine Center. (n.d.). Retrieved January 6, 2014, from http://www.uvaspine.com/ligaments-tendons-and-muscles.php

White, A., & Panjabi, M. (1990). *Clinical biomechanics of the spine* (2nd ed.). Philadelphia: Lippincott.

Wiebe, L., Christopoulos, C., Tremblay, R., & Leclerc, M. (2011). Shake Table Testing of a Rocking Steel Frame Designed to Mitigate Higher Mode Effects. *STESSA 2012,* 703–708-703–708.

Zee, Mark de, Lone Hansen, Christian Wong, and John Rasmussen. "A Generic Detailed Rigid-Body Lumbar Spine Model." *Journal of Biomechanics*. 40. (2007): 1219-1227. Print.

Zhou, S.H., I.D. McCarthy, A.H. McGregor, R.R.H Coombs, and S.P.F. Hughes. "Geometrical Dimension of the Lower Lumbar Vertebrae-Analysis of Data from Digitised CT Images ." *European Spine Journal*. 9. (2000): 242-248. Print.

## Appendix A: Model Creation Process

The following Figures and captions will illustrate the model creation process.

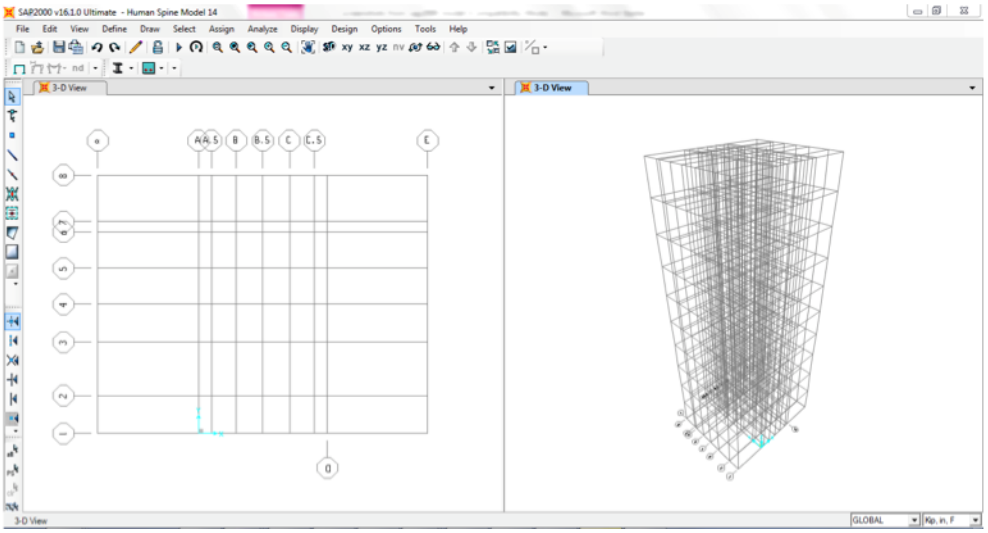

Figure A.1: Step 1: Create Three Dimensional Format Grid

Step 2: Input Material and Section Properties into SAP2000

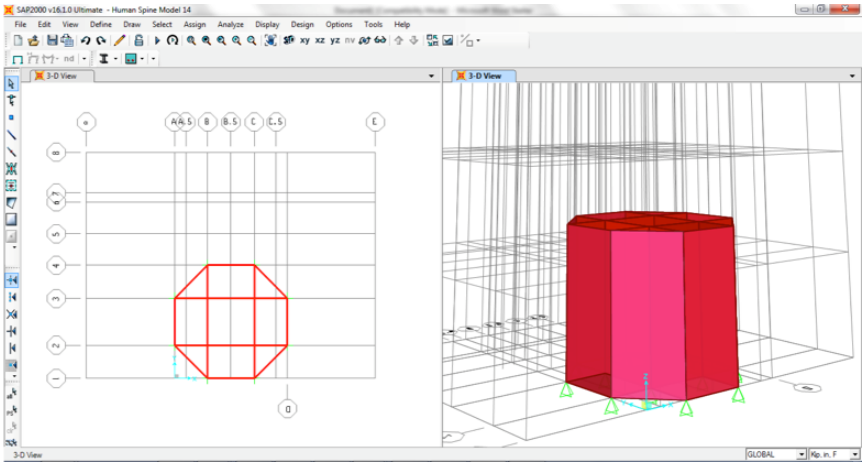

Figure A.2: Step 3: Create the Vertebral Body

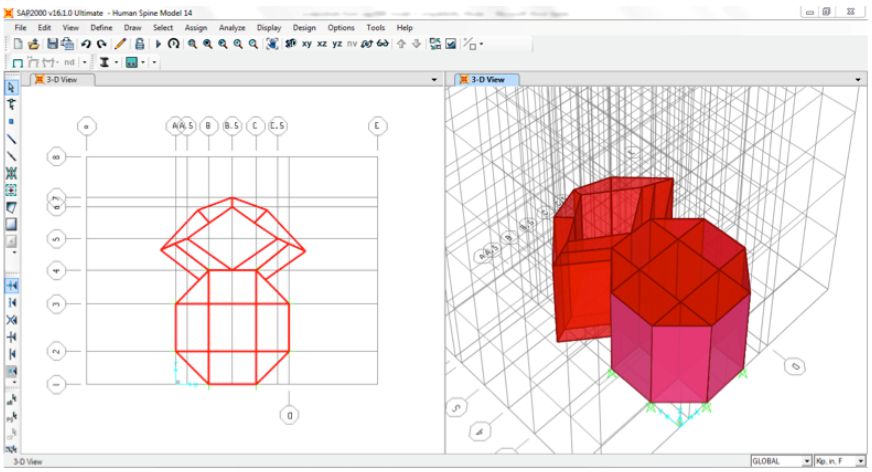

Figure A.3: Step 4:Create the Spinal Canal

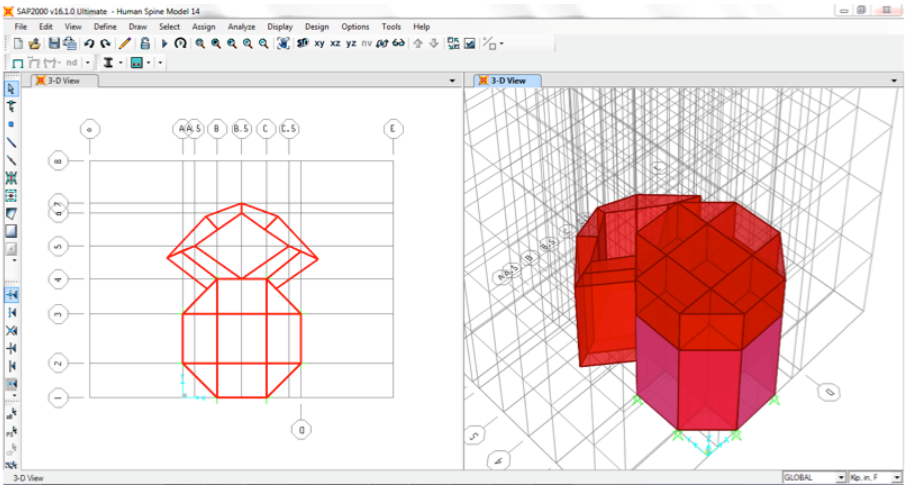

Figure A.4: Step 5: Create the Intervertebral Disk

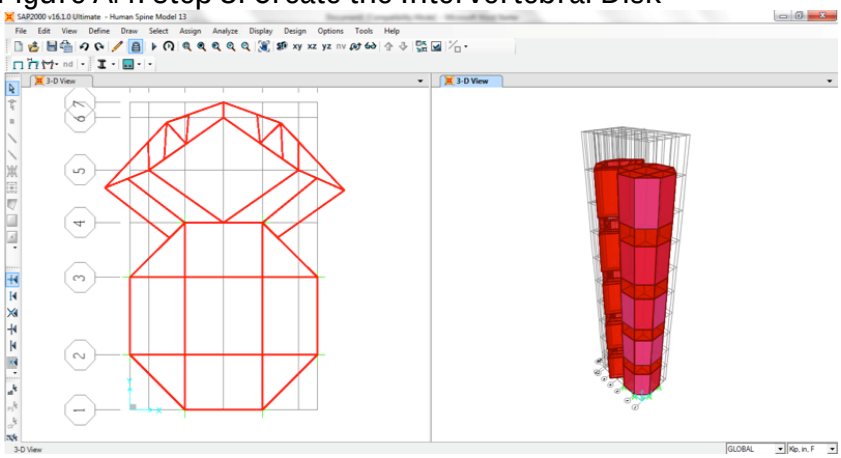

Figure A.5: Step 6: Create the L1-L5 Vertebral Bodies and Intervertebral Disk

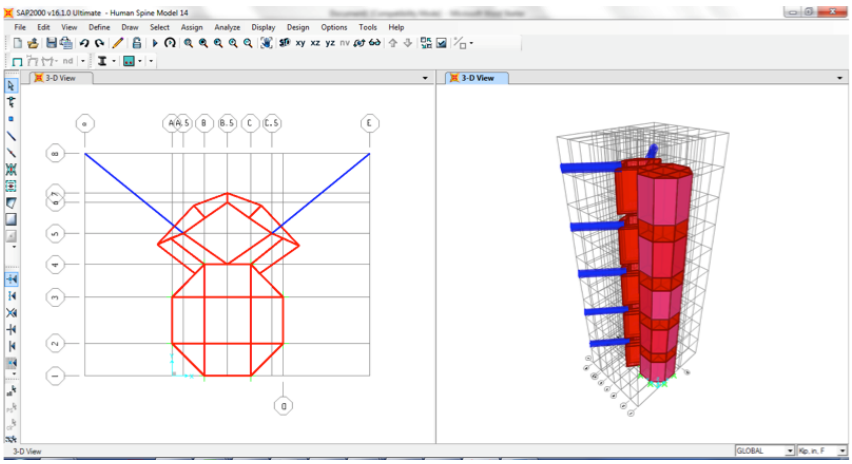

Figure A.6: Step 6: Create the Transverse Processes

Step 7: Create the Spinous Processes

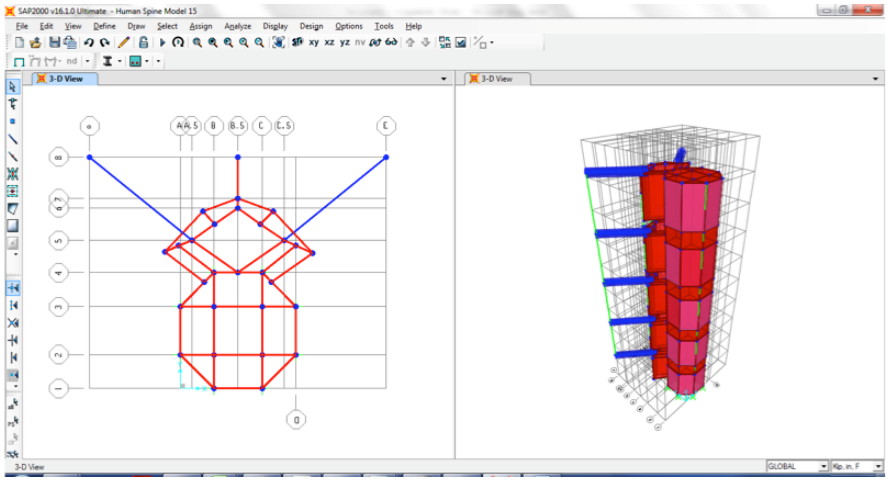

Figure A.7: Step 8: Create the Lumbar Region Ligaments (Final Model)

# Appendix B: Base Shear Versus Roof Displacement Plots

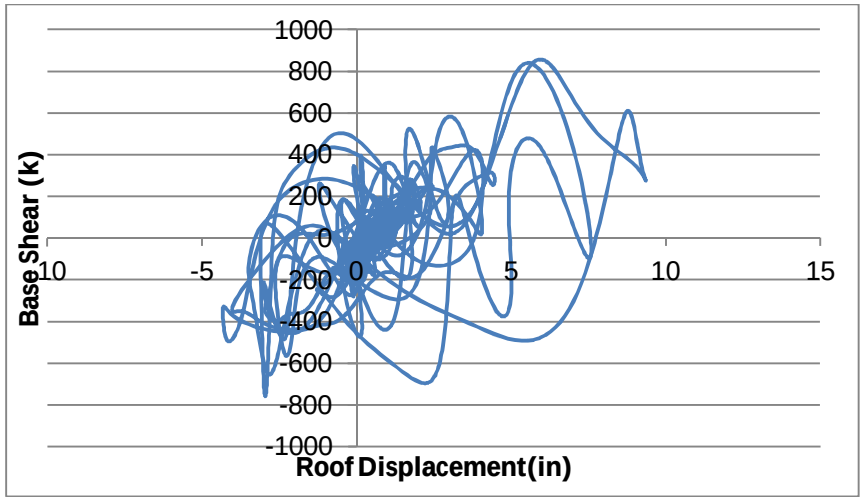


Figure B.1:Segmented PT Strands and Hysteretic Damper Hector Mine

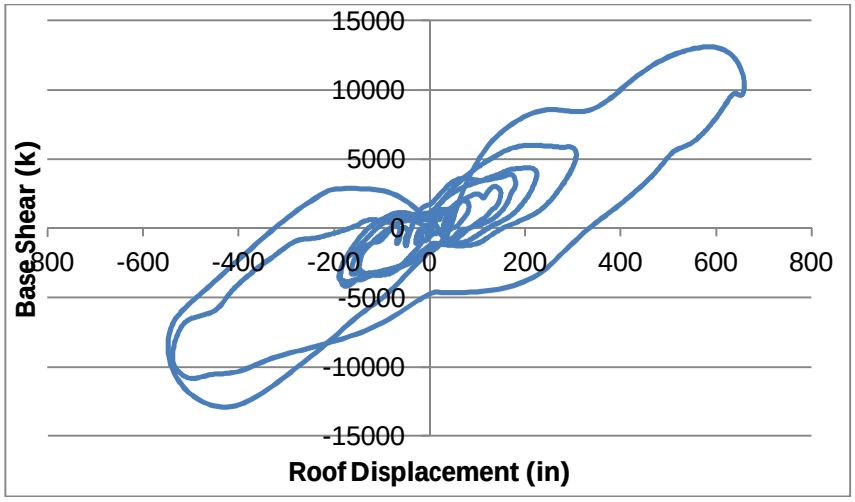


Figure B.2:Segmented PT Strands and Hysteretic Damper Erzincan

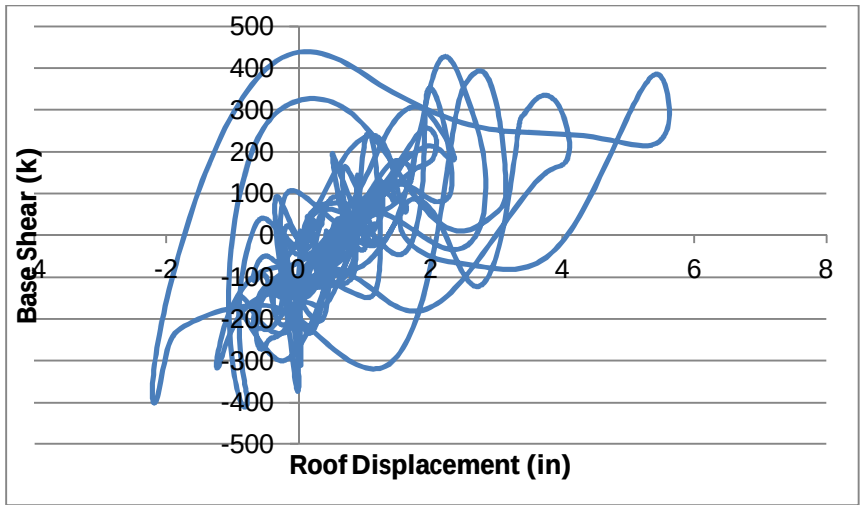


Figure B.3:Segmented PT Strands and Hysteretic Damper Manjil, Iran

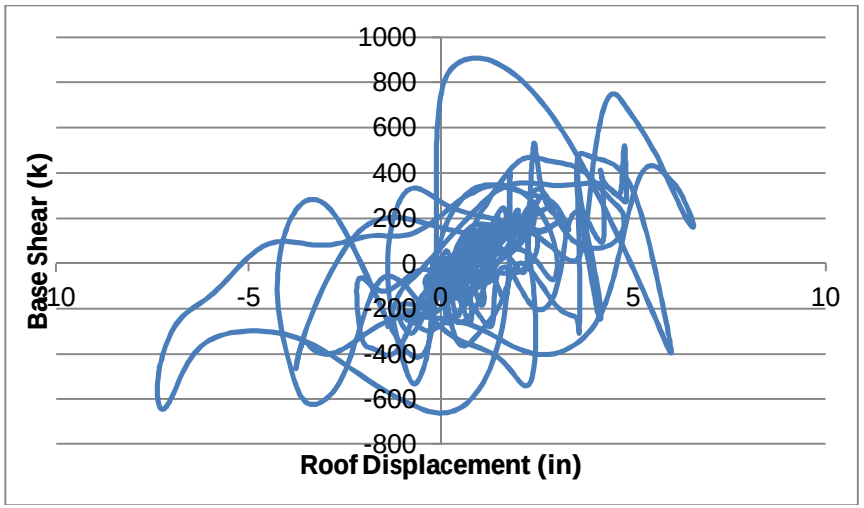


Figure B.4: Segmented PT Strands and Hysteretic Damper San Fernando

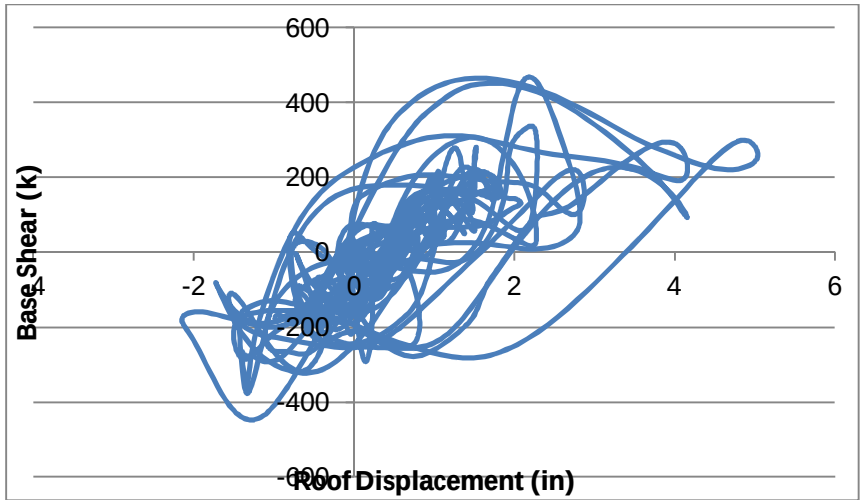


Figure B.5:Segmented PT Strands and Hysteretic Damper Loma Prieta

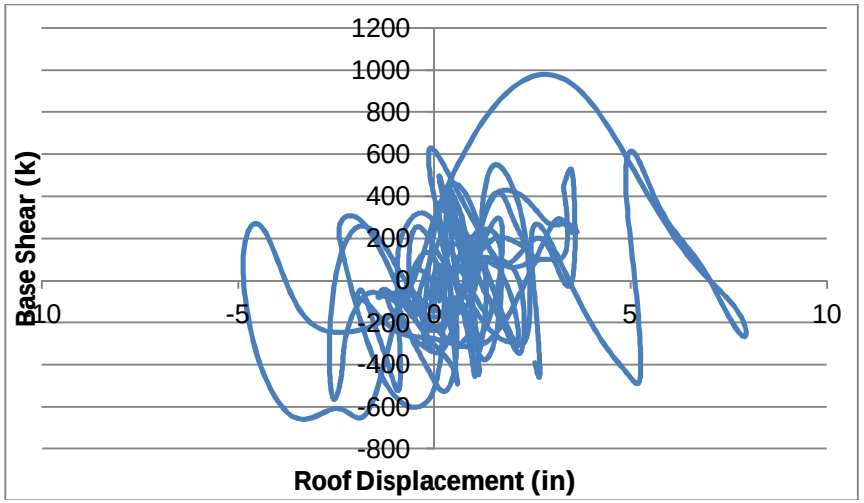


Figure B.6: Segmented PT Strands and Hysteretic Damper Nahanni

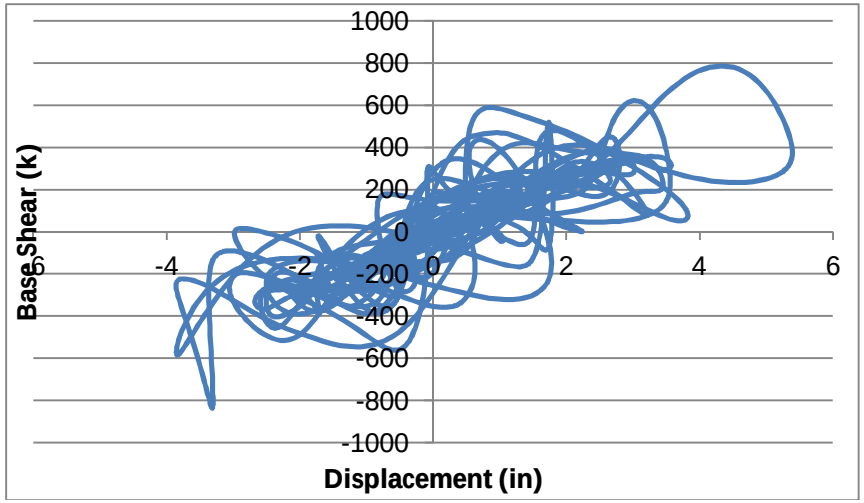


Figure B.7: Segmented PT Strands and Hysteretic Damper Northridge

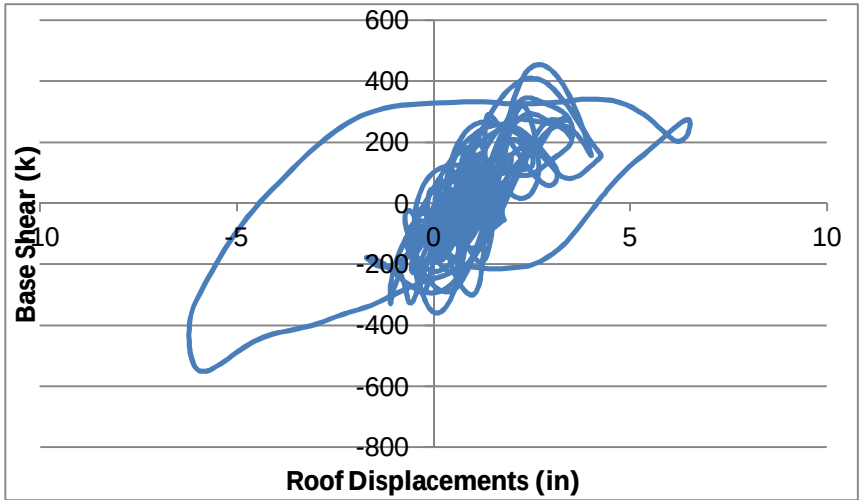


Figure B.8: Segmented PT Strands and Hysteretic Damper Cape Mendocino

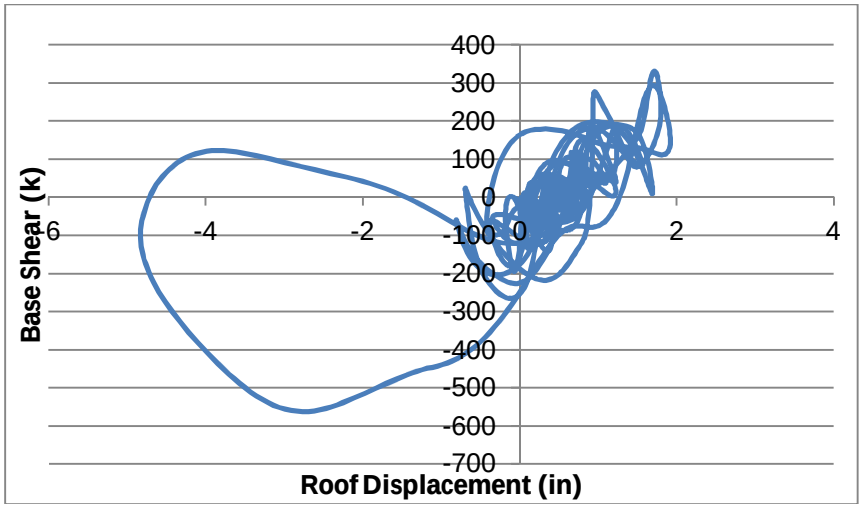


Figure B.9: Segmented PT Strands and Hysteretic Damper Imperial Valley

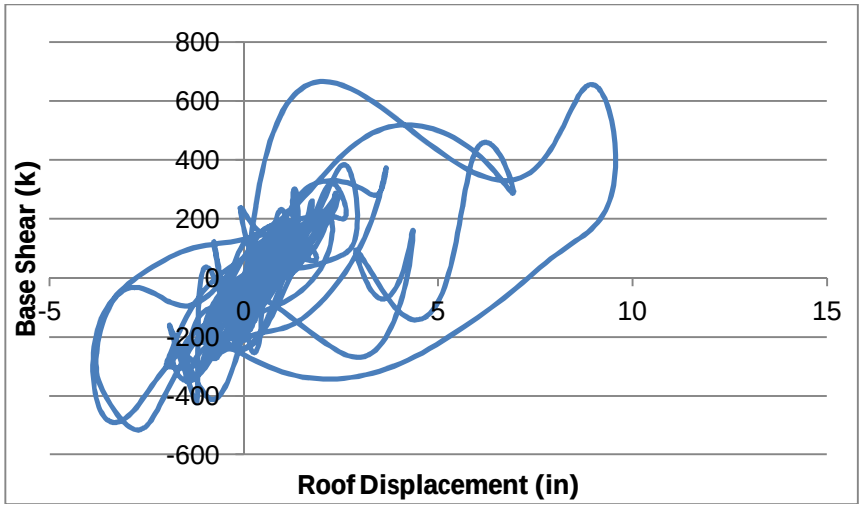


Figure B.10: Segmented PT Strands and Hysteretic Damper Lander's

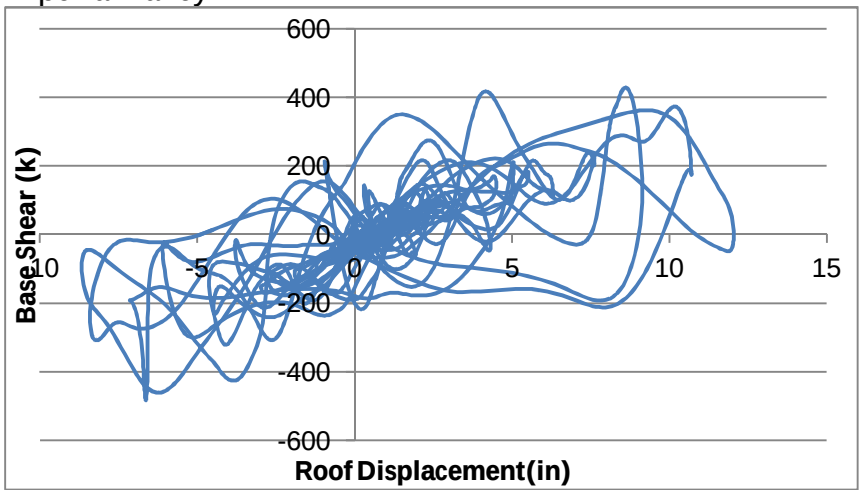


Figure B.11:Segmented PT Strands and Viscoelastic Damper Hector Mine

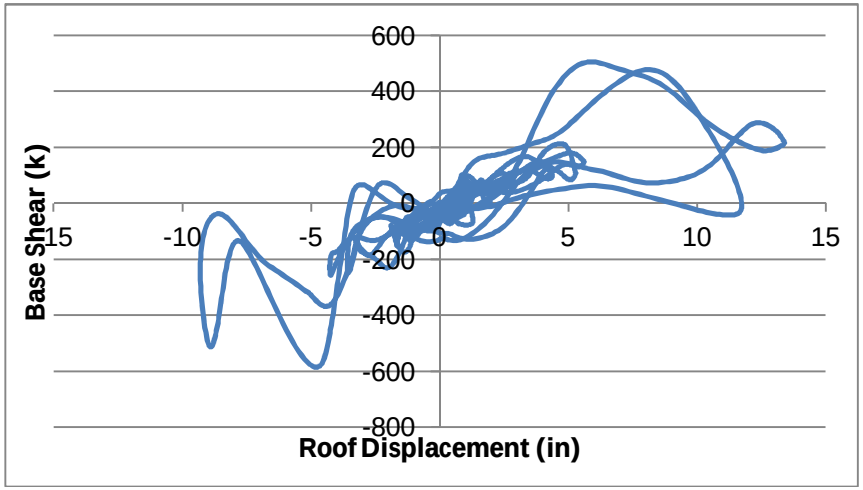


Figure B.12:Segmented PT Strands and Viscoelastic Damper Erzincan

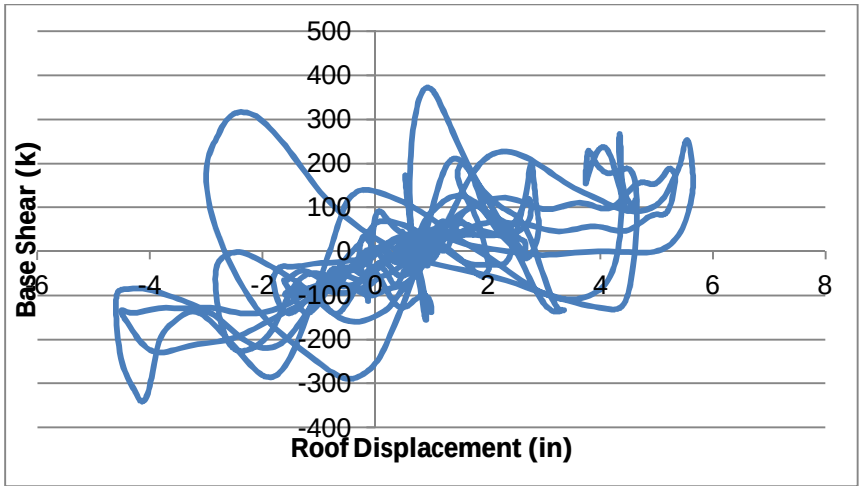


Figure B.13:Segmented PT Strands and Viscoelastic Damper Manjil, Iran

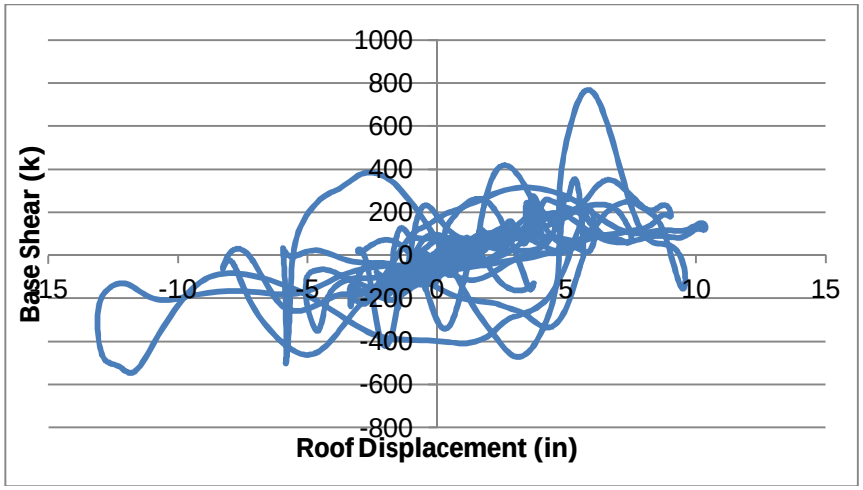


Figure B.14Segmented PT Strands and Viscoelastic Damper San Fernando

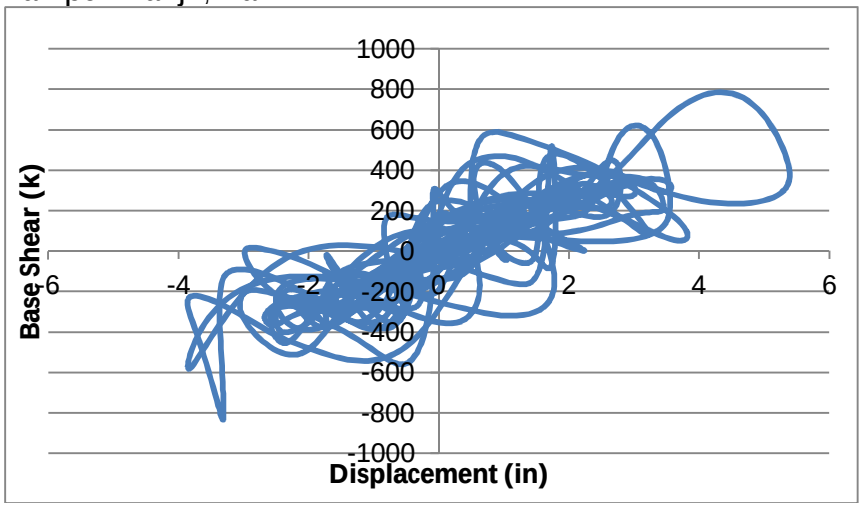


Figure B.15: Segmented PT Strands and Viscoelastic Damper Northridge

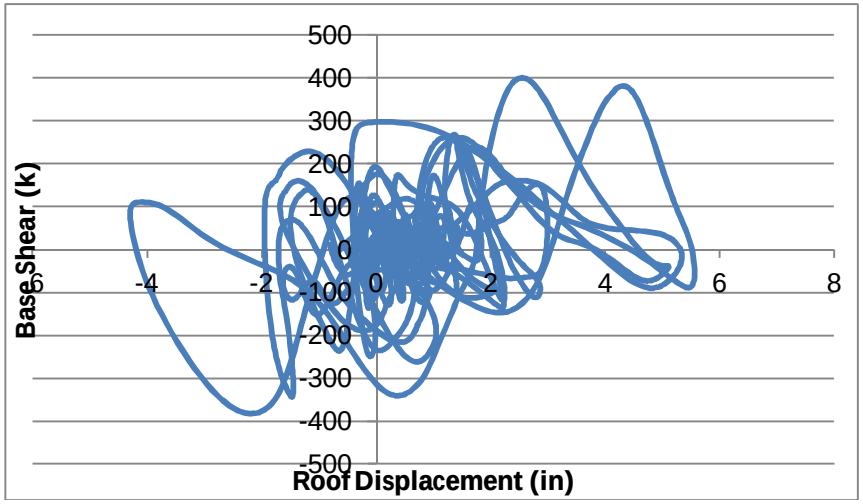


Figure B.16: Segmented PT Strands and Viscoelastic Damper Loma Prieta

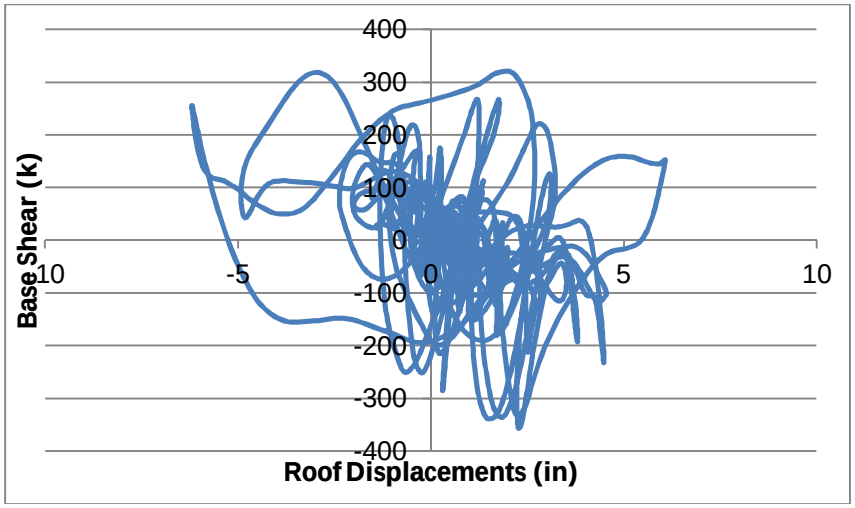


Figure B.17:Segmented PT Strands and Viscoelastic Damper Nahanni

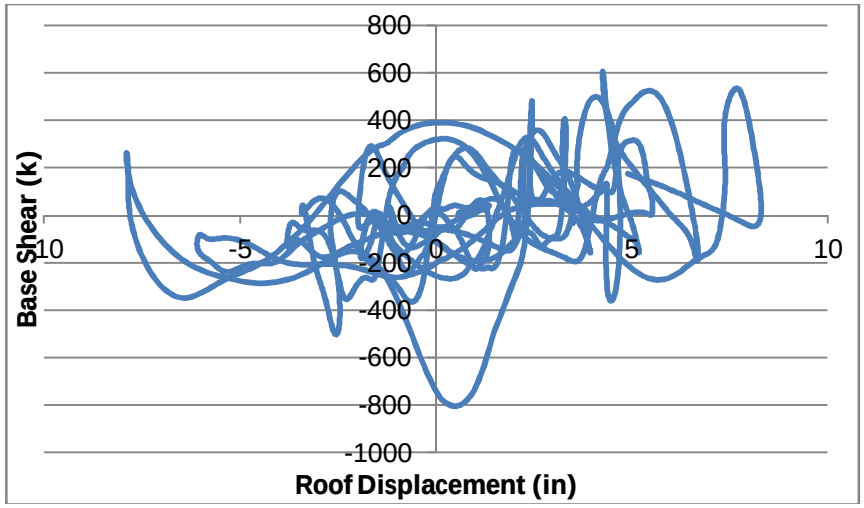


Figure B.18:Segmented PT Strands and Viscoelastic Damper Cape Mendocino

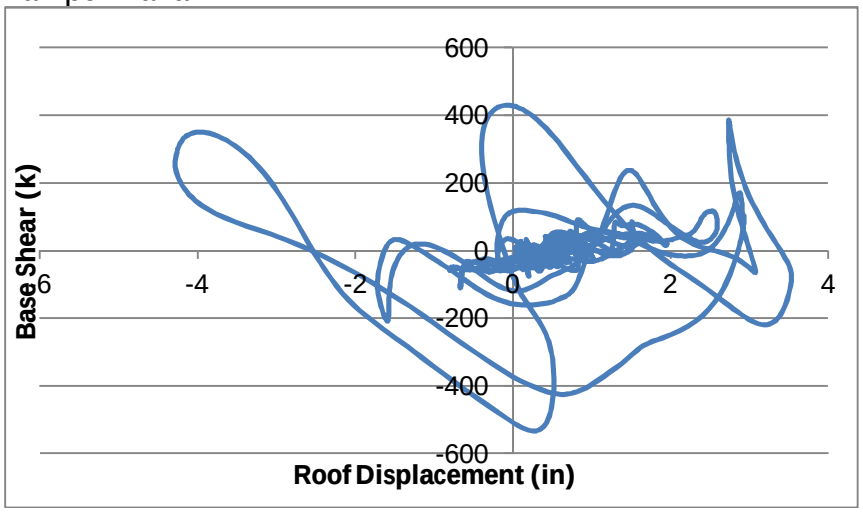


Figure B.19: Segmented PT Strands and Viscoelastic Damper Imperial Valley

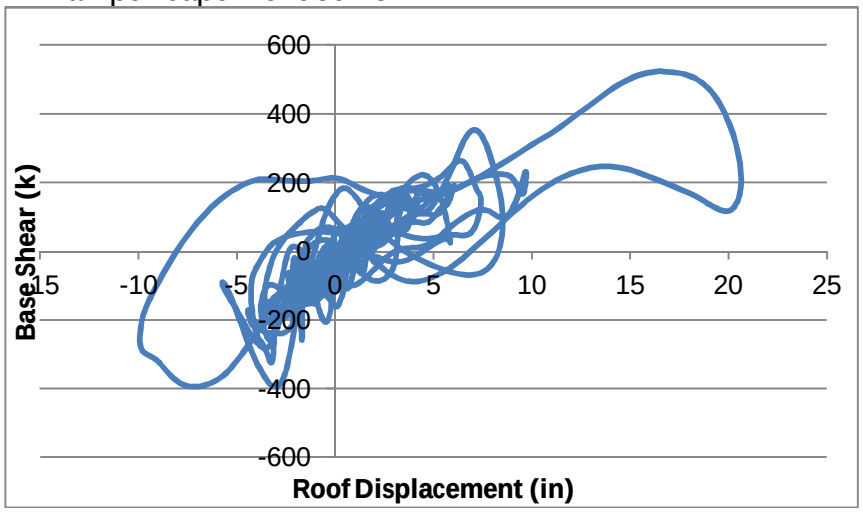


Figure B.20:Segmented PR Strands and Viscoelastic Damper Lander's

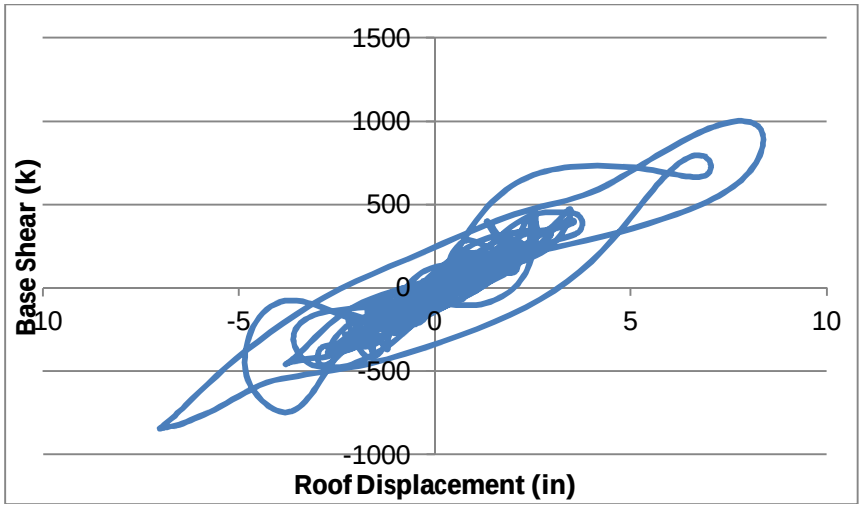


Figure B.21:Continuous PT Strands and Viscoelastic Damper Lander's

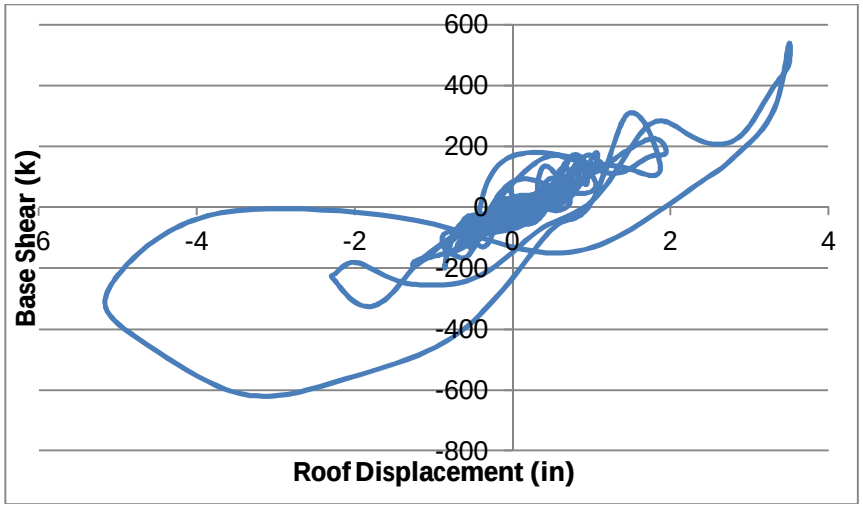


Figure B.22:Continuous PT Strands and Viscoelastic Damper Imperial Valley

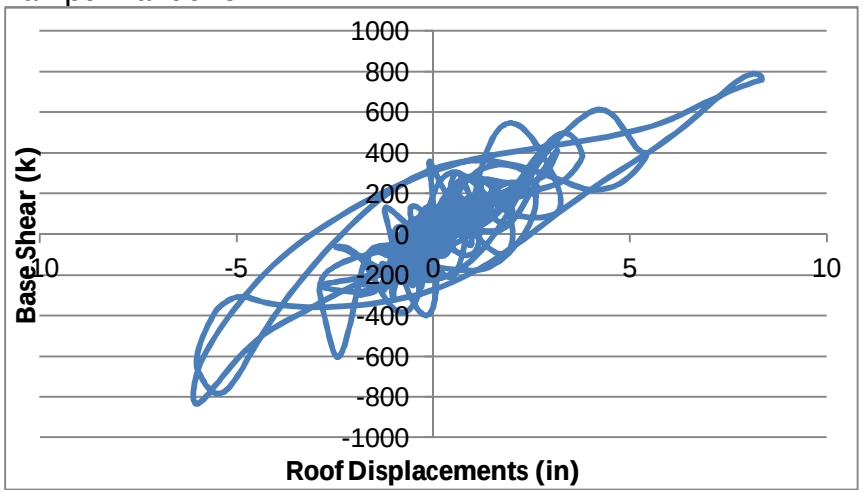


Figure B.23: Continuous PT Strands and Viscoelastic Damper Cape Mendocino

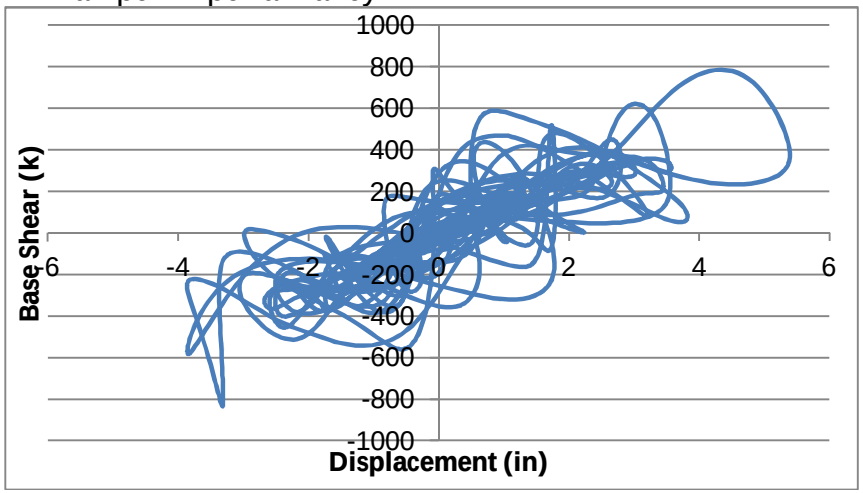


Figure B.24:Continuous PT Strands and Viscoelastic Damper Northridge

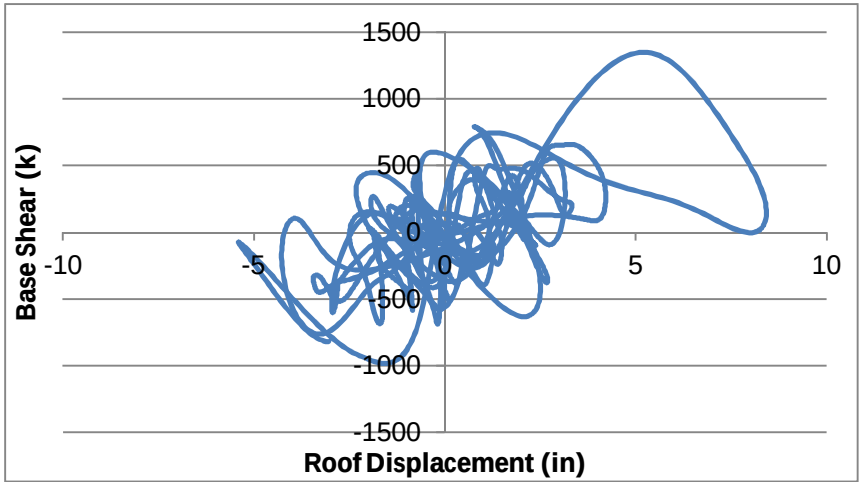


Figure B.25:Continuous PT Strands and Viscoelastic Damper Nahanni

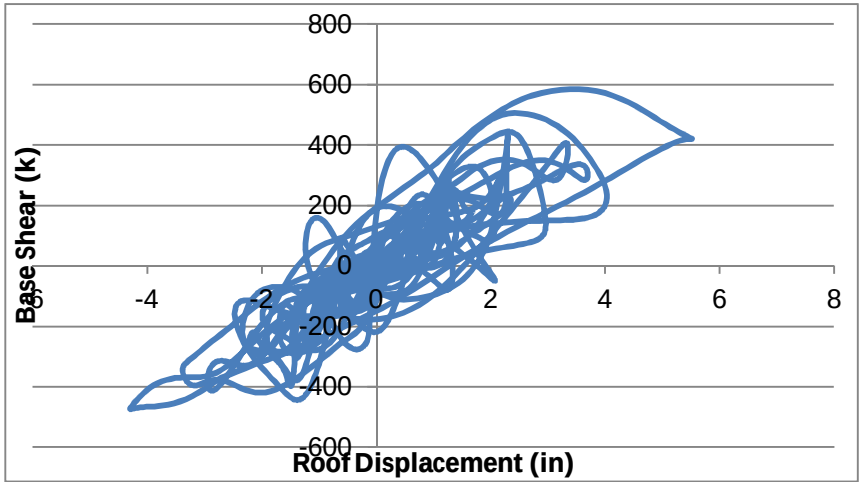


Figure B.26:Continuous PT Strands and Viscoelastic Damper Loma Prieta

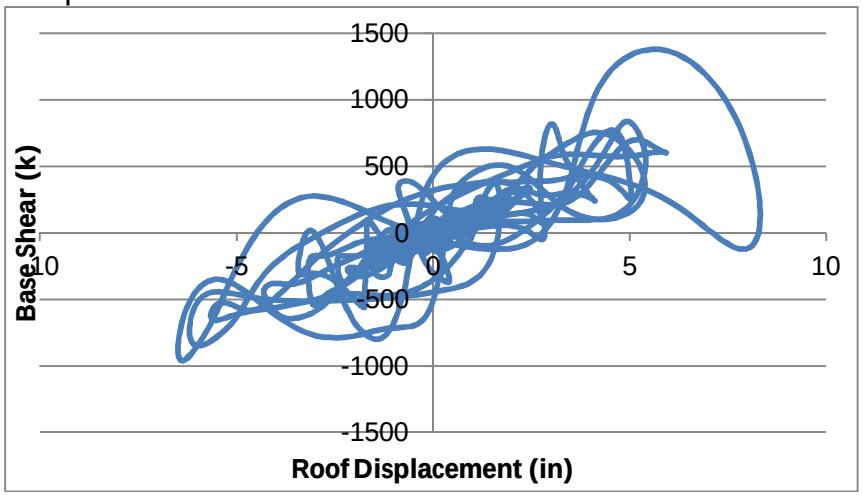


Figure B.27:Continuous PT Strands and Viscoelastic Damper San Fernando

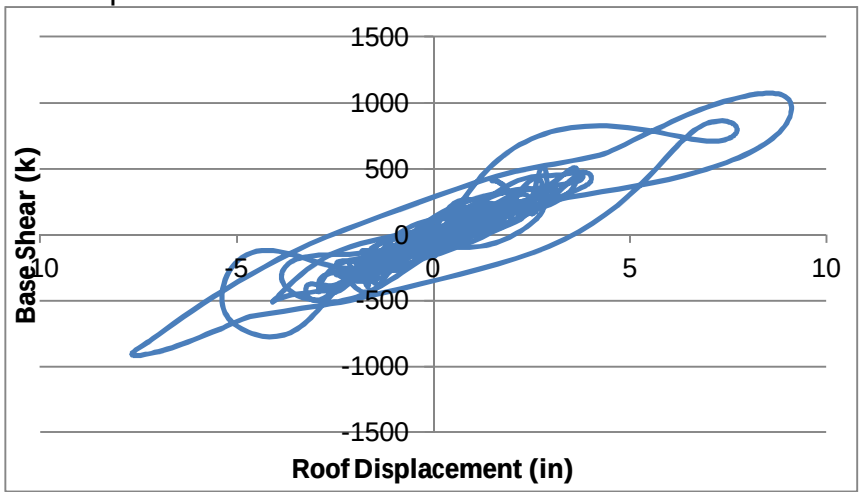


Figure B.28:Continuous PT Strands and Viscoelastic Damper Manjil, Iran

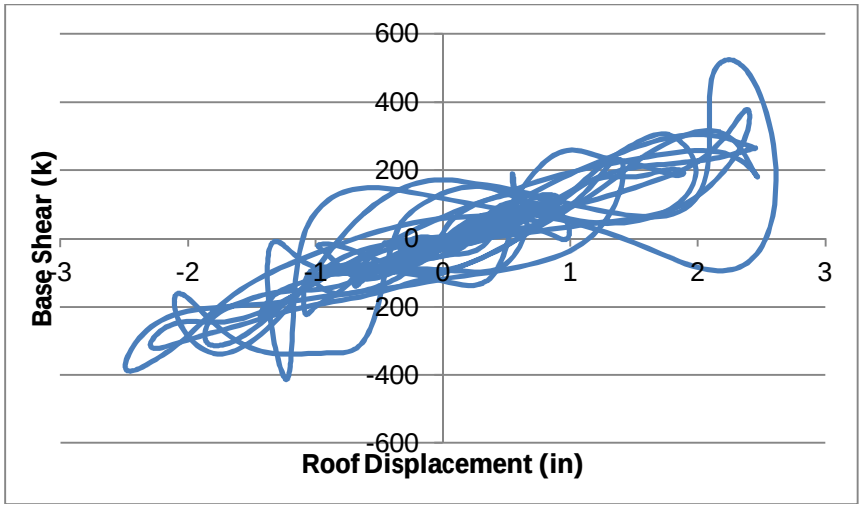


Figure B.29:Continuous PT Strands and Viscoelastic Damper Erzincan

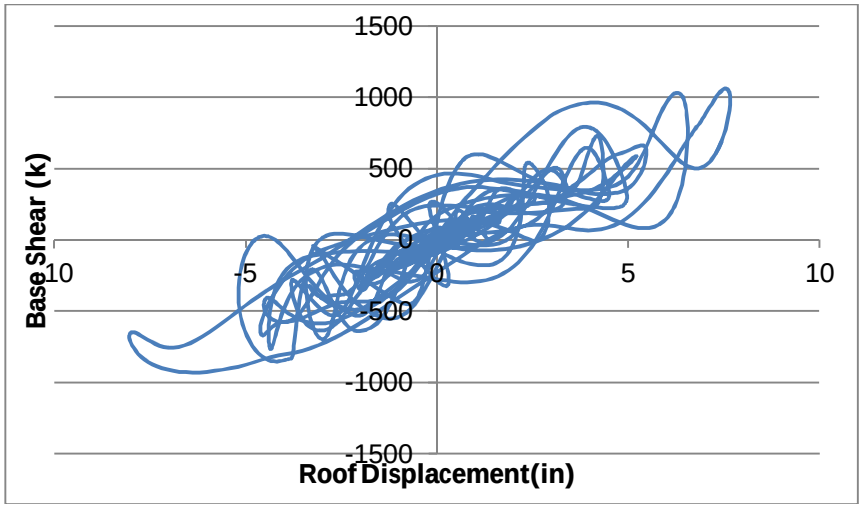


Figure B.30:Continuous PT Strands and Viscoelastic Damper Hector Mine

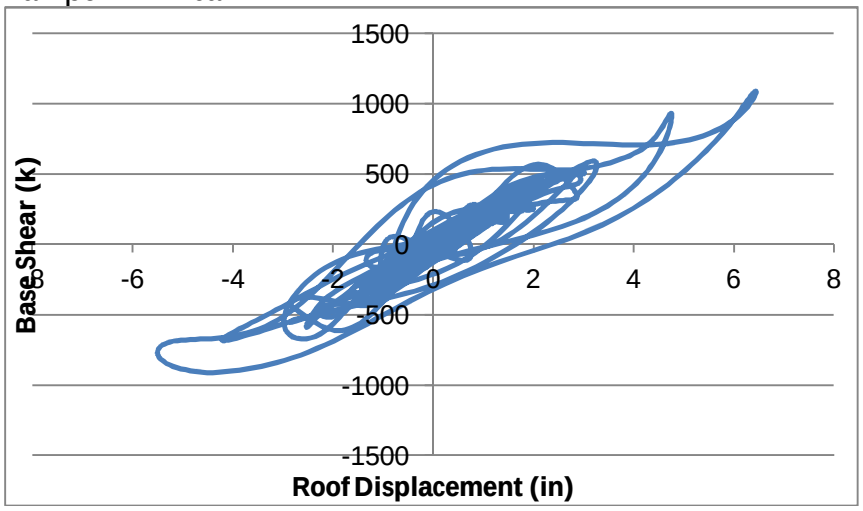


Figure B.31:Continous PT Strands and Hysteretic Damper Lander's

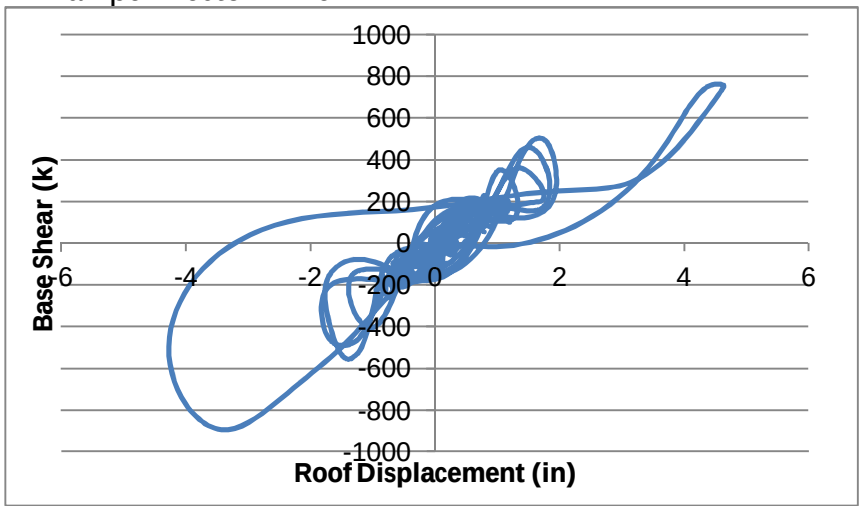


Figure B.32:Continuous PT Strands and Hysteretic Damper Imperial Valley

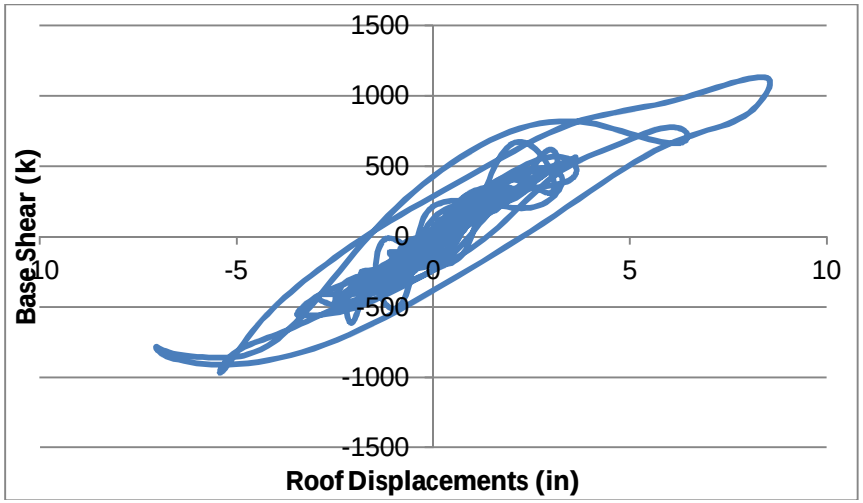


Figure B.33:Continuous PT Strands and Hysteretic Damper Cape Mendocino

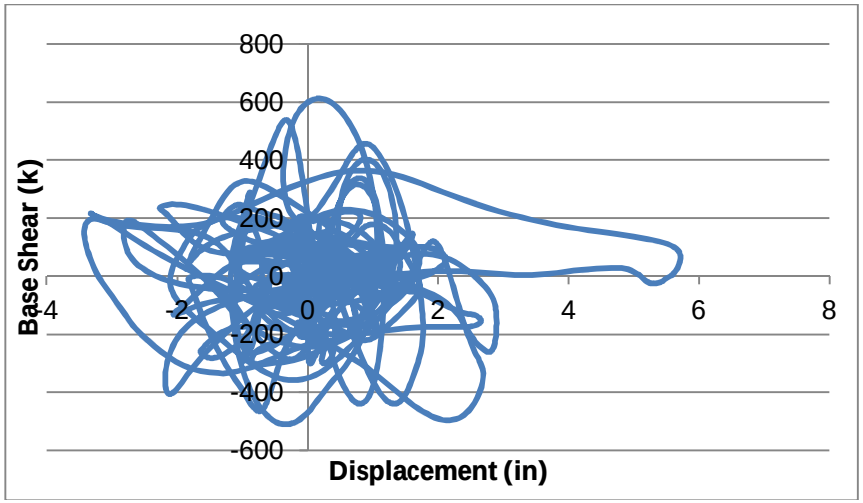


Figure B.34:Continuous PT Strands and Hysteretic Damper Northridge

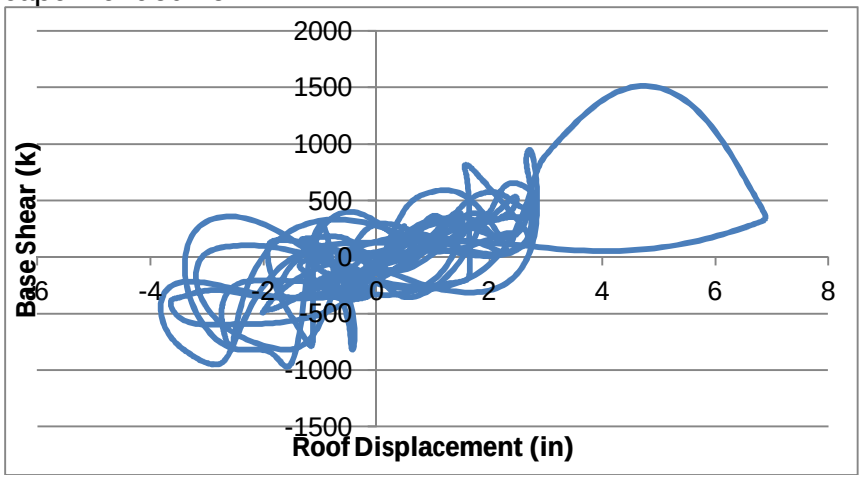


Figure B.35:Continuous PT Strands and Hysteretic Damper Nahanni

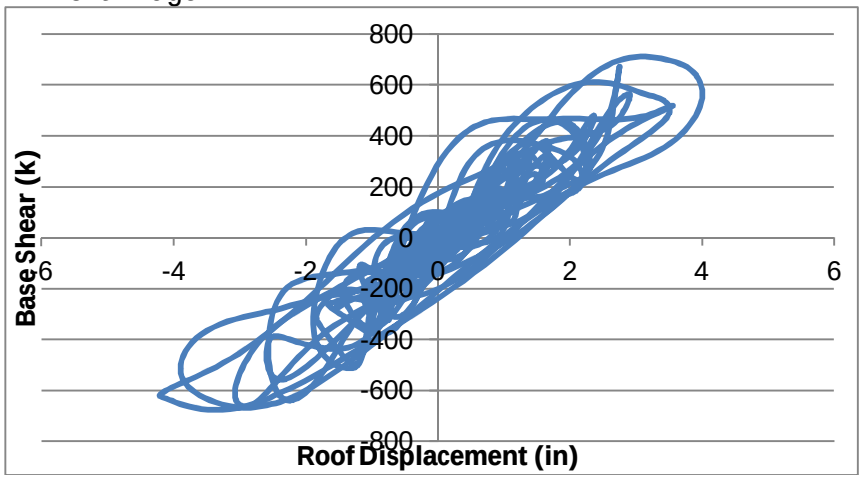


Figure B.36:Continuous PT Strands and Hysteretic Damper Loma Prieta

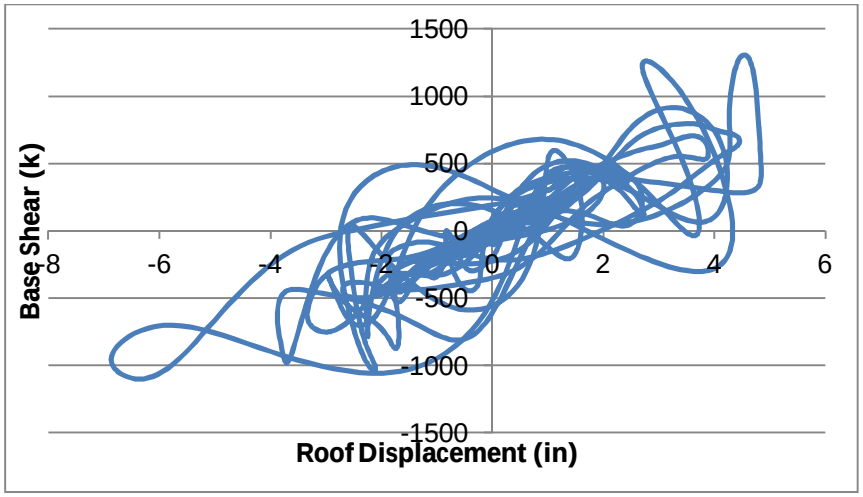


Figure B.37:Continuous PT Strands and Hysteretic Damper San Fernando

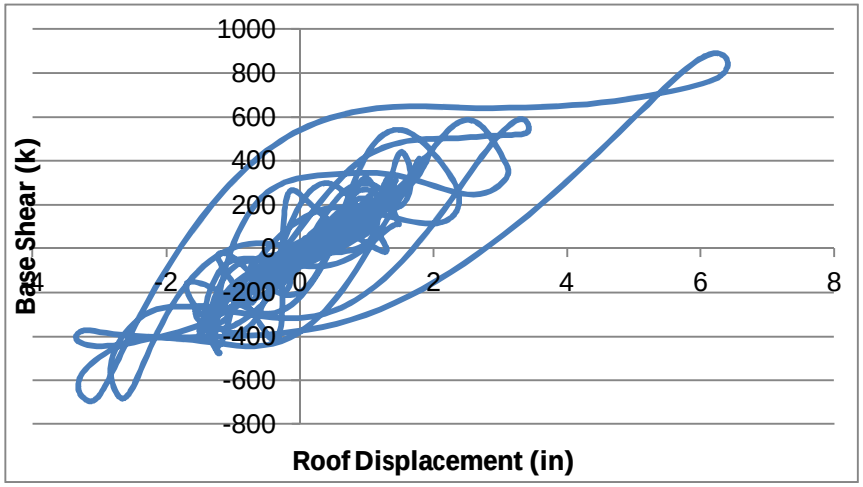


Figure B.38:Continuous PT Strands and Hysteretic Damper Manjil, Iran

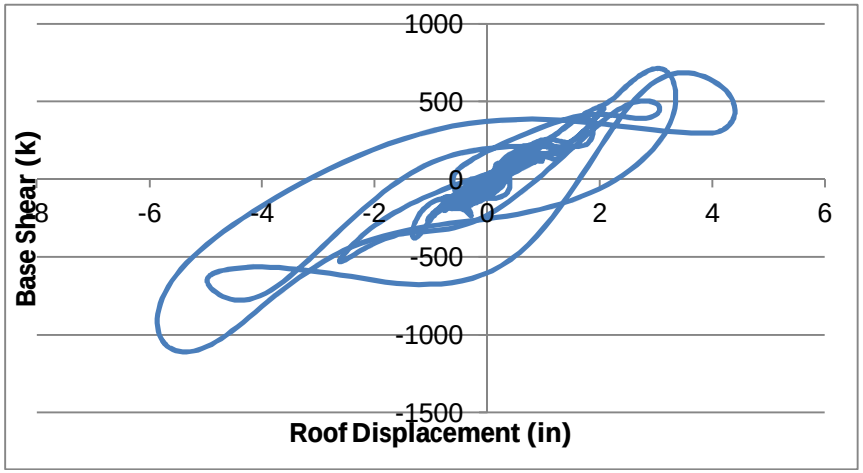


Figure B.39: Continuous PT Strands and Hysteretic Damper Erzincan

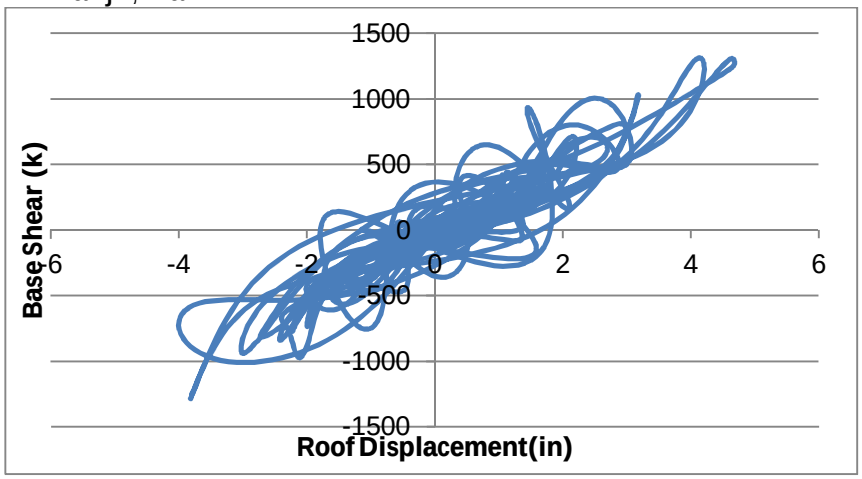


Figure B.40: Continuous PT Strands and Hysteretic Damper Hector Mine